Sensitivity Enhancement Approaches in Microwave-Microfluidic Sensors and Design of a Compact and Cost-effective RF Sensor Readout System

By

Niloofar Sharafadinzadeh

A thesis submitted in partial fulfillment of the requirements for the degree of

Master of Science
in
Electromagnetics and Microwaves

Department of Electrical and Computer Engineering
University of Alberta

© Niloofar Sharafadindzadeh, 2020

Abstract

Microwave resonators have proved their capability as sensing devices in a wide range of applications such as lab on chip, environmental sustainability, and industrial applications, not only for analysis in the solid and liquid phase, but also recently in gaseous environments. Planar microstrip resonators made from split ring resonators (SRRs) have shown relatively sharper resonances and simultaneously increased sensitivity due to their higher coupling to the surrounding signal lines. These sensors are amenable to miniaturization, automation, mass production, and wireless interconnection due to CMOS compatibility, low cost and a facile fabrication process.

Such microwave resonators also offer noninvasive sensing through contact-less probing, which adds to their flexibility of usage and maneuverability for in situ characterization. For certain industrial applications such as material characterization in microfluidic channels, it is crucial to use a highly sensitive device which identifies small variations in concentration. There are many approaches to increase the sensitivity of the microwave resonators. Two passive methods are proposed in this work: gap extension of the SRR, and embedding material under test (MUT) inside the substrate.

To investigate the effect of gap extension on microwave planar resonators' sensitivity, microstrip split rings are utilized as conventional half-wavelength resonators with sensitive spot for dielectric sensing in the gap. The sensor is configured in three different mixed electric and magnetic couplings and the sensitivities, in terms of frequency and amplitude variation, are analyzed under exposure to given materials. The passive resonators at ~2 GHz are simulated with permittivity values of samples ranging from 5 through 30. The resonator gap is engineered with an inward extension for higher sensitivity, where a uniform enhancement up to more than 20% in

frequency-sensitivity is obtained to reach $\frac{change\ in\ frequency}{change\ in\ permittivity} = 6.17MHz$ for all coupling configurations, while the amplitude based sensitivity is preserved. An experimental application of the highly sensitive sensor is introduced in non-contact concentration measurement of glucose within wide range of 1-15 g/dL with steps of 1 g/dL.

In this work, microwave planar sensors are discussed for liquid characterization, mainly microfluidic application. Three common sensors are implemented in complementary split ring resonator, extended gap split ring resonator, and conventional circular split ring resonator resonating at 1.7, 1.9, and 3.6 GHz, respectively. Sensitivity of material on top of the resonator is analyzed, and is modified with respect to the volume of material under test for more comprehensive evaluation of sensor's performance. Circular resonator is found to be the optimum in terms of sample volume and offers up to 50% higher sensitivity for permittivity range from 1-30.

This sensor is further developed into embedding the material under test inside its substrate and the sensitivity is also enhanced on average by ~ 45% for bulk material sensing of the same permittivity range. In practical verification of the embedding concept, water sample concentrated with 10%-50% methanol is placed above/inside substrate and remarkable improvement of 360% in sensitivity is observed for the latter when PTFE tubes are installed. Finally, microfluidic channels are uniquely implemented inside the substrate of circular split ring resonator and distinct signatures are detected, which proved the concept of sensitivity enhancement in resonators while minimizing the sample volume.

In addition, the proper instrument is needed to capture the data from microwave resonance-based sensors in the field. Vector Network Analyzer (VNA) is the major equipment that is vastly used to measure and monitor the performance of RF devices. VNAs are multifunctional and very accurate tools that are used for various applications in this field. Due to their many features and capabilities, they are often bulky and expensive equipments that consist of different RF modules. This study also focuses on developing a compact, cheap, and yet accurate RF sensor read-out system to capture the amplitude of transmission response of SRRs; this novel circuitry is the first step in revolutionizing the practical use of microwave and RF sensors that focuses on miniaturization and performance of such high-demand equipment. This study focuses on sensitivity enhancement of passive SRRs, integrating them with microfluidic channels, as well as developing a read-out system to measure amplitude of transmission profile of the SRRs.

Preface

Chapter 3 of this thesis has been accepted and published on January 8th, 2018, as Niloofar Sharafadinzadeh, Mohammad Abdolrazzaghi, and Mojgan Daneshmand “Highly Sensitive Microwave Split Ring Resonator Sensor Using Gap Extension for Glucose Sensing”, 2017 IEEE MTT-S International Microwave Workshop Series on Advanced Materials and Processes for RF and THz Applications (IMWS-AMP). I was the lead investigator, responsible for all major areas of concept formation, fabrication, measurements and analysis, as well as manuscript composition. Mohammad Abdolrazzaghi helped with measurements and contributed to manuscript edits. Dr. Mojgan Daneshmand was the supervisory author on this study and was involved throughout the project in concept formation and manuscript composition.

Chapter 4 of this thesis has been accepted and published on November 14th, 2019, as Niloofar Sharafadindzadeh, Mohammad Abdolrazzaghi, and Mojgan Daneshmand “Investigation on Planar Microwave Sensors with Enhanced Sensitivity from Microfluidic Integration”, Elsevier Sensors and Actuators A: Physical research paper. I was the lead researcher, responsible for all major areas of concept formation, fabrication, measurements and analysis, as well as manuscript composition. Mohammad Abdolrazzaghi had advisory role and contributed to the manuscript edits. Dr. Mojgan Daneshmand was the supervisory author on this study and was involved throughout the project in concept formation and manuscript composition.

Figures in Chapter 2 are used with permission from the applicable sources.

Dedication

This work is wholeheartedly dedicated to my beloved parents, Naser and Mojgan, and my love, Ali, who are my sources of inspiration and give me strength during challenging times, who generously and continuously provide their moral, emotional, and loving support. I am grateful for their patience when I had faced tough times in the course of my education, for their unconditional love and encouragement that leads me toward the right path, and for their enlightening wisdom in every aspect of my life.

I would also like to dedicate this work to my caring and loving sisters, Nikta and Yekta, who never stop inspiring me by their hard work and dedications in their lives, and bringing me joy and enthusiasm every step of the way. This work would have never been possible if I did not have the support and patience of my loved ones.

Acknowledgments

This work has been made possible by the support and inspiration of many people. Frist of all, I would like to present my sincere recognition to my supervisor Dr. Mojgan Daneshmand who has provided me with her support, guidance and patience throughout my studies under her supervision. It has been a great honor to work with an inspirational and encouraging supervisor like Dr. Daneshmand. Secondly, I would like to thank Dr. Masoud Baghelani for his guidance and suggestions through our collaboration on one of my projects. I would also like to appreciate Dr. Ali Kiaee for his insightful technical discussions and consultations that helped me to improve my knowledge and experience.

My sincere appreciation goes to my dear colleague and friend Mohammad Abdolrazzaghi who helped me from beginning of my graduate studies till the end. He provided technical discussions and insightful suggestions to improve my research and technical knowledge. He has been a great, thoughtful and helpful mentor, as well as a reliable and trustworthy colleague during measurements and experiments. I would also like to thank my friends and colleagues in microwave-to-millimeter (M2M) research group, Sameir Deif, Zahra Abbasi, and Navid Hosseini in the past three years at University of Alberta. I would like to extend my gratitude to sincerely respectful Dr. Pedram Mousavi and his research team for their generous support on providing some electrical components which has made this work possible.

Along the support of my colleagues and friends, I acknowledge Natural Sciences and Engineering Research Council of Canada (NSERC), Alberta Innovate and Technology Futures (AITF) and CMC microsystem for their constructive support in providing the funding for the present research and utilized equipment.

Table of Contents

Abstract ii

Preface v

Dedication vi

Acknowledgments vii

Table of Contents viii

List of Tables xii

List of Figures xiii

List of Abbreviations xvi

1 Introduction 1

1.1 Motivation 1

1.2 Objective 2

1.3 Thesis Outline 3

2 Literature Review 5

2.1 Sensors Overview 5

2.2 Microwave Resonators Overview 6

2.2.1 Planar Microwave Resonators vs Microwave Cavities 7

2.2.2 Basic Operation of a Conventional Open Loop Microwave Resonator 7

2.3 Applications of Microwave Resonators 8

2.3.1 Material Characterization 9

2.3.2 Liquid Sensing in Oil and Gas Industry 10

2.3.3 Liquid Sensing for Biomedical Applications 11

2.3.4 Liquid Sensing for Structural Health Monitoring 14

2.4 RF Readout Circuitry 14

2.4.1 Working Mechanism of VNA 15

2.4.2 S-Parameters 16

3 Sensitivity Enhancement Using Gap Extension 19

3.1 Simulations 20

3.1.1 Simulation of SRR 20

3.1.2 Simulation of the Extended Gap SRR 22

3.2 Experiments and Measurements 23

3.3 Summary 26

4 Sensitivity Enhancement by Embedding MUT into Substrate and Integration with Microfluidic Channel 28

4.1 Introduction 28

4.2 Outline 29

4.3 Applications of Methanol Sensing 30

4.4 Simulation and Analysis 30

4.4.1 Electrical Field Distribution 32

4.4.2 Comparison of Sensors with MUT on Top 33

4.4.3 Embedding MUT inside the Substrate 37

4.4.4 Permittivity Analysis 40

4.5 Measurements and Results 42

4.5.1 Measurements Using PTFE Tubing ... 42
4.5.2 Measurements Using Microfluidic Channel ... 46
4.6 Summary ... 48
5 Design of a Compact and Cost-effective Microwave Sensors Readout Circuitry ... 50
5.1.1 Objective ... 51
5.2 Building Blocks of the System ... 52
5.3 Hardware Design ... 53
5.3.1 Power Board ... 54
5.3.2 Voltage Control Oscillator (VCO) ... 55
5.3.3 Attenuator ... 55
5.3.4 Low Pass Filter (LPF) ... 56
5.3.5 Device under Test (DUT) ... 56
5.3.6 Power Detector (PD) ... 57
5.3.7 Digital-to-Analog Convertor (DAC) ... 57
5.4 Digital Design ... 58
5.4.1 Microcontroller Unit (MCU) ... 58
5.4.2 Analog-to-Digital Convertor (ADC) ... 59
5.4.3 Direct Memory Access (DMA) ... 60
5.4.4 Universal Asynchronous Receiver Transceiver (UART) ... 60
5.4.5 Synchronous Serial Controller (SSC) ... 61
5.5 Software Design ... 62

5.5.1 Graphical User Interface (GUI) 63

5.5.2 MATLAB Functions 64

5.6 Experiments and Measurements 66

5.6.1 Initial Glucose Sensing Measurements 68

5.6.2 Effect of Low Pass Filter and Attenuator 71

5.6.3 Manual Calibration Procedure 73

5.6.4 Resonators Profiles with Improved Setup 74

5.6.5 Improved Glucose Sensing Measurements 76

5.7 Summary 79

6 Conclusion and Future Work 81

6.1 Thesis Conclusions and Accomplishments 81

6.2 Suggestions for Future Work 82

References 84

Appendix A Manual Instructions to Use RF Sensor Readout System 97

A. 1 Calibration Procedure 97

A. 2 Narrow Band $\boldsymbol{S21}$ Amplitude Measurement 98

List of Tables

Table 3-1 Frequency and amplitude sensitivity with respect to permittivity variations 23

Table 4-1 Sensitivity comparison with respect to permittivity 35

Table 4-2 Modified sensitivity comparison with respect to permittivity 36

Table 4-3 Lumped elements of Circular-SRR 39

Table 4-4 Complex dielectric constants of water and methanol [82] 41

Table 4-5 Mixture of methanol and water 43

Table 4-6 Normalized Frequency Error 45

Table 4-7 Normalized Frequency Error for Microfluidic Channel 48

Table 5-1 Comparison of resonance parameters of the three SRRs using VNA and the readout system 75

List of Figures

Fig. 2-1 A conventional split ring resonator (SRR) [5] and its lumped-element equivalent circuit model.. 7

Fig. 2-2(a) Asymmetric SRR [22], (b) conventional SRR [23], (c) DSRR [24], (d) co-planar sensor [25].. 9

Fig. 2-3 Schematic design of co-planar microwave resonator [27] 12

Fig. 2-4 Schematic design of DSRR used in [29] 13

Fig. 2-5 Basic concept of a vector network analyzer [46] 16

Fig. 3-1 (a-c) Case1, Case 2, Case 3, three different SRR orientations (gap = 1.5mm)............... 20

Fig. 3-2 (a-c) Case 1, Case 2, Case 3, Three models for extended gap SRR in different orientations (gap = 1.5mm).. 21

Fig. 3-3 Frequency (a) and amplitude (b) variations in SRR structure due to *different permittivity values* 21

Fig. 3-4 Frequency (a) and amplitude (b) variations in extended gap SRR structure due to different permittivity values.. 22

Fig. 3-5 Experimental frequency (a) and amplitude (b) shift of the proposed sensor at various glucose concentrations 24

Fig. 3-6 Experiment set-up for glucose sensing using modified SRR.. 24

Fig. 4-1 Layouts and dimensions [mm]: (a) CSRR: w = 1, g = 1, L_1 = 35, L_2 = 5; (b) EG-SRR: w = 2.4, g = 1, s = 0.5, L_1 = 18, L_2 = 12, L_3 = 7.6; (c) Circular-SRR: w = 5, s = 1.5, g_1 = 4, g_2 = 1, r_1 = 14, r_2 = 7.5.. 29

Fig. 4-2 Tangential electric field distribution: (a) CSRR; (b) EG-SRR; (c) Circular-SRR.......... 32

Fig. 4-3 HFSS model of the sensors from MUT sensing analysis: (a) CSRR; (b) Ext-GSRR; (c) Circular-SRR 33

Fig. 4-4 Frequency shift (a-c) and sensitivity comparison (d) of sensors with respect to relative permittivity that varies from 1 to 30 34

Fig. 4-5 Normalizing the sensitivity of sensors to volume under the test (V_{CSRR} = 353µL, $V_{EG\text{-}SRR}$ = 182 µL, $V_{Circular\text{-}SRR}$ = 135 µL; V = cross section area of tube x resonator's gap) 36

Fig. 4-6 Embedding MUT into the substrate and cross section of the structure (a-b) and sensitivity comparison of Circular-SRR when MUT is on top and embedded inside the substrate (Carved-SRR) (c) 38

Fig. 4-7 Equivalent circuit model for Circular-SRR (a), S21 profile in HFSS and ADS (b) 38

Fig. 4-8 Effective permittivity and loss tangent of the water-methanol mixture at two operating frequencies shown in (a) and (b) respectively 41

Fig. 4-9 Fabricated structure of sensors: (a) CSRR; (b) EG-SRR; (c) Carved-SRR 42

Fig. 4-10 Experiment set-up for methanol concentration sensing 43

Fig. 4-11 Limit of detection for: (a) CSRR; (b) EG-SRR; (c) Carved-SRR 44

Fig. 4-12 Measured normalized frequency variations in three sensors due to different methanol concentrations 45

Fig. 4-13 (a) 3D schematic of the design (mm), and fabricated model of sensing structure for microfluidic measurements: w = 1, s = 0.5, d = 2, g = 0.5, L_1 = 18, L_2 = 10.5 (b) top view of the sensor (c) fabricated sensor's top view 47

Fig. 4-14 Transmission profile for concentrations (%) of 0 (only water), 10, 20, 30, 40, 50, 100 (only methanol), and bare sensor 48

Fig. 5-1 Block diagram of power connections (a) and RF modules in the system (b) 52

Fig. 5-2 Digital configuration of microcontroller and its peripherals (dashed lines are external connections) 53

Fig. 5-3 Low noise power board supplying digital and analog circuits 54

Fig. 5-4 VCO frequency response generating a tone at 1.219GHz and unwanted harmonics 56

Fig. 5-5 Visual features and building blocks of the GUI for the proposed network analyzer 63

Fig. 5-6 Original experiment setup with power splitter, spectrum analyzer, and the syringe to inject glucose solutions for sensing measurements 68

Fig. 5-7 Initial glucose sensing measurements with no enhancive components and calibration.. 70

Fig. 5-8 Effect of LPF and Attenuator on the system in 4 possible scenarios 71

Fig. 5-9 Calibration setup using a female-to-female connector as thru 73

Fig. 5-10 Transmission profile of three resonators ($SRRa, SRRb, SRR(c)$) measured with the system and VNA 76

Fig. 5-11 Improved setup that includes the power board, attenuator and the low pass filter 77

Fig. 5-12 Glucose sensing measurements using the enhanced system as compared to the VNA 78

List of Abbreviations

MUT	Material Under Test
SRR	Split Ring Resonator
RF	Radio Frequency
CMOS	Complementary Metal-Oxide Semiconductor
CSRR	Complementary Split Ring Resonator
PTFE	Polytetrafluoroethylene
VNA	Vector Network Analyzer
HFSS	High Frequency Structural Simulator
VCO	Voltage Control Oscillator
PD	Power Detector
TL	Transmission Line
ADS	Advanced Design System
DUT	Device Under Test
GUI	Graphical User Interface
PCB	Printed Circuit Board
DI Water	Deionized Water
WC	Water Cut
DSRR	Double Split Ring Resonator
COD	Chemical Oxygen Demand
I/O	Input/Output
DMFC	Direct Methanol Fuel Cells
MCU	Microcontroller Unit
LPF	Low Pass Filter

1 Introduction

1.1 Motivation

Despite the variety in microwave resonators and their applications in industry, sensitivity enhancement is a challenge that yet to be solved by scientists and engineers. This work proposes a simple approach to increase the sensitivity of a conventional SRR for material characterization purposes. A slight geometric modification in SRR structure allows for better sensitivity in measuring vital biomedical compounds such as glucose. According to lab measurements, this small variation in the shape of the SRR leads to a uniform enhancement of 20% in frequency sensitivity which is translated in 6.17MHz.

To further investigate the ways to improve the performance of such sensors, three microwave resonance-based sensors are compared, complementary split ring resonator (CSRR), the proposed geometrically modified SRR, and conventional circular SRR. Then using the most sensitive out of three, the placement of MUT on top or embedded inside the sensor is investigated for further performance enhancement. It is concluded that embedding the sample material inside the substrate of the device improve the sensitivity by 45%. In this study methanol was used as the substance of interest. In brewing and distillery industry, it is crucial to monitor and control the concentration of methanol to produce a high quality alcoholic beverage. Hence, this work focuses on liquid characterization using high sensitive microwave sensors integrated with microfluidic channels for small volume sample materials.

One popular measuring equipment in the field of RF and microwave engineering is Vector Network Analyzer (VNA). VNAs are used at various stages of developing a product or a system; Engineers use VNA repeatedly to verify the performance of their designed components such as filters, antennas, resonators, couplers, etc. This powerful tool is not only used by engineers, but also, by manufacturers. In the production line VNAs are used to ensure all the products meet the design specifications. They are also used for troubleshooting RF and microwave systems.

Although VNAs are in high demand both in academia and industry, their disadvantages are primarily the bulkiness and expensive cost. To solve this issue, this work proposes to design and develop a cost-effective, compact and efficient alternative system that is capable of measuring the frequency response of a device under test (DUT) in real-time and providing features such as plotting S21, calculating the quality factor (Q-factor), and indicating the resonance frequency and amplitude. This systems comes with a user-friendly GUI (Graphical User Interface) and a built-in calibration. This is a novel study that steps into revolutionizing VNA industry. This work promises and delivers a miniature system on a PCB that performs as well as a conventional massive VNA which costs a few thousand dollars. These projects will be discussed in full details in the next chapters of this thesis.

1.2 Objective

The main focus of this thesis is to investigate high RF devices, namely microwave resonance based sensors and their sensitivity. Based on proposed methods above and the importance of sensitivity enhancement of such devices for liquid sensing applications, this thesis aims to use simple but effective approaches to improve the performance of these sensors. The modified sensors then are tested in experimental procedure to verify the sensitivity enhancement. This work is expected to show how simple geometric modification as well as placement of MUT can impose better functionality and introduce a wider range of application for microwave planar resonators.

In addition, this work focuses on design and implementation of a RF readout circuitry which is capable of plotting the frequency response of a microwave resonator as DUT. A user friendly GUI is designed for such system so user can enter the operating frequency range and number of points to sample. This system is an alternative to bulky expensive VNA and is expecting to replace the conventional readout instrument by showing promising and comparable results, small and compact size, and cheap cost of preparation. This system anticipate to be used in the test fields where RF and microwave devices are utilized for various sensing applications, and there is a demand for such readout system that is mobile and easy to use.

The main goal and objective of this work is to study the potential of enhancing the sensitivity of simple and conventional SRRs and use them in small sample volume liquid sensing applications such as microfluidics. In addition, this work promises a novel, state-of-the-art, and convenient alternative network analyzer readout system for RF and microwave devices. To achieve these goals, first, planar microstrip microwave resonators are studied and compared in terms of functionality and performance in liquid sensing applications such as glucose and methanol concentration measurements. Later, the most sensitive device is then integrated with a microfluidic channel in a non-conventional fashion of embedding the MUT inside the substrate. This method shows promises of integrating the humble microwave resonators with sophisticated structures as microfluidic channels for various applications.

Furthermore, the RF readout system is composed of RF modules such Voltage Control Oscillator (VCO) and Power Detector (PD) as well as a microcontroller (MC) as the brain of the system. The promise of a compact and cheap alternative VNA is fulfilled by using these trivial yet effective components. To further illustrate the capabilities of such system, the sensing measurements are performed using the proposed system.

1.3 Thesis Outline

This thesis is composed of six chapters.

- An introduction to the motivation objective of this study is mentioned in Chapter 1.
- Chapter 2 will be an introduction and a literature review of existing microwave resonators for liquid sensing applications their advantages and disadvantages, followed by a brief literature review of RF systems for reading and monitoring RF devices.
- Chapter 3 describes the design, fabrication, and measurement procedure of a highly sensitive SRR tested for glucose sensing applications.
- Chapter 4 is a comprehensive comparison between three types of planar microwave resonators in terms of their sensitivity. In this chapter the most sensitive resonator is selected to be further examined in terms of MUT placement and integration with microfluidic channel for small volume liquid sensing application, namely methanol concentrations in water.
- Chapter 5 introduces a new RF system as a readout circuitry for RF devices and microwave resonators. This chapter describes the building blocks of such systems, and explain each component's functionality in depth. The design, implementation, debug and troubleshoot process of this circuitry is explained as well as the measurements and results. The sensor used in Chapter 3 is tested under the new proposed readout system and the resulting frequency response verifies the validity of this system.
- At last, Chapter 6 summarizes the conclusions of this thesis and outlines the possibilities of future research in this field.

2 Literature Review

2.1 Sensors Overview

Sensors are vastly used in our daily lives; from the personal cell-phone mobile, to cutting-edge nano electronics technology. The modern techniques used in today's sensing applications are raising interest for many researches around the world. Manufacturers are competing to provide the most novel, innovative, efficient and sophisticated sensors to industries. Several types of sensors that are used in industry are strain gauges, accelerometers, ultrasonic sensors, passive acoustic sensors, etc. These sensors are expensive, difficult to mount on large targets for structural health monitoring (SHM) applications, easily damaged in harsh environments, and cannot continue to operate for long time intervals [1].

Other current methods used in various sensing applications are optical and THz sensors. The disadvantages of optical sensors are low reproducibility, high insertion losses, and complex fabrication process which can compromise the resolution of such sensors for high-accuracy applications [2]. On the other hand, THz sensors used in substance detection especially explosive materials, show many limitations in this application. For instance, some of the explosives have similar absorption frequencies as some ordinary substances and that makes these sensors effective enough as they show large number of falls positive. High atmospheric humidity during measurements, opaque packaging, and inhomogeneity of the substance surface also lead to low efficiency [3]. To compensate for the existing challenges, a fast-growing research in microwave sensors is under study worldwide.

Microwave resonance-based sensors have been chosen over the prevailing sensors due to their planar structure which allow for simple fabrication process, low manufacturing cost, CMOS compatibility, and flexible configuration. In addition to their compact structure, the presence of electromagnetic field lines in the sensor's proximity leads to non-contact sensing applications for situations where maintenance of testing materials is crucial and also where the material under test is toxic or contaminating and can cause damage to the sensor [4], [5], [6]. Therefore, microwave sensors are a great candidate for non-contact sensing applications to monitor the variation of the dielectric properties of material under test, especially in harsh environmental conditions [7]. On the other hand, microwave sensors are able to translate the changes in the MUT and the environment of study into measuring quantities in a very short amount of time, almost instantly. Hence, these sensors can be used for spectral and real-time measurements [8].

In addition, Microwave sensors have higher operational range of frequencies as opposed to low frequency sensing systems. This immunes microwave sensors from noise interference with the high frequency system. In addition, at high frequencies microwave resonators are favorable over low frequency sensing methods as they can measure the capacitance of the resonating element as a sensitivity measure whereas evaluating the capacitance at higher frequencies using conventional methods is not possible [9], [8], [10]. The basic operations, applications and the physics of such microwave resonators are discussed in the next section.

2.2 Microwave Resonators Overview

A resonator is a structure that at a particular frequency, it will have oscillations with the maximum amplitude. Due to this feature, microwave resonators can be used as filters, oscillators, frequency meters, tunable amplifiers, and microwave sensors [9]. Microwave sensors divide into two categories, planar structures and microwave cavities such as waveguides. The former exhibits more advantages compared to microwave cavities which are not the focused of this work. Planar microwave sensors are compact in size and due to their flexible structure, they can be mounted in various objects such as pipelines in oil and gas industry, or human body to monitor vital bodily fluidics such as glucose for biomedical applications.

2.2.1 Planar Microwave Resonators vs Microwave Cavities

Despite the high-quality factor that waveguides provide, the bulky and large size of this resonators eliminate them for various sensing applications that are size-sensitive. Substrate integrated waveguides (SIWs) are in great interest as they not only provide a high-quality factor as conventional waveguides, but also, they maintain a planar structure. The drawback of SIWs is the cost and complex fabrication process. Among different types of resonant sensors, planar resonators are most common due to their low profile, CMOS integrability, robust and compact design, low-cost fabrication, and flexible to be printed on non-uniform surfaces [9], [8], [10].

2.2.2 Basic Operation of a Conventional Open Loop Microwave Resonator

In order to understand the sensing principle of microwave resonance-based sensors, a half-a-wavelength conventional split ring resonator (SRR) is studied in terms of its equivalent circuit model, resonance frequency, and the existing coupling that enables the sensing applications.

Planar microwave resonators consist of a resonating element that is edge coupled to a microstrip transmission line (TL). In this configuration, small variations in the environment

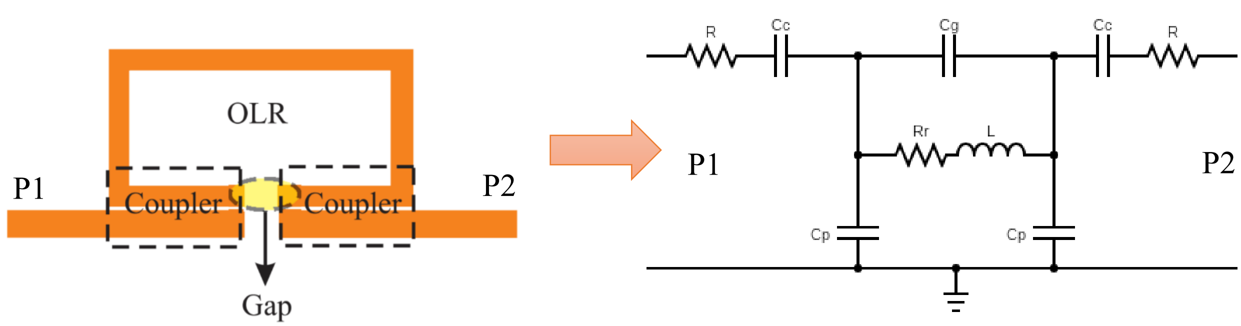

Fig. 2-1 A conventional split ring resonator (SRR) [5] and its lumped-element equivalent circuit model

reflects on the resonance properties of the resonating element, and it is shown as a shift in resonance frequency defined according to (2-1).

$$f_{resonator} = \frac{1}{2\pi\sqrt{LC}} \quad (2\text{-}1)$$

Fig. 2-1 shows the lumped-element equivalent circuit model of the SRR, where Cc indicates the coupling capacitance by the ring and TL, Cg is the capacitance created by the gap of the ring, and Cp indicates the capacitance between the ground plane and microstrip line and the dielectric region of substrate in the middle, and the resistors indicate the resistive properties of the sensor [5], [11]. The sensitivity due to frequency shift is limited by the coupling between the resonator and the adjacent TL. This coupling is shown in **Error! Reference source not found.** and it is odeled as a capacitance called Cc [10], [5]. This equivalent coupling capacitance Cc along with the capacitance due to the gap of the resonating ring (Cg) creates an effective capacitance that has a significant effect on the resonance frequency of the coupled system. The effective capacitance is substantially impacted by sample material's permittivity. Hence when the permittivity of material under test is changing the resultant capacitance seen by the resonator is changed, which results in a shift in frequency. It is also worth mentioning that, once the capacitance is changed, the loading of the circuit is different and this also results in a shift in amplitude of the transmission profile of the microwave circuit.

2.3 Applications of Microwave Resonators

Microwave spectroscopy is used in sensing applications, this state-of-the-art measurement technique has its own drawbacks. The Vector Network Analyzer (VNA) used for this method is very expensive and not viable for most application. In addition, the open-ended dielectric prob used for such measurements must be in-contact with material under test (MUT) which disqualifies this method for non-contact, and real-time sensing [12]. As oppose to spectroscopy, the resonant-based sensing nature of microwave sensors makes them a great candidate for non-contact measurements

Microwave resonators have been used in a wide range of applications for sensing purposes, such as material characterization [13]–[15], [4], liquid [7], [16]–[18], and gas detection [2], [8], [9], [10] biomedical application [3], [9], [19]–[22], pipeline and coated metal sensing [12], [23], [24] etc. Microwave sensors have various features that are significant for sensing applications including non-contact measurements and material characterization. Fig. 2-2 shows a few example of planar microwave resonators [5], [25]–[27].

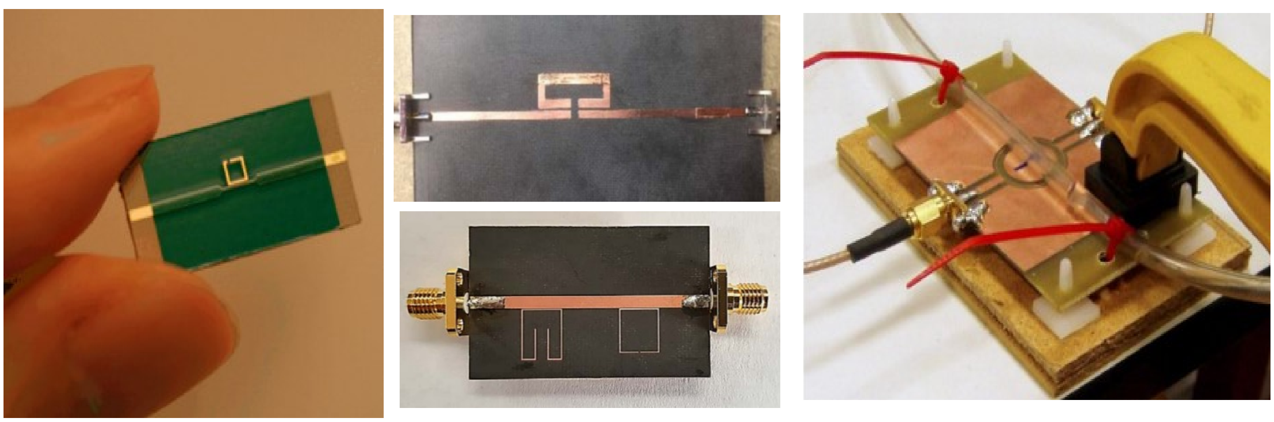

Fig. 2-2(a) Asymmetric SRR [22], (b) conventional SRR [23], (c) DSRR [24], (d) co-planar sensor [25]

2.3.1 Material Characterization

The most significant feature of microwave planar sensors that separates them from other devices is their contactless working operation. This feature allows planar microwave sensors to detect highly toxic and dangerous chemicals with no contact and also can cope with situations where no direct access between MUT and sensor is available such as blood in body [1]–[3], [8], [9], [7], [10], [13], [16], [17], [19]–[21], [15], [19]. The working principle of most microwave sensors is based on the variations in frequency response due to change in materials' complex permittivity. Hence, the selectivity makes it possible for microwave sensors to distinguish between many materials and/or chemicals that are present in the ambience under test. This leads to multi-material sensing studies such as human bodily fluids, and concentration monitoring of certain compounds in food and drinks [3], [9], [19]–[22].

Therefore, multi-material sensing is significant for healthcare and biomedical applications as well as food and beverage industries. The other feature that makes these sensors convenient is integrated sensing. For many biological applications, it is required to characterize and determine the content/ingredients of certain liquids/mixtures. To acquire accurate measurements, radio frequency (RF) interactions with microfluidic systems have been encountered, and that leads to integrated sensing using planar microwave resonators [13], [28]–[34].

2.3.2 Liquid Sensing in Oil and Gas Industry

In many industrial processes, it is vital to detect the concentrations of constituent liquids. A microwave-based sensor to detect solution type and its concentration has been the research topic of many scientists and engineers. One of these studies is done by *Korostynska et. al.* in [35]. Their proposed sensor is primarily used to measure NO_3 concentrations and chemical oxygen demand (COD) as a quality measure of the treated wastewater. This work proves the microwave resonator's ability to distinguish between different solutions (NO_3) at different concentration levels. This type of device has the advantages of non-destructive, real-time response, non-ionizing radiation, and no additional chemical was required during the measurements.

Zarifi et al. introduces a liquid-liquid interface detection sensor based on microwave split ring resonator for oil and sand industry [36]. In this study, planar resonators are chosen over the other techniques due to their easy implementation, ability to perform in non-contact fashion, and moderate sensitivity to changes of the ambient environment. It is observed that as the sensor moves along the immiscible sample of two liquids, results in resonance and Q-factor variations. These variations are due to the change in permittivity of different liquids and their loss factor. Furthermore, the great advantage is that the microwave resonant sensor is also responsive even with the existence of a lossy medium, e.g. water.

Karimi et al. experiment a water cut (WC) sensing method using an open shunt stub (T-resonator), which provides open circuit transmission and is usable for various pipe sizes [16]. The advantages of this design are low cost fabrication and obtaining minimum repeatability. However, WC sensors are not the most effective methods for real time monitoring of water content during oil production.

2.3.3 Liquid Sensing for Biomedical Applications

In addition to oil and gas industry, microwave resonant sensors have been studied by many researchers in chemical, biology and medical applications. For instance, ethanol is used in various fields such as the pharmaceutical, medical diagnosis, academic, and beverage industries to name a few. Therefore, ethanol concentration sensing is one of the subjects that researchers have investigated. *Salim et al.* propose a sensor using two concentric CSRR [37]. The sensitivity of this design is tested for various concentrations of ethanol in deionized (DI) water. The results suggest that microwave resonator is low-cost, reliable, reusable, and effective for low concentration measurements.

Despite the easy and low-cost fabrication of microwave resonators for biomedical applications, low sensitivity is a challenge for biosensors. In addition to the planar structure of resonant based sensors, co-planar type structures are other version of microwave sensing devices with major impacts on biomedical applications. For instance, to investigate the fluid properties in biomedical applications, a co-planar microwave resonator has been put to test by *Mason et al. in* [27]. Fig. 2-3 shows the schematic of the proposed co-planar resonator in this work. This method

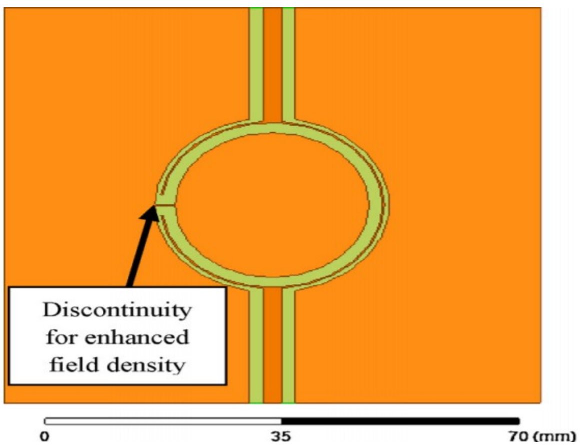

Fig. 2-3 Schematic design of co-planar microwave resonator [27]

is done in a non-contact interaction of non-thermal intensity microwave signals with the sample solution. This paper demonstrates the sensitivity of the sensor to glucose dilutions. To study this structure, various concentrations of glucose are tested using this sensor.

Measuring size, volume and dielectric property of liquids are significant in medical and chemical applications [29]. In this paper, a modified split ring resonator (double split-ring resonator, DSRR) as shown in Fig. 2-4 is used. This work investigates the effect of gap size in DSRR sensing behavior. To extract the segment length and speed, the relation between sensor response and time is studied. Knowing the length of the liquid and radius of the tube, one can easily calculate the volume of the liquid segment. Permittivity can also be calculated using the shift in resonant frequency and changes in bandwidth. This technique is suggested to be adaptable for medical, biological, and chemical real-time and lab-on-chip applications.

Diabetes is one of the most common chronic diseases in the world that could lead to death

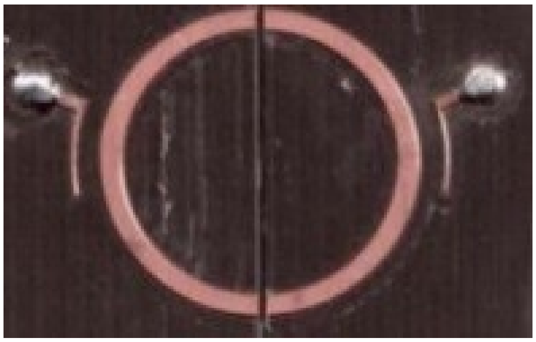

Fig. 2-4 Schematic design of DSRR used in [29]

or blindness, heart failure, kidney failure and physical disability [38], [39]. This metabolic disease happens when blood glucose level is outside of the normal range (0.89 mg/mL to levels exceeding 3.5 mg/mL) [37]. Patients with diabetes need to monitor their blood glucose on a daily basis, and in some cases they need to take medications in order to control their glucose level [40]–[42]. Hence, early diagnosis and blood glucose monitoring is crucial for patients and healthcare providers to effectively tackle this disease [38], [43].

This requires a major need for an accurate, highly sensitive, and stable method for glucose sensing in clinical monitoring [44]. The most common glucose monitoring method that is widely used at home consists of a monitoring system that requires a drop of blood for glucose concentration evaluation. This process has to be repeated several times during a day, which is time consuming and uncomfortable for patients. In order to alleviate the diagnosis process, there has been a growing interest in designing a device that is capable of non-invasive and continuous measurement conditions [42].

For one, open-ended coaxial probes are used to measure the complex permittivity of biological analytes and liquids, while large size, high cost, and low penetration depth are among their drawbacks [40]. In addition, commercialized glucose biosensing techniques based on electrochemical, optical, piezoelectric, thermal, or mechanical principles are invasive, thus not suitable for in situ measurement conditions [39], [44].

On the other hand, microwave planar sensors that exploit various types of sensing elements have attracted the attention of many researchers due to their compact size, accurate, non-invasive, label-free, and real time measurements of biological or chemical MUT, e.g. here glucose [43]. The resonant-based sensors employ a resonator with hotspot that is sensitive to dielectric property of its environment and is specialized for dielectric MUT sensing in non-contact fashion [45].

2.3.4 Liquid Sensing for Structural Health Monitoring

Electromagnetic waves lose energy as they propagate through a lossy medium, due to low conduction. Hence, sensing in a lossy medium has always been a challenge in the field of microwave sensors. Engineers have further investigated the effect of microwave resonators in lossy media such as fluid carrying water. Water penetration in an infrastructural insulating coating is a rising concern in the industry, as it will eventually lead to corrosion. Hence, it is of a great importance to develop a method to monitor water diffusion in coatings. In one study done by *Khalifeh et al.* [37], an open microstrip resonator is designed to monitor water diffusion in organic coatings. In another research, real-time measurements using microwave microfluidic sensor are studied to monitor size, speed, and dielectric property of liquid segments.

2.4 RF Readout Circuitry

In general RF readout systems are the most important equipment to measure RF and microwave devices in both academic labs and industrial manufacturing companies. This equipment is capable of providing the performance and functionality of RF networks. By sending a high frequency excitation to the device under test, the RF readout system is able to monitor and measure the response. This helps researchers and designers to verify the operation of the designed network and compare with the simulated version [46]. The wide range of operational frequency of such devices make them ideal candidate for RF and microwave devices in various applications. This emphasizes on the high demand and popularity of RF readout systems.

There are many types of RF readout systems, each designed to measure a specific parameter or a feature of device under test. The three types of RF readout systems are: Scalar Network Analyzer (SNA), Vector Network Analyzer (VNA), and Large Signal Network Analyzer (LSNA) [46]. SNA is the simplest type of RF network analyzers that is designed specifically to measure the scalar properties of the network, such as the amplitude properties of the device under test. Whereas, LSNA is the most sophisticated instrument among the RF analyzers. This instrument is able to measure various properties of DUT under large signal condition. For instance, LSNA provides full analysis despite the harmonics and non-linearity of a network. However, VNA is the most useful and popular among researchers and engineers.

2.4.1 Working Mechanism of VNA

Among many features of the VNA, measuring transmission and reflection responses when DUT is excited are the most sought-after features. Monitoring reflected and transmitted waves over the operating frequency range provides insightful information about the characteristics of DUT. The VNA uses a source to generate an excitation, and a set of receivers to capture the changes to the excitation signal caused by DUT.

The excitation signal, or technically known as incident wave, enters the DUT, and the VNA measures the reflected wave from the input side, as well as the wave that goes through the DUT, known as transmitted wave. VNA calculates the resultant wave and compares it to the incident wave. This is how the characteristic of DUT is determined by a VNA [47]. Fig. 2-5 illustrates a simple schematic of working mechanism of a VNA, with incident, reflected, and transmitted waves [46]. Although the VNA provides both phase and amplitude information, this chapter focuses mainly on amplitude measurement with respect to frequency variations, i.e. transmission profile.

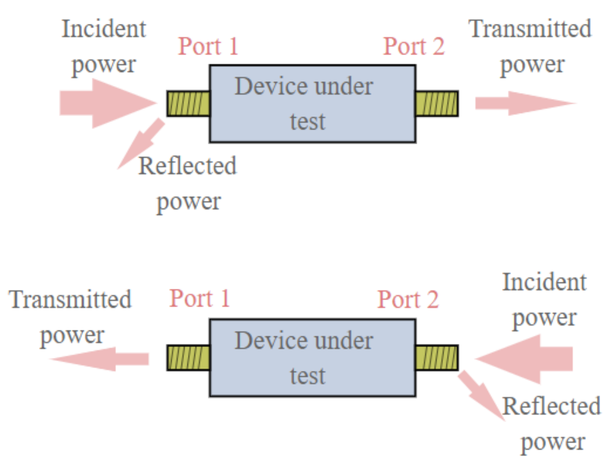

Fig. 2-5 Basic concept of a vector network analyzer [46]

2.4.2 S-Parameters

Measuring the voltages and currents at the microwave frequencies is problematic as direct measurements involve magnitude and phase of the high frequency wave in a certain direction. To resolve this, a representation that is more compatible with direct measurement, the concept of incident, reflected and transmitted waves is defined, scattering matrix [48].

Scattering matrix provide insightful description of the microwave network as seen through its ports. This matrix relates the voltage wave incident on the ports to the reflected waves from the ports. These scattering parameters (S-parameters) of a microwave network can be directly measured using a VNA. Since, in this thesis all the microwave resonators have one input and one output, the scattering matrix calculations are written for a 2-port network. (2-2) shows the scattering matrix for a 2-port network and its relation with incident and reflected voltage waves. In this equation V_i^- indicates the amplitude of the voltage wave reflected from port i, and V_i^+ is the amplitude of the voltage wave incident on port i [48]. Hence $[S]$ is referred to as scattering matrix which contains the S-parameters.

$$\begin{bmatrix} V_1^- \\ V_2^- \end{bmatrix} = \begin{bmatrix} S_{11} & S_{12} \\ S_{21} & S_{22} \end{bmatrix} \begin{bmatrix} V_1^+ \\ V_2^+ \end{bmatrix} \qquad (2\text{-}2)$$

In practice, it is not common to calculate the whole matrix when measuring a microwave network; but calculating some individual scattering entities gives important information on the characteristics of the network. A specific S-parameter is determined as

$$S_{ij} = \frac{V_i^-}{V_j^+}\Big|_{V_k^+ for\ k \neq j} \qquad (2\text{-}3)$$

(2-2) indicates that S_{ij} is determined by calculating the ratio of voltage wave reflected from port i and voltage wave incident on port j. This is done when port j is excited by an incident wave of V_j^+ and the incident waves on all other ports except j are set to zero, which translates in terminating all other ports by a matched load to eliminate the effect of reflection from unwanted ports [48]. In this analogy, S_{ii} represents the reflection coefficient seeing through port i, and S_{ij} is transmission coefficient from port j to port i.

Therefore in the case of a 2-port network, S_{11} and S_{21} are reflection coefficient of input and transmission coefficient from input to output, respectively. The main focus of this thesis is determining only the amplitude of S_{21} of the designed microwave resonator; because investigating the transmission coefficient of the DUT provides insight to how this resonator transmits the wave through output when input is excited. Hence S_{21}determines the characteristics of the microwave network under test. Chapter 5 explains in detail how amplitude of $S_{21}$is calculated in this thesis.

Due to rising need in a portable, accurate and inexpensive network analyzers, authors of [49] proposed a novel VNA design that is made of a standing-wave probing device and a tunable phase shifter. This design uses one power detector (PD) as oppose to conventional VNAs that operate based on multiple power measurements. The proposed system is designed for an X-band (8.2-12.4 GHz). Despite being cost effective, this design has struggled to solve the issue with size.

In this thesis, a portable, accurate, compact and small RF readout circuitry is proposed which can measure the transmission profile of a resonator-based microwave sensor as well as material characterization sensing measurements. This novel and simple design is made of readily-available off-the-shelf components, such VCO, PD, microcontroller (MC) board, and a power board. This is a narrow band RF sensor readout circuitry whose result is compared with a high end Cobalt VNA from Copper Mountain. The details of this design is fully discussed in Chapter 5.

3 Sensitivity Enhancement Using Gap Extension

In this study, a simple SRR and a modified SRR with extended gap, as metamaterial inclusions, are found to be sensitive to surrounding media's dielectric property. Simulations of three different orientations with respect to the I/O transmission lines are discussed to investigate the most effective design. Thereafter, the optimum sensor is designed in HFSS and fabricated. Solutions with different glucose concentrations are prepared to investigate the frequency response of the sensor in dealing with the external material.

Sensitivity enhancement of microwave resonance-based sensors has always been a challenge for researchers and engineers. These sensors are vastly used in various fields of applications; therefore, it is crucial for microwave sensors to provide high accuracy and sensitivity, especially in biomedical, food and beverage applications. In these fields, where small liquid samples are under test, the sensitivity of the device plays an important role. This is the main motivation of this study to work on boosting the performance of microwave split ring resonators (SRRs) in liquid sensing applications. Two approaches to increase the sensitivity is proposed in this thesis. The firs one is geometrically modifying the gap of SRR to change the electromagnetic field distribution, and hence the sensitivity of the device. This study is done for glucose sensing applications.

The other approach is embedding the material under test (MUT) into the substrate rather than placing on top of the device. This technique is done for methanol sensing and further investigations have been done for small volume of samples by introducing microfluidic channel in the set-up. The second method is discussed in Chapter 4.

3.1 Simulations

3.1.1 Simulation of SRR

In this section, a simple SRR has been simulated using ANSYS HFSS in three different orientations with regards to I/O microstrip transmission line. Then, the modified SRR with the extended gap is introduced and simulated. In these simulations, frequency and amplitude variations with respect to changes in electrical properties of MUTs, mainly complex permittivity, are studied. Fig. 3-1 shows the three placements of the SRR on a Rogers 5880 substrate with permittivity of $\varepsilon_r = 2.2$ and dielectric loss tangent of $\tan\delta = 0.0009$, whose thickness measures 0.8 mm. The dimensions of the SRR are 20mm in long side, 15mm in short side, 2.4mm in microstrip width, and 0.5mm in spacing between transmission line and ring resonator, which leads to a resonance frequency of 1.863 GHz.

All the simulations in this study are done for a sample material with size of 2mm x 4mm x

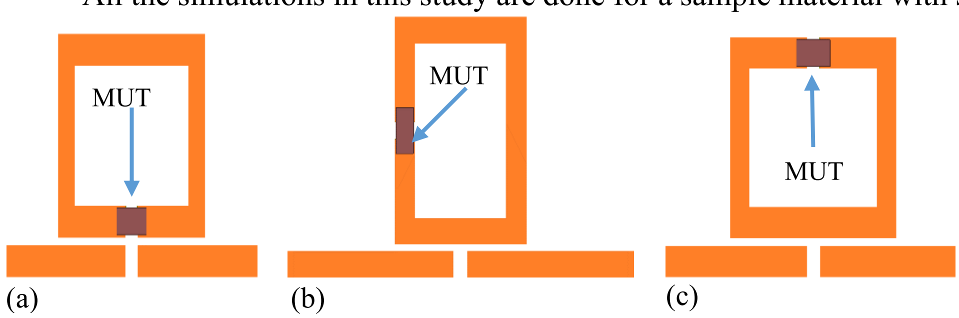

Fig. 3-1 (a-c) Case1, Case 2, Case 3, three different SRR orientations (gap = 1.5mm)

2mm and its permittivity value varying from 5 to 30 in step size of 5, this also includes air as the base line. Also the gap size for this design is 1.5mm. Fig. 3-3 illustrates the frequency and amplitude variations in regards to different permittivity values, where f_0 and A_0 present resonant frequency and amplitude, respectively.

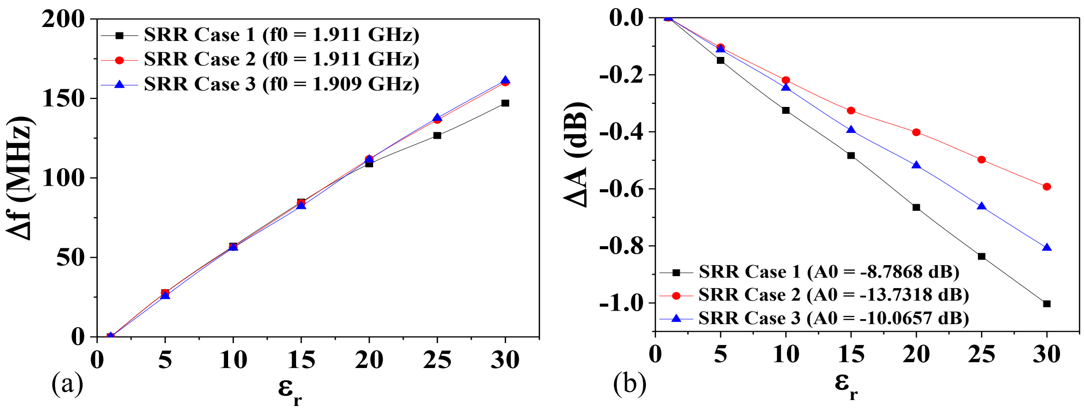

Fig. 3-3 Frequency (a) and amplitude (b) variations in SRR structure due to *different permittivity values*

According to the simulation, Case 1 is the most responsive in terms of amplitude variations, while the frequency profile of this structure does not show significant variations. In pursuit of a design for higher sensitivity we have engineered the configuration of the gap to interfere more with the MUT. Hence, SRR with extended gap is introduced.

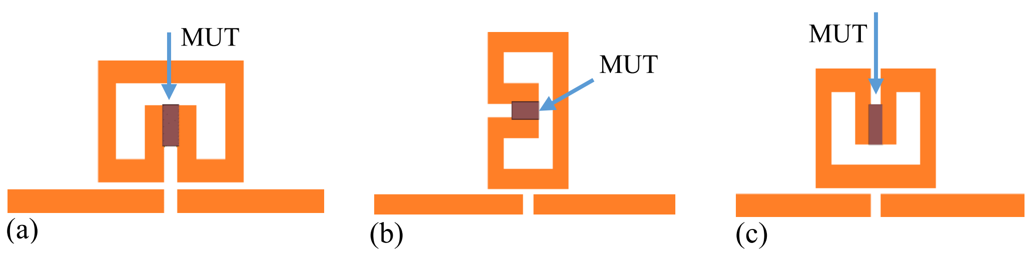

Fig. 3-2 (a-c) Case 1, Case 2, Case 3, Three models for extended gap SRR in different orientations (gap = 1.5mm)

3.1.2 Simulation of the Extended Gap SRR

The modified SRR with three different rotations is shown in Fig. 3-2. This structure is preferable over simple SRR because the gap extension provides more interaction between the MUT and microwave resonant power, whose perturbation would change the resonant frequency, hence results in better sensitivity in the structure. Fig. 3-4 illustrates linear relationship between permittivity values and frequency response in terms of resonant frequency and amplitude of the structure.

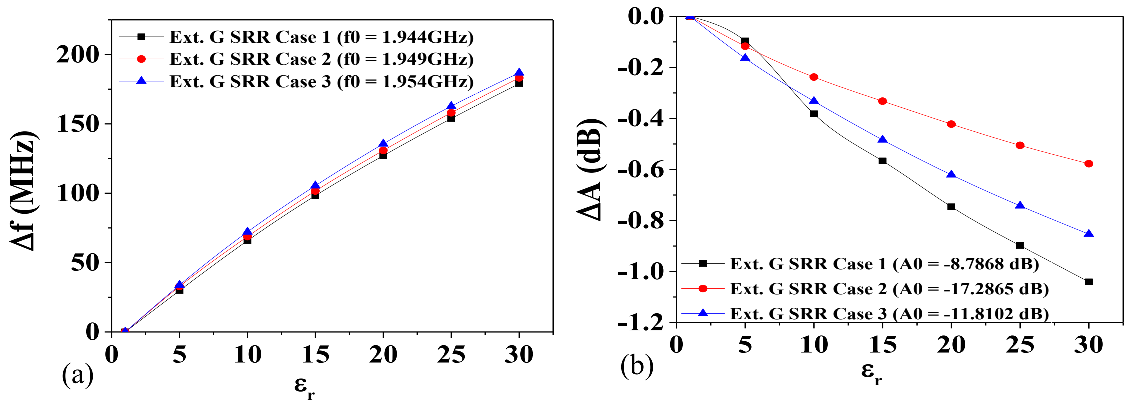

Fig. 3-4 Frequency (a) and amplitude (b) variations in extended gap SRR structure due to different permittivity values

In comparison between the conventional and the proposed sensors, not only the amplitude variation of Case 1 is superior both in the simple and modified SRRs, but also in frequency, a frequency-based sensitivity enhancement of up to 20% is obtained for ${\varepsilon_r}_{MUT} = 30$, where modified SRR is employed and according to Table 3-1, $\frac{\Delta f}{\Delta \varepsilon_r}$ is improved from 5.07 MHz up to 6.17 MHz (which translates into $\sim 0.3\ \%$ sensitivity with respect to initial resonance frequency). **Error! Reference source not found.** again confirms that the amplitude sensitivity is preserved at its original value. This structure is then with different concentrations. The experiment procedure and the results are discussed in details in the next section. The dimension of the inward extension is 5.2mm.

Table 3-1 Frequency and amplitude sensitivity with respect to permittivity variations

	Frequency Sensitivity ($\Delta f/\Delta \varepsilon_r$) MHz		Amplitude Sensitivity ($\Delta A/\Delta \varepsilon_r$) dB	
Δε	Conventional SRR	Gap Ext. SRR	Conventional SRR	Gap Ext. SRR
5	6.93	7.45	-0.037	-0.041
10	6.33	7.31	-0.036	-0.042
15	6.05	7.01	-0.034	-0.040
20	5.72	6.68	-0.035	-0.039
25	5.27	6.40	-0.034	-0.037
30	5.07	6.17	-0.034	-0.035

3.2 Experiments and Measurements

A modified SRR with extended gap proposed in this study is used for measurements (Fig. 3-3 (a)). The gap size is chosen to be 2.5mm in this experiment due to practical size of the tube that is intended to fit within the gap. NI PXIe 5632 VNA is used to collect data regarding frequency and amplitude profile. Glucose solutions are prepared by mixing 30g of glucose with 100mL of deionized water (DI). Two pumps are used in this experiment in order to dilute the prepared glucose sample. The high-concentration glucose solution (30g/dL) with stepwise flow rate of 3.33 mL/hr increments is diluted with 50 mL/hr constant flow rate of DI water. The test is performed for second time to ensure the repeatability. All the liquid solutions are injected through PTFE tubes, with inner diameter (ID) of 1/16” and outer diameter (OD) of 1/8”. Fig. 3-6 illustrates the experiment set-up for glucose sensing using modified SRR.

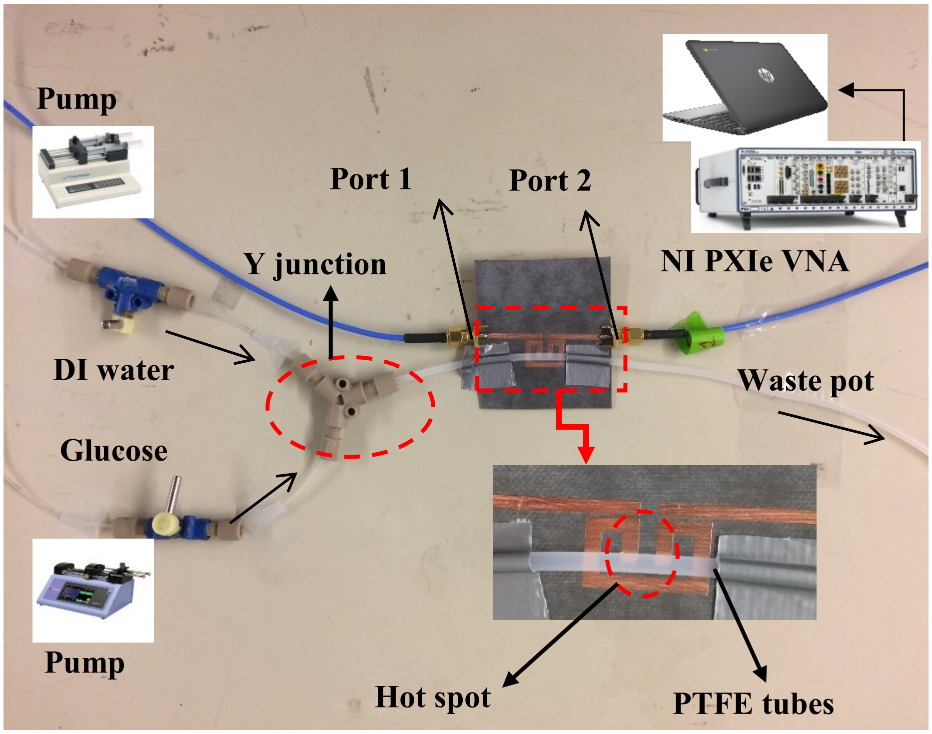

Fig. 3-6 Experiment set-up for glucose sensing using modified SRR

As concentration of glucose increases, the frequency and amplitude response of the proposed sensor vary, accordingly. Frequency and amplitude variations are given in Fig. 3-5 (a) and (b), respectively. Based on these results, it is observed that both profiles exhibit smooth and linear responses.

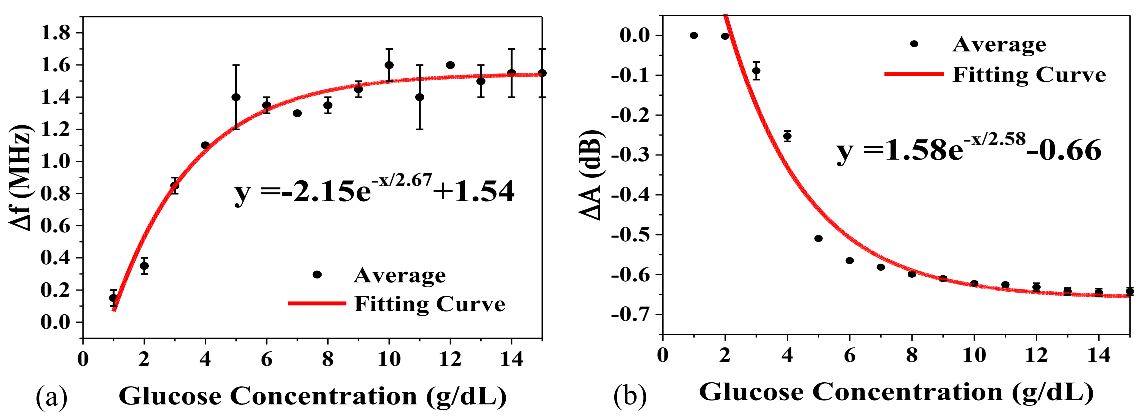

Fig. 3-5 Experimental frequency (a) and amplitude (b) shift of the proposed sensor at various glucose concentrations

In addition, it is shown in the Fig. 3-5 that the proposed structure can detect up to 1.6 MHz shift in frequency and 0.63dB shift in amplitude for concentration variations of 1-15 g/dL. This suggests that the proposed sensor can be used for glucose sensing in low concentrations by monitoring the amplitude profile of the device due to its abrupt changes. However, the amplitude of the sensor reaches saturation at higher concentrations, *i.e.* higher than 10g/dL.

The saturation can be explained by understanding that at higher concentrations, the permittivity of the material is increased. At higher permittivity values, material act as a lossier medium where electromagnetic field propagation attenuates, and therefore the sensitivity of the microwave sensor decreases and reaches saturation. This can be explained by considering the wave velocity in a medium which is defined as [6], [7]:

$$v = \frac{c}{\sqrt{\varepsilon_{eff}}} \qquad (3\text{-}1)$$

where c is the speed of light ($3 \times 10^8 m/s$) and ε_{eff} is the effective permittivity of the wave propagation environment. With the increase of permittivity the wave velocity decrease which translates into slower wave propagation and hence lossy medium. Less electromagnetic wave propagation in microwave sensors results in less sensitivity to variations in sample materials in terms of their permittivity properties. In addition, another way of determining resonance frequency of microwave resonators is as follow [7]:

$$f_r = \frac{c}{2\lambda_g\sqrt{\varepsilon_{eff}}} \qquad (3\text{-}2)$$

where $\lambda_g$represents the guided wavelength. According to this relation, higher permittivity values have less significance on the resonance frequency of the microwave sensors, which results in less responsivity from such structures.

On the other hand, frequency profile behaves in linear fashion as well. Therefore, when sample material experiences high concentrations of glucose, frequency profile is investigated instead of amplitude of the sensor. Also, the provided experimental data could be fitted with exponential expressions as given inside the graphs, which is useful to resolve intermediate solutions.

The advantages of the modified SRR sensor suggested in this work is both low and high glucose concentration detection using amplitude and frequency response, respectively. However the drawback of this design is experiencing noise in frequency profile, hence poor resolution, which is typical characteristic of passive sensors specifically in approaching limit of detection in sensing. Future work revolves around improving the sensor's resolution using an active feedback loop to compensate for any electrical loss and to boost the resolution of the system, where preliminary steps are taken in [23].

3.3 Summary

In this study, microwave split ring resonator is utilized as a passive planar sensor for material characterization. The transmission profile of the two-port sensor is monitored for resonant frequency and amplitude variations. Three planar configurations in couplings with SRR are analyzed in the resonant frequency of 2 GHz. Then, the gap of resonators is modified in geometry with an inward extension to enhance the sensitivity. The same analysis of material characterization is done over the newly developed sensors and 20% enhancement in frequency based sensitivity is achieved for materials with $\varepsilon_r = 30$ with no degradation in amplitude based sensitivity.

The best configuration is selected to be used in sensing for biomedical applications of glucose concentration sensing. Different portions of sensing are resolved using whether amplitude or frequency within wide range of 1-15 g/dL. Considerable sensitivity in frequency is recorded with the passive sensor. Higher resolution in sensing is under exploration for next generations of the proposed sensor in future work.

4 Sensitivity Enhancement by Embedding MUT into Substrate and Integration with Microfluidic Channel

4.1 Introduction

To further extend the sensitivity enhancement investigations, two simple SRRs and a complementary SRR (CSRR) are compared in terms of their sensitivities in this chapter. The most sensitive design is then picked to be examined further in terms of MUT placement. Aside from extending the SRR's gap explained in previous chapter, the other approach to enhance the microwave resonators' sensitivity is embedding the material under test (MUT) into the substrate rather than placing on top of the device. This technique is done for methanol sensing and further investigations have been done for small volume of samples by introducing microfluidic channel in the set-up.

Microwave resonant-based sensing is a recent developing technology that is being investigated by many researchers over the past decade. Microwave resonators are used in numerous industrial, medical, and biomedical sensing applications ranging from material characterization, environmental system monitoring, biomolecule detection, and concentration study [5], [50], [51], [52]–[58]. Among various types of microwave resonators, planar structures have proven to be the ultimate candidate for sensing purposes due to their simple and low-cost fabrication, compact size, non-contact sensing, and CMOS compatibility [29], [45], [51], [59]–[62], [63].

In terms of performance, microwave split-ring resonators (SRRs) have proven to have good sensitivity due to high coupling between the resonator and the transmission line (TL) [50], [8], [59], [64]–[66], [67]. Relatively high quality factor of such resonators makes them suitable for characterizing lossy medium such as liquid and gas [68]–[72], [6]. Material characterization with SRRs have been a topic-of-interest among many researchers. *Mason et. al.* proposed a microwave-resonant sensor to determine the physiological levels of glucose for biomedical applications [27]. Non-contact liquid sensing with microwave resonators was shown in [73], [74].

Integrating active sensing with machine learning algorithms for higher sensing resolution was introduced by *Abdolrazzaghi et. al.* [6]. Humidity and moisture detection in environmental systems using SRRs was investigated by [4]. Organic-vapor sensing and detection of volatile organic compounds using microwave sensors with high selectivity and sensitivity were investigated by [8], [10].

4.2 Outline

Despite all the studies, the battle between sensitivity and simplicity of the sensors continues to challenge the researchers. The objective of this study is to optimize liquid characterization with respect to sensitivity and sample size using microfluidic channel. To do that, sensitivity of three most common microwave resonant-based sensors shown in Fig. 4-1**Error! Reference source not found.**, namely, complimentary split ring resonator (CSRR), SRR with extended gap (EG-SRR), and Circular-SRR, are compared with concentrations of liquid solutions.

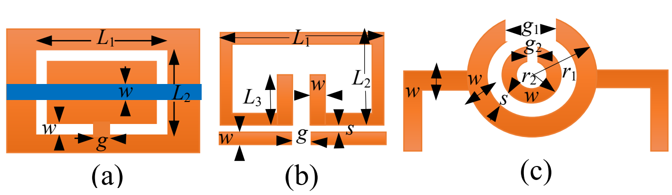

Fig. 4-1 Layouts and dimensions [mm]: (a) CSRR: w = 1, g = 1, L_1 = 35, L_2 = 5; (b) EG-SRR: w = 2.4, g = 1, s = 0.5, L_1 = 18, L_2 = 12, L_3 = 7.6; (c) Circular-SRR: w = 5, s = 1.5, g_1 = 4, g_2 = 1, r_1 = 14, r_2 = 7.5

This study then proposes embedding the sample within the substrate of the sensor, resulting in modified structure (Carved-SRR) that enhances the sensitivity for small-scale measurements. A unique configuration of microfluidic channel inside the sensor is examined that demonstrates the concept of integrating SRRs with materials under test for highly sensitive performance.

It is shown that the proposed technique of de-embedding the liquid in the resonator substrate is preferred choice for microfluidic sensing. In an attempt to exploit the functionality of the sensor, methanol is chosen to be used in concentration study due to its extensive application in numerous applications.

4.3 Applications of Methanol Sensing

Methanol concentration sensing is used in developing direct methanol fuel cells (DMFCs). Concentration of methanol in DMFCs plays an important role, as it affects their electrical performance and efficiency. Higher methanol concentration in DMFCs increases fuel loss and reduces the efficiency [75], [76]. Monitoring methanol and water concentration in DMFCs facilities has a crucial role in design improvement and performance enhancement [77].

Also determining methanol concentration is significant in food and beverage industry. When fermenting alcoholic drinks, methanol is naturally produced, which is toxic for human consumption. Moreover, it is crucial to identify the precise methanol content, as its tolerance limit varies for different types of drinks. Hence, a highly sensitive method is needed during the quality-control process of food and beverages [78], [79].

4.4 Simulation and Analysis

In this study, three planar microwave resonant-based sensors are compared in terms of sensitivity. Because the configuration of the material under test as well as the sample volume is different from one sensor to another, one traditional and two modified SRRs are designed and compared in this paper [26], [80]. Conventional CSRR, SRR with extended gap (EG-SRR), and a circular-SRR are the candidates for this concentration study.

The configuration of these sensors and their dimensions are illustrated in Fig. 4-1. Unlike the case of circular-SRR and EG-SRR, where the microstrip traces are designed on top of 0.8 mm-thick Rogers 5880 substrate, resonating element in CSRR configuration is etched from the ground plane at the bottom of the substrate, while transmission line is printed on top. In transmission profile of these resonators, a notch is expected for CSRR and circular-SRR due to continuous TL, while EG-SRR demonstrates a peak for transmission profile, S21.

In either case, the sensing parameter is frequency (not amplitude), therefore, this apparent difference in sensors' response is ignored when discussing their sensing functionality, which is mainly based on resonance frequency variation. Moreover, 0.8 mm-thick Rogers 5880 is used as the substrate of CSRR and EG-SRR, where in the circular SRR a thicker one (3.18 mm) is employed as it will be discussed more in following sections.

The choice of CSRR slot-width is based on simulation analysis (not given for brevity) to achieve the maximum sensitivity. In addition, rectangular SRR is found to be more sensitive to MUT when its gap is extended. In this situation, higher coupling is produced, and more capacitance undergoes variation. Moreover, since the circular SRR is patterned on thicker substrate, thicker transmission lines are also required for 50-Ohm realization. Considering these notes, the initial resonance frequencies of the sensors are 1.7, 1.9, and 3.6 GHz for CSRR, EG-SRR, and circular SRR, respectively.

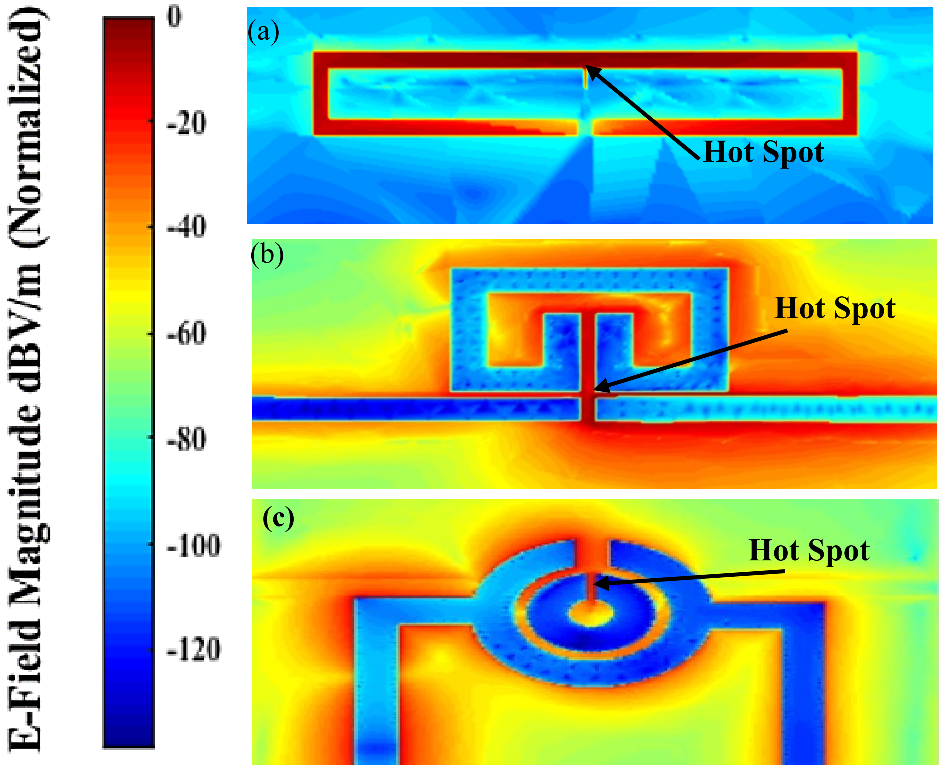

Fig. 4-2 Tangential electric field distribution: (a) CSRR; (b) EG-SRR; (c) Circular-SRR

4.4.1 Electrical Field Distribution

To identify the most sensitive region, the "hot-spot", of the planar sensors, it is crucial to study the electric field distribution near the resonating element. The sensing mechanism is based on interactions of the electromagnetic fields with the MUT whose dielectric loss tangent is 0.01 and permittivity is variable over the range of 1 to 30. It is shown that when an MUT is placed on the resonator's hot-spot, there will be a frequency shift in the transmission profile (S_{21}) of the sensor. This shift is caused by variations in effective dielectric properties of the region close to the hot-spot. The resonator can be modeled as a parallel RLC circuit, whose capacitance (C) is affected by permittivity of MUT and the substrate itself; leading to a change in the resonance frequency of the resonator as formulated below:

$$f_{resonator} = \frac{1}{2\pi\sqrt{L_s C_s}} \tag{4-1}$$

where L_s and C_s are inductance and capacitance of the resonator circuit model, respectively.

Based on simulation results in Fig. 4-2, the areas with the highest intensity of electrical field distribution holds the maximum sensitivity, also known as hot-pot. The blue-colored areas indicates the presence of the metal conductor, and this is as expected since tangential electric field is theoretically zero on a conductive surface. The electric field distribution of these three sensors and their hot-spots are illustrated in Fig. 4-2, which is desired for MUT placement.

4.4.2 Comparison of Sensors with MUT on Top

Based on this information and using ANSYS HFSS software, S_{21} profile and sensitivity of these sensors to permittivity variations for some MUT are investigated. The frequency shift of these sensors is studied for wide range of relative permittivity from 1 (free space) to 30 (lossy medium approximation). Fig. 4-3 shows the HFSS model of the sensor loaded with MUT with square cross section of 3.18 mm x 3.18 mm to model PTFE tube with outer diameter of 3.175 mm which will be used in measurements.

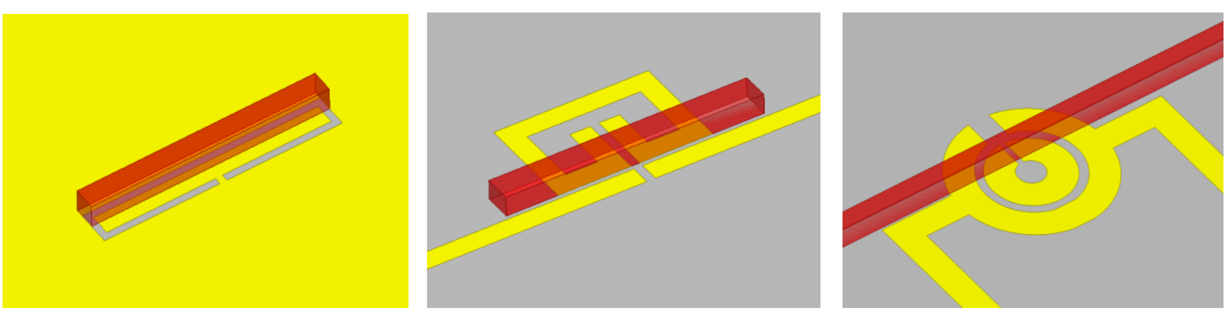

(a) (b) (c)

Fig. 4-3 HFSS model of the sensors from MUT sensing analysis: (a) CSRR; (b) Ext-GSRR; (c) Circular-SRR

A quantity that helps us compare the sensors with each other regardless of their geometrical differences and even frequency of operation is sensitivity that is defined as follows:

$$S = \frac{\Delta f}{f_0} \qquad (4\text{-}2)$$

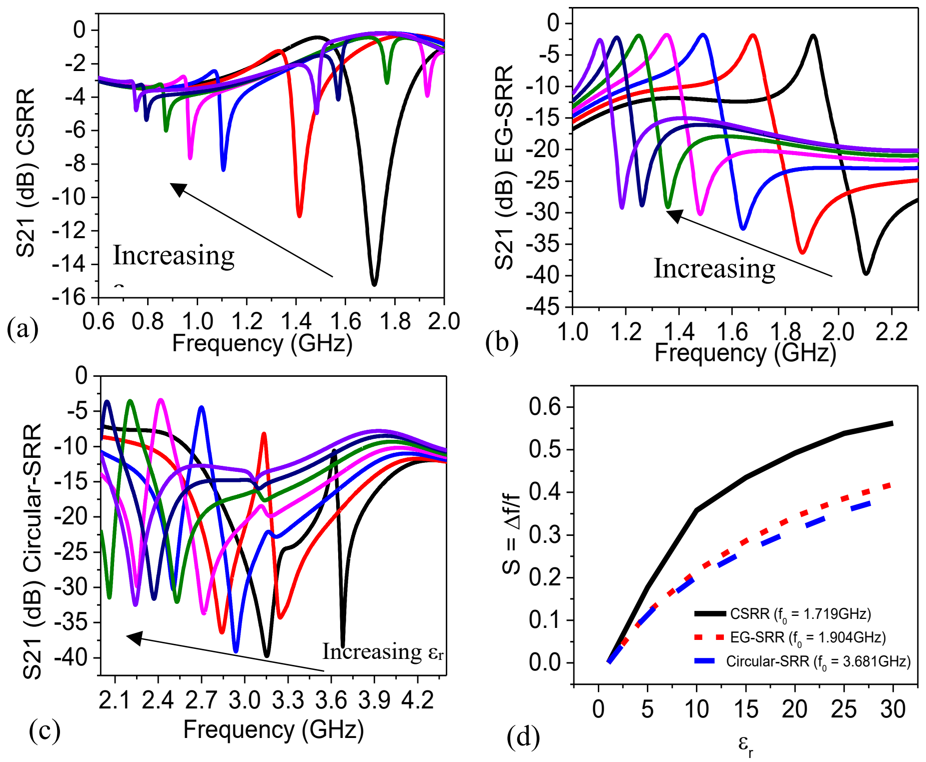

Fig. 4-4 Frequency shift (a-c) and sensitivity comparison (d) of sensors with respect to relative permittivity that varies from 1 to 30

where f_0 indicates the resonance frequency and Δf is the frequency shift of the resonator when facing various permittivities. Although the selected sensors operate at different resonance frequencies, the results shown in this paper are normalized to the corresponding frequency to allow for better and accurate performance comparison. Fig. 4-4 (a-c) shows the frequency shifts in insertion loss in parametric study of these structures for various permittivity values that ranges from 1 to 30. Fig. 4-4 (c) shows two resonances for Circular-SRR, which are due to the presence of two resonating rings in this specific structure. For the purpose of this paper the higher resonance frequency is considered to be the resonance frequency, which for the case of free space ($\varepsilon_r = 1$) is 3.681GHz. It is also to note that the graphs plotted in Fig. 4-4 (d) are normalized to their individual resonance frequencies.

This graph demonstrates the conventional definition of sensitivity, which is usually applied for single sensor; however, in the stated discussion, a comparison between different configurations is put forward. Hence this definition is not comprehensively describing the functionality of the sensor since it conveys no explicit information regarding the volume (V) of sample.

Volume is an important factor in sensing high-tech applications where the sample size is crucial, for example biomedical analytes. In addition, emphasizing on the volume reduces the impact of the size of the resonator. Therefore, normalization to sample volumes need to be taken into account when comparing the sensitivity. This provides useful information on device performance with smaller sample size which is applicable in commercial and pharmaceutical applications. Table 4-1 summarizes the corresponding sensitivity values for each resonator in Fig. 4-4 (d).

Table 4-1 Sensitivity comparison with respect to permittivity

Permittivity	Sensitivity $(S = \frac{\Delta f}{f_0})$		
	CSRR (f0=1.719GHz)	Ext-GSRR (f0=1.904GHz)	Circular-SRR(f0=3.6810GHz)
1	0	0	0
5	0.17743	0.11811	0.11763
10	0.35777	0.21627	0.20158
15	0.43514	0.28714	0.2627
20	0.49215	0.34278	0.31242
25	0.5381	0.38583	0.35615
30	0.56254	0.41942	0.39093

Although Fig. 4-4 (d) and Table 4-1suggest that CSRR provides higher sensitivity, the effect of volume under the test needs to be considered. Therefore, these results are normalized to the volume of the MUT as shown in Fig. 4-5 and Table 4-2 with the definition given below:

$$S_{mod} = \frac{\Delta f}{f_0 V} \quad (4\text{-}3)$$

where S_{mod} represents the modified sensitivity as a function of volume of the material.

Table 4-2 Modified sensitivity comparison with respect to permittivity

Permittivity	Sensitivity ($S_{mod}[\frac{1}{\mu L}]$)		
	CSRR (f0=1.719GHz)	EG-SRR (f0=1.904GHz)	Circular-SRR(f0=3.6810GHz)
1	0	0	0
5	0.5	0.66653	0.87134
10	0.9	1.20033	1.49315
15	1.2	1.5812	1.94593
20	1.3905	1.88994	2.31419
25	1.52035	2.12366	2.63817
30	1.58938	2.31121	2.89575

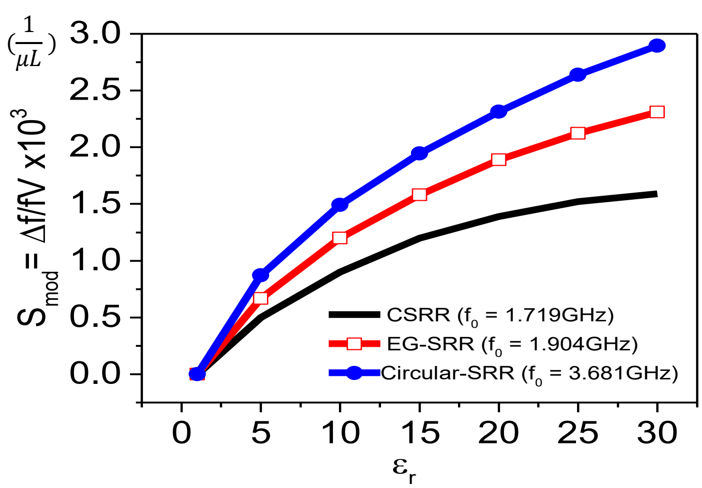

Fig. 4-5 Normalizing the sensitivity of sensors to volume under the test (V_{CSRR} = 353μL, $V_{EG\text{-}SRR}$ = 182 μL, $V_{Circular\text{-}SRR}$ = 135 μL; V = cross section area of tube x resonator's gap)

Volume of the MUT is defined as sample volume seen by the sensitive region of the resonator. It is shown in Fig. 4-2 (a-c) that this region is in fact the gap for EG-SRR and Circular-SRR and the length of cavity in CSRR. According to this figure, EG-SRR and Circular-SRR both provide higher sensitivity up to 50% improvement compared to CSRR. However, since the minimum volume required of the Circular-SRR is less than EG-SRR ($V_{Circular\text{-}SRR} = 135\mu L$ and $V_{EG\text{-}SRR}=182.02\mu L$), the former provides better overall performance, especially for small sample measurements in microfluidic application.

As a result, the performance of Circular-SRR is further investigated in this section. In addition, Fig. 4-5 proves that the Circular-SRR provides a promising trend for sensitivity as permittivity increases. Although eventually these graphs approach a steady state at higher permittivity values, the most responsive and sensitive resonator reaches this state at a higher permittivity (> 30). This is the reason that Circular-SRR is chosen to pursue the investigation further in this paper.

4.4.3 Embedding MUT inside the Substrate

The aim of this section is to add to sensitivity of the Circular-SRR. It is shown in literature that a great amount of electromagnetic energy is stored within the substrate; therefore, placing an MUT inside the substrate is expected to increase its electromagnetic interactions with the resonator, and ultimately leads to enhanced sensitivity [24], [81].

The depth to which the MUT is embedded into the substrate is not a factor when the cross section of the substrate is uniform. This is because the parallel plate capacitance seen by the MUT is from the resonator to ground plane. To enhance the sensitivity of Circular-SRR, the MUT is embedded in substrate (placed between resonator and ground plane), which is called, hereafter, Carved-SRR.

This arrangement is illustrated in Fig. 4-6 (a) and (b), and enhanced sensitivity due to this configuration is observed in HFSS simulation plotted in Fig. 4-6 (c). It is evident that the resonance frequency for such configurations depends on relative permittivity of the substrate ($\varepsilon_{r_{sub}}$), as well as relative permittivity of MUT ($\varepsilon_{r_{MUT}}$), which can be described as:

$$C_s = f(\varepsilon_{r_{sub}}, \varepsilon_{r_{MUT}}) \tag{4-4}$$

where C_s acts as the effective capacitance in parallel RLC resonator in (4-1).

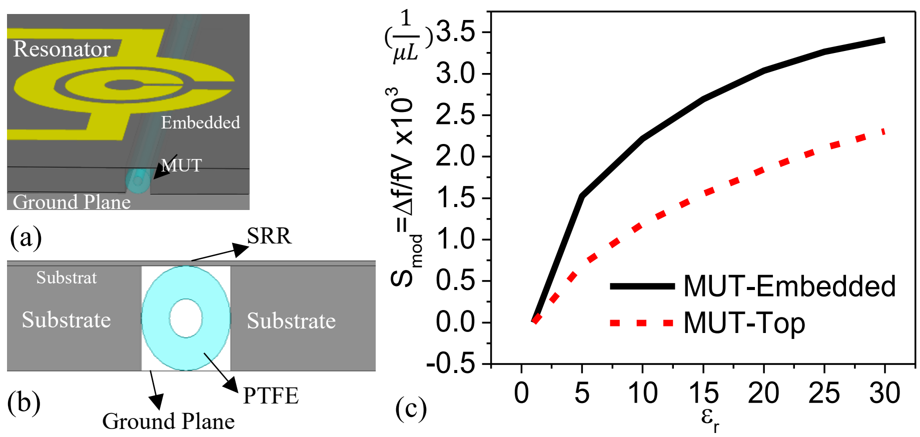

Fig. 4-6 Embedding MUT into the substrate and cross section of the structure (a-b) and sensitivity comparison of Circular-SRR when MUT is on top and embedded inside the substrate (Carved-SRR) (c)

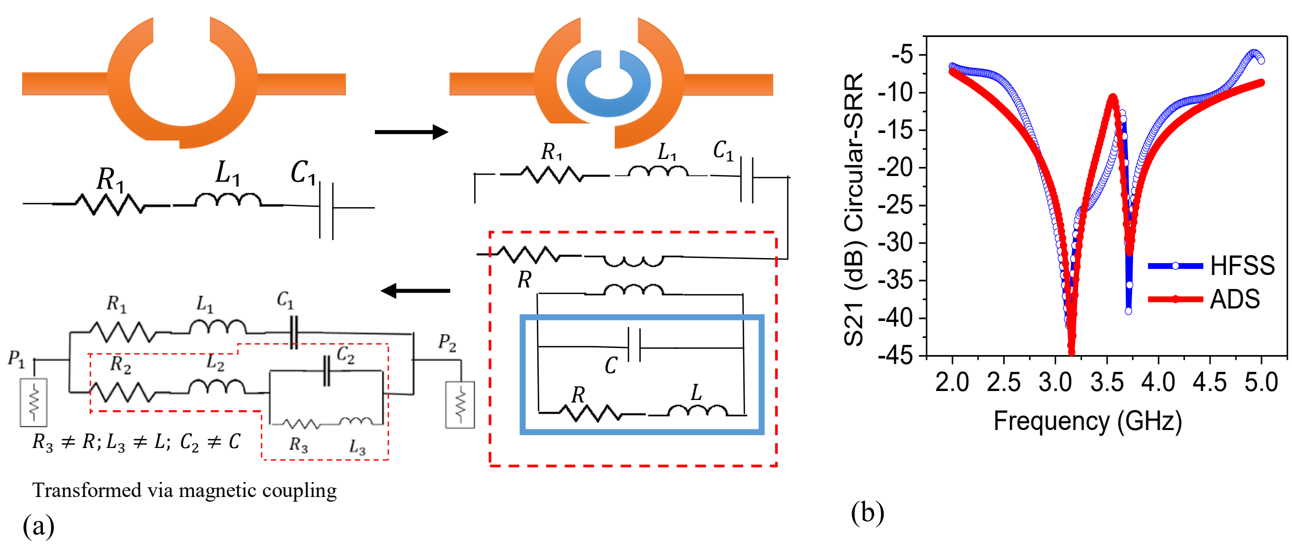

Fig. 4-7 Equivalent circuit model for Circular-SRR (a), S21 profile in HFSS and ADS (b)

Table 4-3 Lumped elements of Circular-SRR

Parameters	Values
Ports	$P_1 = P_2 = 50\Omega$
Resistors	$R_1 = R_2 = 1m\Omega$; $R_3 = 115.91m\Omega$
Inductors	$L_1 = 1pH$; $L_2 = 10nH$; $L_3 = 214.916pH$
Capacitors	$C_1 = 229.616fF$; $C_2 = 9.44265pF$

In addition, Fig. 4-7 (a) shows an equivalent circuit model of Circular-SRR and its lumped elements. This structure consists of two asynchronous ring resonators due to their different sizes. The dashed red outline RLC circuit (C_2,$R_{2,3}$,$L_{2,3}$) represents the magnetic coupling transformation by introducing the inner ring resonator. Also, C_1 represents the capacitance due to the gap of the bigger ring as well as the spacing between the rings. The other elements are lumped elements of the transmission line of the resonator.

Fig. 4-7 (b) shows the magnitude of the transmission profile (S21) for Circular-SRR. This figure compares the profile obtained from HFSS model with the equivalent circuit modeled in ADS. It is clear that this circuit with lumped elements indicated in Table 4-3 is a close approximation to model Circular-SRR as ADS simulations are aligned with HFSS. Also, two notch resonances from two ring resonators represent themselves in Fig. 4-7 (b). The outer resonator, however, is electrically connected to the input/output transmission lines, thus more external loading is on it and less equivalent quality factor is resulted.

Better Q-factor at the higher resonance frequency makes it ideal for sensing application, and hence 3.68GHz is used rather than 3.13 GHz. This can be shown in the following calculations where quality factor is the ratio of resonance frequency to the difference of +3dB frequencies in

(4-5) where $f_{+3dB,L}$ and $f_{+3dB,H}$ are 3dB above in amplitude compared to resonance value. $f_{+3dB,L}$ and $f_{+3dB,H}$ are lower and higher frequencies between the resonance notch frequency, f_0.

$$Q = \frac{f_0}{f_{+3dB,H} - f_{+3dB,L}} \qquad (4\text{-}5)$$

Right Resonance: $f_0 = 3.68\ GHz, f_{+3dB,L} = 3.709\text{GHz}, f_{+3dB,H} = 3.718\ GHz, Q = 409$

Left Resonance: $f_0 = 3.134\ GHz, f_{+3dB,L} = 3.104\text{GHz}, f_{+3dB,H} = 3.152\ GHz, Q = 65$

This clearly proves that the notch at higher frequency has better Q-factor, and hence better sensitivity.

As shown in (4-1), the resonance frequency depends on L_s and C_s of the circuit, and by placing MUT inside the substrate, the dependency of capacitance C_s on MUT maximizes that affects the resonance frequency and sensitivity significantly. Even though embedding a channel in substrate may imply challenging fabrication procedure, design and building this sensor can be simply done by prevailing innovative 3D-printing technologies.

4.4.4 Permittivity Analysis

It is required to understand the changes in effective permittivity (ε_{eff}) and loss tangent ($tan\delta$) of water-methanol mixture at ~2 GHz and ~4 GHz (range of operation for the sensors). First, it is necessary to obtain the complex dielectric constant of methanol and water at frequencies of interest. According to [82], the frequency-dependent complex dielectric constants of water and methanol are approximated as governed by Maxwell-Garnett expression as follows:

$$\varepsilon_{MG} = \varepsilon_h \frac{\varepsilon_h + \frac{1+2f}{3}(\varepsilon_i - \varepsilon_h)}{\varepsilon_h + \frac{1-f}{3}(\varepsilon_i - \varepsilon_h)} \qquad (4\text{-}6)$$

which approximates the effective permittivity of a mixture [83]. In this formula ε_{MG} stands for the approximated effective permittivity, f is the volume fraction of the mixing substances, ε_h and ε_i are the host's and inclusion's permittivity values, respectively.

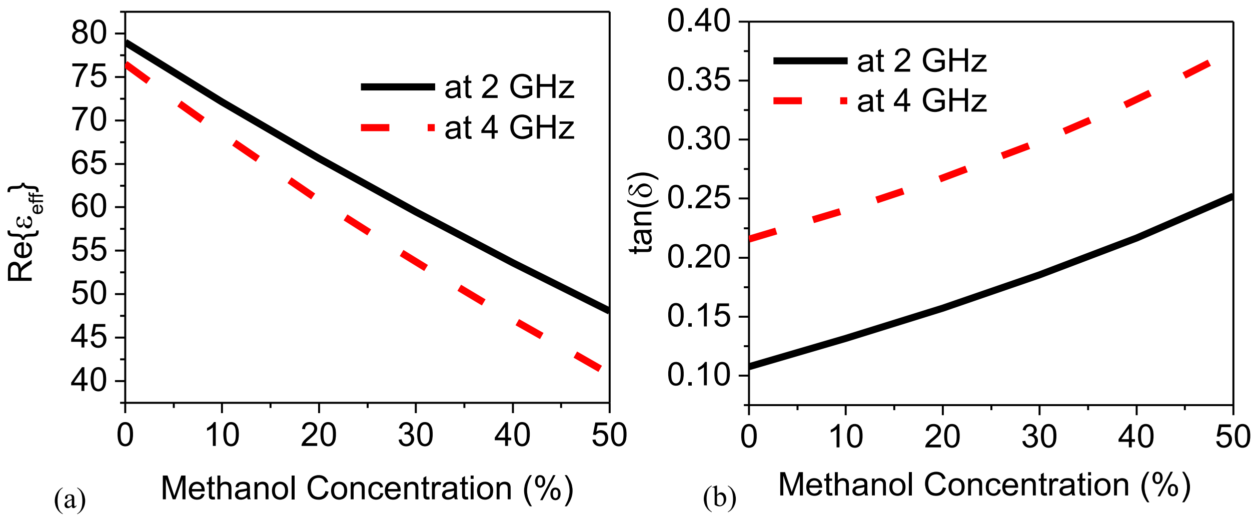

Fig. 4-8 Effective permittivity and loss tangent of the water-methanol mixture at two operating frequencies shown in (a) and (b) respectively

Table 4-4 Complex dielectric constants of water and methanol [82]

Substances	Frequency	
	2 GHz	4 GHz
Water	$79 - j8.5$	$76.5 - j16.5$
Methanol	$24 - j13.5$	$14.5 - j13$

Using the complex dielectric constants shown in Table 4-4 and Maxwell-Garnett approximation given in (4-6), the effective permittivity and loss tangent of methanol-water mixture at different concentrations are plotted in Fig. 4-8 (a) and (b) respectively. Fig. 4-8 (a) signifies the range of permittivity corresponding to 0-50 % concentration of methanol in water that brings about relative permittivity within range of (42-77) at 4 GHz and (48-80) at 2 GHz.

In addition, Fig. 4-8 (b) shows that as the concentration of methanol increases, the loss tangent of the mixture also increases, and hence at higher concentrations the medium under the test becomes lossier. It is noteworthy to mention the effect of frequency on both plots that the mixture's effective permittivity drops faster with concentration at higher frequencies. Moreover, the solution is lossier at higher frequency, and this even becomes amplified for higher concentrations of methanol.

4.5 Measurements and Results

Three microwave resonant-based sensors are studied in this paper to compare their sensitivity to methanol concentration variations in water at room temperature (25℃). These sensors are fabricated with the dimensions stated in Fig. 4-1 (a-c) as shown in Fig. 4-9 (a-c). First, the proof of concept will be verified for PTFE tubing and later it will be examined on microfluidic channel made up from quartz.

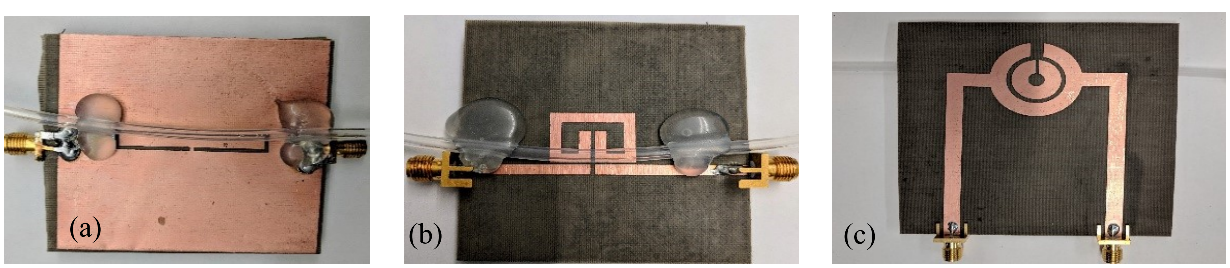

Fig. 4-9 Fabricated structure of sensors: (a) CSRR; (b) EG-SRR; (c) Carved-SRR

4.5.1 Measurements Using PTFE Tubing

In this experiment, PTFE tube with outer diameter of 3.175 mm, wall thickness of 1 mm, and relative permittivity of 2.2 is used to contain methanol-water mixture. Sample configuration will be similar to what is shown in Fig. 4-3, where the cubes are replaced with cylindrical tubes. As discussed in pervious section, the sample material is placed inside the substrate for Carved-SRR, and for this experiment, two Rogers 5880 substrates with thickness of 3.18 mm are used to encapsulate the tube which is covered by resonator and ground sheets from top and bottom, respectively.

The experiment set-up for concentration sensing using the three SRR sensors is shown in Fig. 4-10. Samples with total volume of 50mL for each test are prepared before injection into the tube according to the ratios given in Table 4-5 for required concentrations. For instance, to get a sample with 30% methanol concentration, 15mL methanol is mixed with 35mL of water.

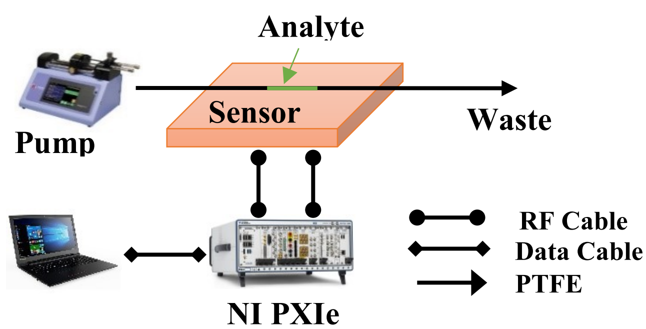

Fig. 4-10 Experiment set-up for methanol concentration sensing

Table 4-5 Mixture of methanol and water

Methanol Concentration	Mixture of Water (w) and Methanol (m)
10%	45 mL (w) + 5 mL (m)
20%	40 mL (w) + 10 mL (m)
30%	35 mL (w) + 15 mL (m)
40%	30 mL (w) + 20 mL (m)
50%	25 mL (w) + 25 mL (m)

Fig. 4-11 shows the measured results for each sample and the error bars are computed as an averaging from three measured values. Error bars shown on the plots indicate that sensing with CSRR (with notch, Fig. 4-4 (a)) conveys more error in center frequency readout. The reason can be the large portion of the tube interacting with the sensor, and apparently the changes in the concentration of the liquid under test is affecting different parts of the resonator differently. This makes the sensor output not stable unless a very huge material size would be used.

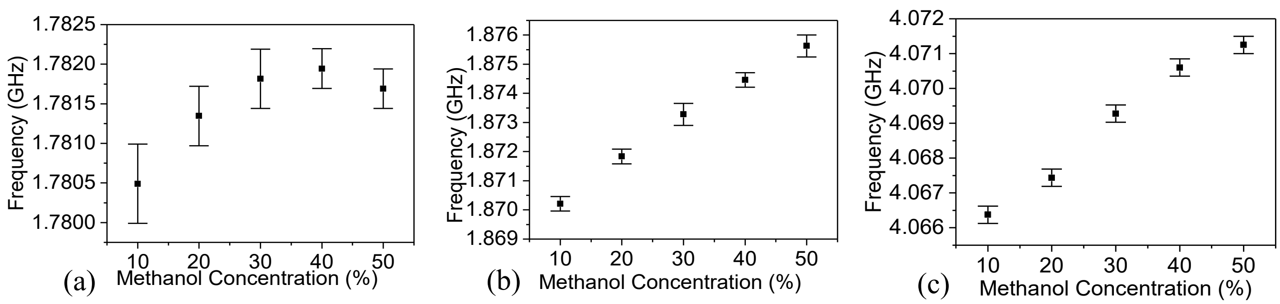

Fig. 4-11 Limit of detection for: (a) CSRR; (b) EG-SRR; (c) Carved-SRR

Whereas Carved-SRR (with notch, Fig. 4-4 (c)), similar to EG-SRR (with peak, Fig. 4-4 (b)), provides higher accuracy in frequency detection, and hence concentration detection. This indicates that Carved-SRR and EG-SRR are more reliable and repeatable than CSRR. Furthermore, it can be observed from Fig. 4-11 (a), that CSRR reaches saturation for methanol concentrations higher than 30%, which confirms the poor performance of this structure.

On the other hand, EG-SRR and Carved-SRR exhibit a linear performance from 10% to 50% methanol concentration. Also, Table 4-6 shows detailed information on resonant frequencies and frequency shifts due to analyte (δf), and the normalized frequency detection error for each structure. It is evident that the normalized error for carved sensor is an order of magnitude lower than its counterparts, a benefit of the proposed design for highly sensitive applications.

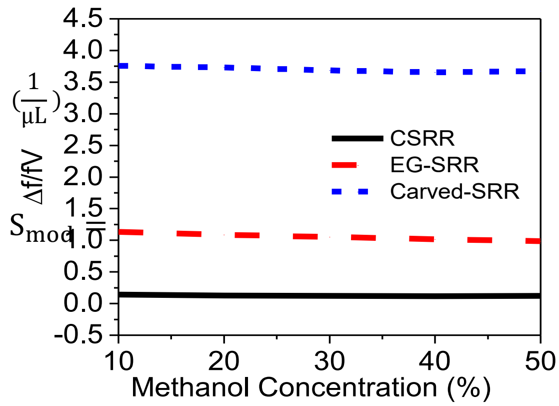

Fig. 4-12 Measured normalized frequency variations in three sensors due to different methanol concentrations

Fig. 4-12 shows the sensitivity variations with methanol concentration which indeed would translate into much smaller absolute permittivity changes. Hence it would be more reliable to study the effect of methanol concentration on the sensitivity of the device under test (DUT). In Fig. 4-6 the plot reaches a steady state for higher permittivity which for methanol and water is roughly 30

Table 4-6 Normalized Frequency Error

	CSRR			EG-SRR			Carved-SRR		
Methanol Concentrations	f (GHz)	$\times 10^5 \delta f$ (kHz)	$\times 10^{-4} \frac{\delta f}{f}$	f (GHz)	$\times 10^4 \delta f$ (kHz)	$\times 10^{-4} \frac{\delta f}{f}$	f (GHz)	$\times 10^4 \delta f$ (kHz)	$\times 10^{-5} \frac{\delta f}{f}$
10%	1.7804	5	2.808	1.870	2.5	1.336	4.066	2.5	6.147
20%	1.7813	3.75	2.105	1.871	2.5	1.335	4.067	2.5	6.146
30%	1.7818	3.75	2.104	1.873	2.5	1.334	4.069	2.5	6.143
40%	1.7819	2.5	1.403	1.874	2.5	1.333	4.070	2.5	6.141
50%	1.7816	2.5	1.403	1.875	2.5	1.332	4.071	2.5	6.140

and 80 respectively. The frequency response of each sensor changes with methanol concentration; however, these changes are normalized to each sensor's resonance frequency and sample material volume in each case. This is done to only investigate each sensor response to methanol concentration variations.

Fig. 4-12 shows that for methanol concentration increasing from 10% to 50% the proposed design, Carved-SRR, has the highest sensitivity and responsivity. This agrees with proposed statements in previous sections. Based on this figure, the modified sensitivities for CSRR, EG-SRR, and Carved-SRR are measured to be on average $0.126\mu L^{-1}$, $1.056\mu L^{-1}$, and $3.701\mu L^{-1}$ respectively. This suggests that Carved-SRR is a great candidate for sensing methanol, and its performance is not degraded at higher concentrations despite increase in methanol concentration. These observations are aligned with the simulation results discussed and shown in Fig. 4-6 (c).

4.5.2 Measurements Using Microfluidic Channel

In previous sections the sensitivity of three types of microwave resonators has been discussed and put into comparison. In section 4.5.1 and Fig. 4-9 the embedded method using tubes has been analyzed and discussed. This concept has been also examined using simulation in Fig. 4-6, hence it is concluded that embedded technique indeed boosts the performance of the sensor. Then, the MUT configuration on top versus embedded into the substrate of the most responsive resonator of all three has been investigated, and it has been proposed that embedding sample indeed boost the performance of the sensor.

Therefore, the novelty of this work represents itself as an effective solution for industrially accepted structures that carry low volume fluid, such as microfluidic channels. It is shown that embedding the sample under test in to the substrate of the sensor is in fact a superior measurement. Therefore, this integration would be an ideal candidate for microfluidic sensing where the sample size is very small. This idea is used to integrate the microstrip split ting resonator with microfluidic channel embedded into its substrate to show the method's capability of sensing low percentages of methanol in water.

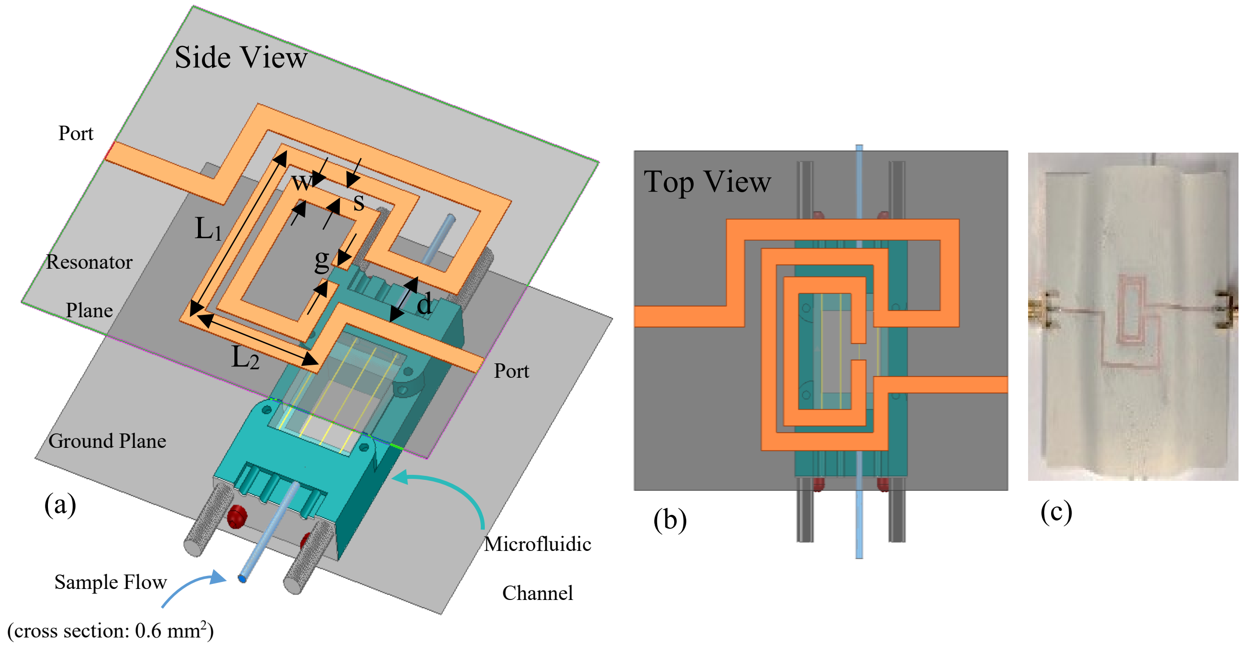

Fig. 4-13 (a) 3D schematic of the design (mm), and fabricated model of sensing structure for microfluidic measurements: w = 1, s = 0.5, d = 2, g = 0.5, L_1 = 18, L_2 = 10.5 (b) top view of the sensor (c) fabricated sensor's top view

An experimental procedure is shown using a microfluidic channel that is embedded within the substrate of an SRR microwave sensor. The schematic of this experiment and the fabricated resonator is shown in Fig. 4-13. In this fabrication a Roger 5880 substrate has been used with thickness of 0.5mm for the ground plane and 0.125mm for which the resonator is printed on. The structure illustrated in **Error! Reference source not found.** represents a geometrically modified Circular-SRR on top layer with the advantage of the analyte being embedded in the sensor to increase the sensitivity with less volume needed. This design supports the proposed idea in previous section which is improving the performance by embedding the sample versus other configurations.

The goal of this experiment is to show that using this method, it is feasible to engage minute samples as low as 15 μL which is illustrated in Fig. 4-14. The shift of frequency from 0% to 100% methanol is measured to be 1 MHz and the amplitude variation in this range of methanol

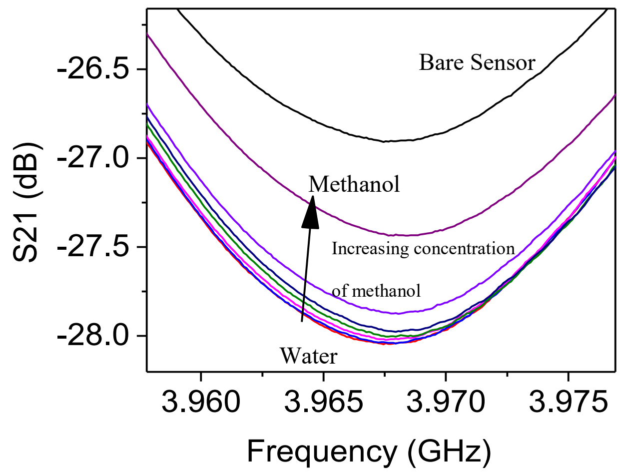

Fig. 4-14 Transmission profile for concentrations (%) of 0 (only water), 10, 20, 30, 40, 50, 100 (only methanol), and bare sensor

concentration is measured to be 0.611 dB. Also, Fig. 4-14 shows that the sensor cannot distinguish for methanol concentrations less than 10%. Table 4-7 shows the normalized frequency error for this experiment. This figure exhibits that the proposed method is responsive to changes in small volume of sample materials, hence it is a superior method of enhancing the sensitivity for microfluidic applications. This technique may be used in micron-scale sensing application, and it can also be used for studying bodily fluids using microfluidic channels.

Table 4-7 Normalized Frequency Error for Microfluidic Channel

Methanol Concentration	$\frac{\delta f}{f}$
10%	0.756E-4
20%	1.260E-4
30%	1.306E-4
40%	1.512E-4
50%	1.764E-4

4.6 Summary

In this study, three microwave resonant-based sensors are compared in terms of their sensitivity and performance for methanol-in-water sensing. Conventional CSRR, SRR with extended gap, and Circular-SRR are the sensors of interest with simulated resonance frequencies of 1.7, 1.9, and 3.6 GHz, respectively. This paper proposes a modified definition of sensitivity that enables comparisons between different sensor configurations. Electric field distribution and hot-spot discussion is studied by numerical simulations in HFSS, and sensitivity analysis is performed along with dielectric constant studies using Maxwell-Garnett's approximation. Exploiting the capacitance within the substrate, material under test is placed inside between the resonator and ground. As a result, a significant enhancement in the sensitivity and performance of the conventional SRR is observed. Simulation and measurement results align together in presenting the Carved-SRR (normal SRR with carved substrate to include material under test) provides better sensitivity and accuracy for lossy liquids with verification on methanol-in-water concentration sensing within range of 0-50%. Furthermore, this method is integrated with microfluidic channel to prove the feasibility of using the embedding technique in small-scale sensing applications in biomedical and biological research.

5 Design of a Compact and Cost-effective Microwave Sensors Readout Circuitry

There is a gap in connecting microwave resonance-based sensors and their use in industry; the limitation is the absence of a measuring instrument that can provide the characteristics of the DUT and its response in the field. VNA is the most common equipment used for that purpose, but due to its large size and high purchase cost, it is not possible to employ this equipment in the field.

RF network analyzers are vastly used to measure the performance and properties of RF and microwave devices. Using this type of equipment, the functionality and reliability of a microwave device or an RF system is verified. One of the most popular equipment that is used to monitor and measure the frequency response of microwave resonators is Vector Network Analyzer (VNA). This powerful and popular network analyzer not only measures the amplitude of the device under test (DUT), but also it is capable of providing the phase information.

In practice, when using microwave resonance-based sensors in the field, there is an inevitable need of a portable, compact and accurate network analyzer, or a read-out system to measure and capture the data acquired by the DUT. Unfortunately, current VNAs are bulky, immobile, and also very expensive to be handled by amateur users. Therefore, there is a gap in industry where microwave and RF devices are used as sensors and yet there is no monitoring and data acquisition instrument. In this chapter, a simple, novel, cost-effective, and compact readout circuitry is proposed that can be used to measure the amplitude of transmission profile (S_{21}), and also can be used during sensing measurements in the field. In addition, this system is compatible with the microwave resonance-based sensors discussed in the previous chapters.

This novel and simple design is made of cheap off-the-shelf components, such VCO, PD, microcontroller unit (MCU), and a power board. A low-pass filter (LPF) and attenuator are used to improve the system performance which will be explained in this chapter in full details. The result obtained with this readout circuitry is compared with a high-end Cobalt VNA from Copper Mountain. Also, please note, since this system only measures the amplitude value of transmission profile and does not consider the phase, hereafter where $S_{21}$is mentioned, it intends to the amplitude value [dB] only.

5.1.1 Objective

This chapter talks about a novel readout circuitry that is specifically designed for microwave resonators and their sensing applications in various fields. Although VNA is a powerful equipment that is capable of measuring various properties and responses of a DUT, the proposed system is focused to measure the transmission response, i.e. S21, of the sensor placed in the loop as DUT. This network analyzer not only provides the transmission profile of the sensor itself, but also allows for sensing measurements using the DUT and some samples for material characterization applications. For instance, the glucose concentration sensing measurement is repeated using this system to verify the functionality of the proposed readout circuitry.

In addition to hardware design, this system provides a trivial and easy-to-use GUI software where user can enter some input parameters such as frequency range of operation and number of points to tune the resolution of result; it also offers an option for averaging for noise and fluctuation reduction. This software gives the user the option to import the S21 response of the sensor captured from a standard VNA. This allows the user to compare the results of the proposed network analyzer with a VNA to verify the accuracy. The proposed system has many building blocks that includes

RF modules, power board and connections, and digital configurations and programing. These building blocks will be explained in details in the following sections.

5.2 Building Blocks of the System

This chapter focuses on the readout circuitry that uses a microwave resonator SRR as a DUT and measures its transmission response. The hardware of this system is made of various sections: power connections, RF modules, and digital boards. Power board is simply a PCB board with some voltage regulators to convert the power plug-in to a clean and low noise DC 5V to power up the RF and digital components.

RF modules are readily-available off-the-shelf components and consist of VCO, attenuators (Att.), low pass filter (LPF), and a PD. The purpose of VCO is to generate frequency span of the system, and PD is responsible for capturing the power level and amplitude of the DUT response. A DAC (digital to analog convertor) is also used to feed the tuning input voltage of VCO to generate frequency span. These are the key components of the system and provide frequency and amplitude information required to plot S21 of the resonator. LPF and attenuator are utilized to improve the performance of the system. Further discussion on the latter components will be done later in the chapter. Fig. 5-1 illustrates the block diagram for power and RF configurations, where

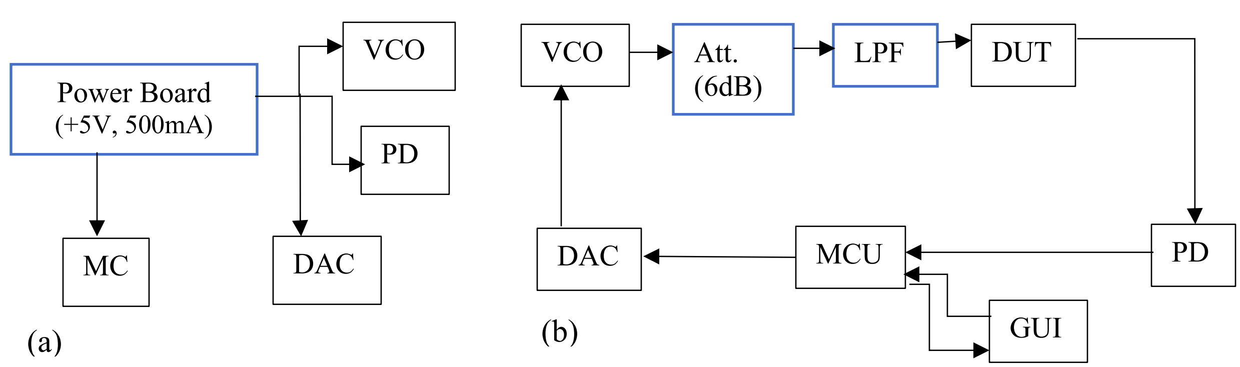

Fig. 5-1 Block diagram of power connections (a) and RF modules in the system (b)

the blue boxes indicate the modules that are added to improve the system after primary results has been captured.

In addition to hardware design aspect of the project, the majority of the work in this chapter is done on the digital configuration and programing of MCU. In this process, many peripherals of MCU are used to develop the desired digital system that can produce the tuning voltages that feed the VCO for frequency generation, and also to capture the power levels from PD to quantify the amplitude of S21. These peripherals include ADC (analog to digital convertor), UART (universal asynchronous receiver transceiver), DMA (direct memory access), and SSC (synchronous serial controller). The functionality of these peripherals within MCU will be discussed later in this chapter. Fig. 5-2 shows the digital configuration of the system inside the microcontroller.

5.3 Hardware Design

In this section, each component will be discussed in full details. Explaining the functionality and performance of the building blocks of the system allow for insightful understanding of the

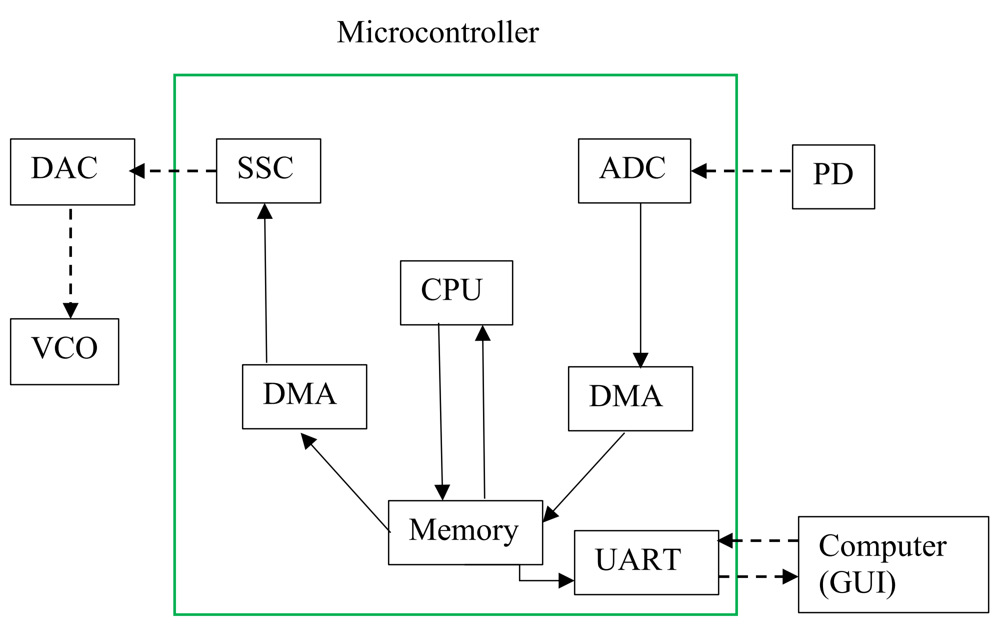

Fig. 5-2 Digital configuration of microcontroller and its peripherals (dashed lines are external connections)

whole system and proves the simplicity of the design. Each RF module will be described in the next sections.

5.3.1 Power Board

Originally the system has been powered by a 3-channel switching bench DC power supply that provides the system with a +5V. However, to minimize the effect of noise and increase the stability on VCO, it has been decided to use a power board that uses a dual, low noise and low dropout voltage linear regulator. This board is a Linear Technology development board that has two output channels with maximum output DC voltage of 5V and 500mA maximum current. Fig. 5-3 shows a snapshot of the power board. The output noise of this power supply is $20\mu V_{RMS}$ in a 10Hz to 100KHz bandwidth [84], which makes it a great candidate for this system.

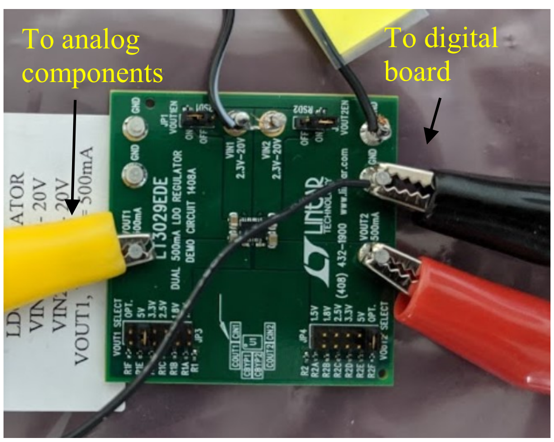

Fig. 5-3 Low noise power board supplying digital and analog circuits

Also, powering up digital and analog components with separate channels isolates the interference of digital noise into analog signals. The primary result of this chapter has been obtained using the bench DC power supply, and then for better performance a second set of measurement is done using this power board. The original and improved results will be compared in the result section of this chapter.

5.3.2 Voltage Control Oscillator (VCO)

As mentioned before, to measure the transmission response of the microwave resonator or any other S-parameters, a source of RF signal generator is required to excite the microwave device. In this project, VCO is responsible for generating the frequency span and more importantly the RF signal at the output which is crucial for DUT excitation. This RF signal will be the input of the DUT whose S21 profile is the target. This RF module has one input, one output, and a V_{cc} DC power supply that is connected to +5V. The input of the VCO is called V_{tune} which stands for tuning voltage. The tuning voltage can be swept from 0 to 25V. For each input voltage point there is a corresponding frequency point that generates a RF signal in that frequency. According to the datasheet [85], the tuning voltage and frequency hold a linear relation. For the max range of input voltage, a frequency span of 1.216 – 2.902 GHz is generated. In addition, the dynamic range of the output power of the VCO is 2.45 dBm [85].

5.3.3 Attenuator

The SMA attenuator is added after VCO for the second round of measurements to improve the performance of the system, more specifically the VCO. This simple module has a 6dB attenuation over a wide band of frequency, 0-6GHz [86]. The reason that this attenuator is added is because, once VCO is attached to the rest of the system, the impedance seen by the output is changed. Hence due to loading effect the output power of the VCO is not stable which implies error in generating output frequency, and this leads to unreliable results. To compensate for the loading effect of VCO and increase the stability of RF signal feeding the DUT, the attenuator is placed after VCO. The 6dB attenuation in transmission is negligible while it has a 12dB attenuation in reflection of the signal. Therefore, placing the attenuator promises for better performance and stability of the system, as well as isolating the VCO from the rest of the system.

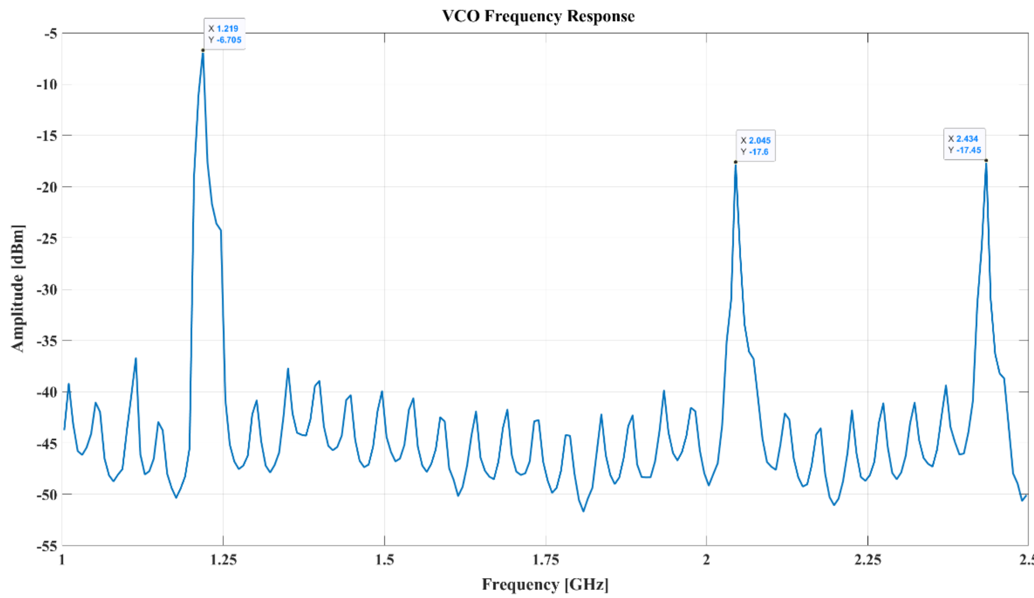

Fig. 5-4 VCO frequency response generating a tone at 1.219GHz and unwanted harmonics

5.3.4 Low Pass Filter (LPF)

In addition to the attenuator, a SMA low pass filter is added to the second round of measurements to enhance the performance of the readout circuitry. This LPF has a cut off frequency of 2.4GHz [87] and, it is used to attenuate the second and third harmonics that get carried on from VCO into PD. To understand this better, VCO frequency response is measured using a DC power supply and a spectrum analyzer (NI PXIe-5601 10MHz-6.6GHz). This experiment generates a single tone RF signal at 1.219GHz. Fig. 5-4 shows the frequency response of the VCO and its main fundamental harmonic at desired frequency, as well as the unwanted peaks. These harmonics introduce error in the amplitude of S21 and make the system inaccurate and unreliable. Therefore, the LPF is added to attenuate the second and third harmonics generated by VCO, and consequently increase the accuracy of the system.

5.3.5 Device under Test (DUT)

For measurement purposes, the microwave resonator that was discussed in both Chapter 3 and 4, extended-gap SRR, is used as the device under test. This microwave sensor is used as the

DUT to capture the transmission profile as well as sensing measurements using high concentration glucose solutions. Basically, the goal is to observe the performance of the resonator using the proposed system and verify the S21 with the transmission profile of the same device measured by VNA. In addition, the sensing measurement results are investigated in terms of the trend and pattern of the frequency shift of the S21. The resonance frequency of this microwave sensor is 1.978GHz.

5.3.6 Power Detector (PD)

PD is one of the other important RF modules in this project that is responsible to capture the output power of the DUT. This specific module has one RF input coming from the DUT and gives the output power as DC voltage levels. Aside from the input and output, a +5V is required to power up the PD. This voltage is fed through the power board that was discussed before. This power detector has a wide bandwidth which operate from 10MHz to 8GHz, its output voltage ranges from 0.5 to 2.1V, and the rang of output power in frequency band of 1 – 5GHz is -40 to 15dBm [88]. The wideband nature of the PD can be problematic, as this module picks up the higher and unwanted harmonics of VCO in the RF signal. This is the reason that a LPF is suggested to eliminate the higher harmonics and reduce the error in the results.

5.3.7 Digital-to-Analog Convertor (DAC)

To generate the tuning voltages feeding into VCO, a very low noise and high voltage digital-to-analog convertor is used to pass the voltages at the output. This DAC produces a very clean analog signal which is crucial for RF components such as VCO. This board has a $2.2\mu V$ output noise which comes from the V_{REF} voltage regulator chip on the board [89].

Microcontroller is in fact programmed in a way that according to the frequency ranges entered by user in GUI, it controls the DAC's output voltages. It is worth to mention that, to increase the efficiency and accuracy of the DAC, the evaluation board is used rather than the stand-alone chip. The evaluation board (EVAL-AD5791SDZ, 20-bit) has all the required voltage regulators, bypass capacitors, voltage division resistors, amplifiers, and buffers. Otherwise, the board deriving DAC chip had to be designed, fabricated, and verified in the lab before using it in the readout circuitry [89]. In addition, in this work the output voltage range of DAC is assumed to be 10V, from the output range of 2-15V, hence the dynamic range of frequency generated by VCO is 1.216 – 2.06 GHz [85], [89].

5.4 Digital Design

In addition to the hardware design, the most important aspect of this project is the digital configuration and programming of the digital component, mainly microcontroller. Microcontroller is the brain of the system that controls and brings separate pieces together and closes the loop.

This device communicates with GUI software through UART communication protocol. The input parameters entered by user in the software will then be used by microcontroller to set DAC output voltages feeding into VCO which ultimately generates the frequency vector, as well as reading ADC levels from the amplitude of PD which indicate the amplitude power of DUT. The firmware development of the microcontroller, deriving its peripherals, and the debugging procedure is explained in the following sections.

5.4.1 Microcontroller Unit (MCU)

Microcontroller unit (MCU) is a small computer in form of a chip that contains one or more CPUs (central processing unit), memory, and configurable input/output peripherals each with different functionality. The MCU used in this work is an ATSAM3X8E manufactured by Arduino and contains a microchip ARM Cortex-M. This is a powerful microcontroller that can be used for various projects. The peripherals that are used in this work include: a 12-bit ADC, UART and SSC protocols, timer counter (TC), and DMA. Configuring these peripherals enables the microcontroller to communicate with RF modules of the network analyzer such as PD, and DAC evaluation board. The MCU is the core of the proposed system and the majority of the workload has been contributed to firmware development of the controller.

5.4.2 Analog-to-Digital Convertor (ADC)

Analog-to-digital convertor is one of the peripherals that is configured within the microcontroller unit. The purpose of using an ADC in this system is to convert the output voltage of the PD into digital values, i.e. ADC code levels, so microcontroller can communicate these values to GUI software where the voltages are translated into power quantities; this provides the software with the amplitude data required to measure S_{21}. In addition, microcontroller reduces the noise presented and carried over in the analog signal coming from RF modules and PD by averaging and digitizing the voltages using ADC.

The MCU contains a 12-bit ADC with 1MHz as maximum sampling frequency; this peripheral is managed by ADC controller register. However, this register is not continuously clocked. There is a power management controller (PMC) that controls the clock system of the peripherals. Therefore, ADC controller master clock (MCK) must be enable in PMC prior to programing the ADC, and the ADC clock frequency is set to its maximum value, 22MHz [90]. When configuring this peripheral, the ADC offset has been assumed to be 0. In addition, ADC is triggered using Timer Counters. When this module is enabled, a waveform is generated to trigger the corresponding peripheral, for example ADC.

In order to save the processing power and time of CPU, PDC (peripheral DMA controller) is used throughout the system design. This module transfers data between the peripherals and the memory, whether on or off the microcontroller. Using PDC reduces the number of clock cycles required for data transfer, hence improves the performance of microcontroller [90]. ADC, as well as other peripherals used in this design, are using this method for data transfer and communication with memory unit.

5.4.3 Direct Memory Access (DMA)

The SAM3X/A series of the microcontroller has a powerful architecture which is designed to maintain a high-speed data transfer. This is done by a multi-layer bus matrix as well as SRAM (static random access memory) banks, PDC and DMA channels that allow for parallel processing and efficient data transfer [90]. DMA has one master interface and one channel, and it acts as a bridge in data transferring between peripherals and destination. This module reads the data from the source and writes it to the destination. A DMA controller handles the transfer between peripherals and memory, and hence it receives triggers from the certain peripherals that are used for the data communications such as SPI, PWM, UART, and SSC. The last two are used in this work for data transfer between peripherals.

5.4.4 Universal Asynchronous Receiver Transceiver (UART)

UART is used for communication and in-situ programming solutions [90]. One of the main characteristics of this module used in this work, is independent receiver and transmitter with a common programmable baud rate generator. The purpose of UART communication in this thesis is to connect the PC laptop to microcontroller in order to transfer data from and to the software ran on the computer.

The developed GUI software is where the input parameters defined by user is transferred to microcontroller, and where the data captured by the system is received and post processed by the software. This is done using a USB-to-TTL serial cable, where the TTL serial end connects to the receiver (Rx) and transmitter (Tx) serial pins on the microcontroller board. The baud rate generator provides the bit period clock named baud rate clock to both Rx and Tx [90]. In the serial communication, the standard baud rate used is 9600, which means the serial port is able to transmit a maximum of 9600 bits per second.

5.4.5 Synchronous Serial Controller (SSC)

As mentioned before, the output voltage of DAC evaluation board is controlled by the microcontroller. Synchronous serial controller is used to transfer the data and commands from MCU to DAC. SSC is a communication link with external devices, and it has independent Rx and Tx and a common clock divider. Each of the Rx and Tx interface with three signals, TD/RD for data, TK/RK for the clock, and TF/RF signal for the Frame Sync [90]. These signals each correspond to a pin on DAC board that enable the board, communicate the data and activate the clock on the board.

Since in this work, the data transfer happens in one direction, from microcontroller to DAC, the main focus is on transmitter signals. According to DAC datasheet [89], the TD corresponds to SDIN, TK to SCLK, and TF to SYNC. These are the serial pin configuration from microcontroller to DAC evaluation board. TD carries the encoded commands and data that determines the performance of DAC, whether it's a read or write command, or if it is the DAC register value, D which defines the output voltage by the following equation [91]

$$V_{out} = \frac{(V_{REFP} - V_{REFN}) \times D}{2^{20} - 1} + V_{REFN} \qquad (5\text{-}1)$$

Where V_{REFN} is the negative input voltage on DAC board, which is $-10V$, and V_{REFP} is the positive input voltage on the board, $+10V$, and D is the 20-bit code programmed from microcontroller to DAC. SYNC, the active low digital interface synchronous input pin, is the frame synchronization signal for the input data. When this signal is low, it enables the input shift register, and data is transferred on the falling edge of the following clocks. The input shift register is updated on the rising edge of the SYNC [91].

5.5 Software Design

Aside from the hardware design aspect of the project, the software development, data acquisition, and processing the data play crucial roles in providing a reliable and functioning system. To employ a user-friendly system that is ideal for in-situ measurements, a trivial and easy-to-use interface is required to allow for input parameters determination, data acquisition, and post-processing to measure and display the desired output. For this purpose, a graphical user interface is developed to yield an accessible environment for user to employ the proposed network analyzer system in the field and capture the S_{21} profile of the DUT for sensing applications.

The software development of this work is done by a powerful multi-paradigm numerical computing environment, known as MATLAB. This program has a feature called App Designer which provides a platform to implement the code and customize the visual aspect of the GUI. To obtain a well-maintained and manageable software, several MATLAB functions have been scripted separately and called back within the GUI code design. Aside from measuring and plotting S_{21}, the GUI provides other features such calibrating the system and importing S_{21}data captured by the Copper Mountain VNA to compare and verify the measured results versus the accurate data from the VNA. This software is also capable of sending error, warning, and notifying messages to the user in different situations.

5.5.1 Graphical User Interface (GUI)

When designing a user interface there are two main factors to think of: the visual design, and programming implementation. The former must be designed in such a way that it is easy to understand, provides necessary features for the application, and has a coherent graphical design.

Customizing the visual aspect of the user interface in MATLAB is very simple and straightforward. Once a new project is created in App Designer, under Design View, there is a platform to build the face of the GUI. This section also provides a library of various interactive components that can easily be dragged and dropped in the platform to create the features of the GUI. Some of these components are axes, buttons, check boxes, drop down menus, edit fields (numerical and text), tables and etc. Fig. 5-5 illustrates the visual features of the GUI developed in this work. As shown in this figure, there is a section for input parameters which are determined by

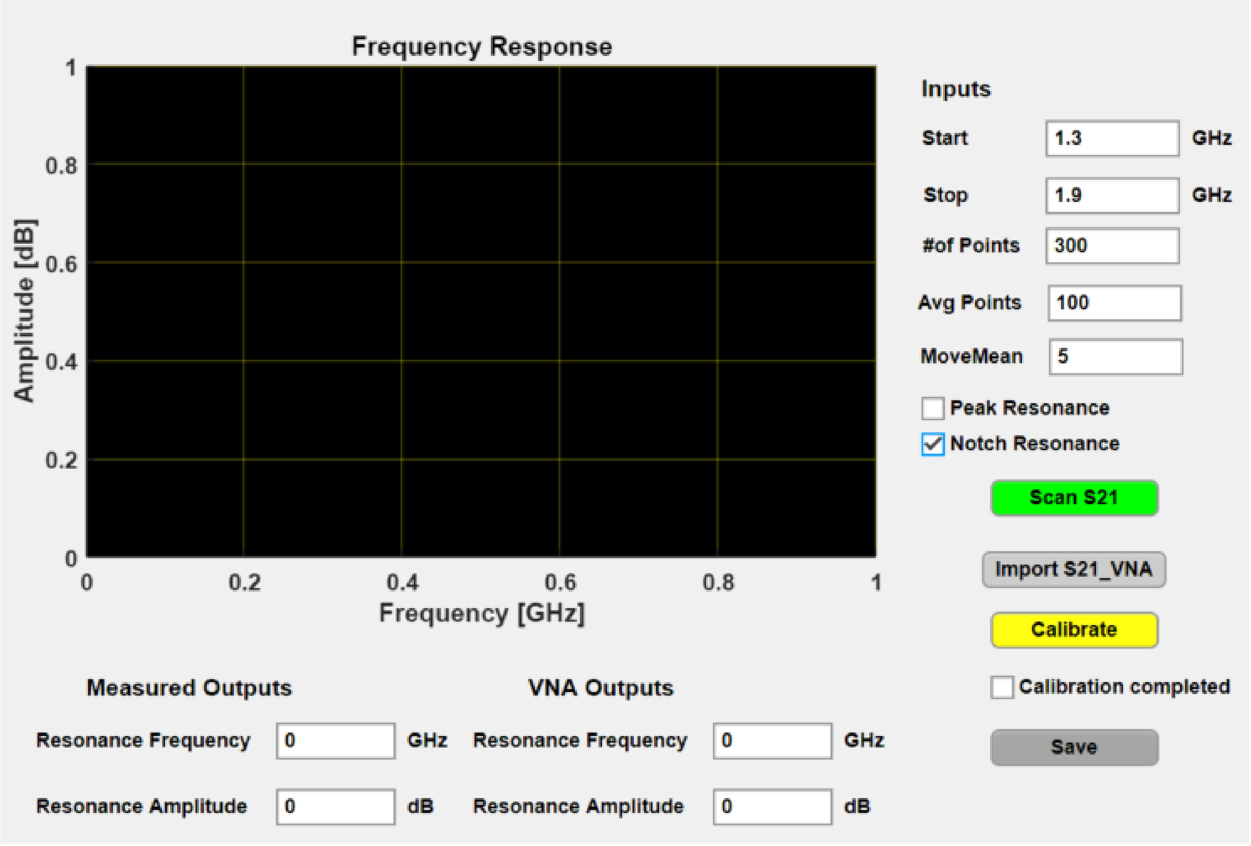

Fig. 5-5 Visual features and building blocks of the GUI for the proposed network analyzer

the user. These are the frequency range, number of points to be sampled, Avg points to average the voltages captured by ADC, and MoveMean determines the number of average points that is used in the built-in move-mean function of MATLAB to average the input power to the DUT from VCO.

The buttons are used to perform the S_{21}measurements, importing the same profile from VNA, and calibration of the system. The check box is chosen when the calibration process is completed. There are two output sections that calculate the resonance frequency and amplitude captured by the proposed system as well as VNA. The main visual feature of this GUI is the axes, where the transmission profile of the DUT is plotted and shown with its amplitude [dB] on y-axis and frequency [GHz] on the x-axis.

Each of the components in GUI design can be accessed under Code View tab in the App Designer platform. In the Code View, each button can be programed to perform a desired function once the button is pushed in the GUI. All the edit fields (in this case numerical) can be read and/or written the values by programming them in Code View. One easy way to implement the codes to perform the desired functionality is to write separate MATLAB functions and call back these functions in the Code View.

5.5.2 MATLAB Functions

To maximize the quality and clarity of the program, one principle function is written to control all the functions used in this design (Control function); this function is applied when user push the button to scan for S_{21}. In this code, the input parameters are checked in case user enters any invalid values. First step is to convert the range of frequency to voltage. This voltage range is in fact the required output voltages that DAC needs to pass to VCO to generate the corresponding frequencies. This is done by interpolating the frequency range entered by user with the voltage and frequency information given in VCO's datasheet [85].

Then Control calls and passes the converted voltage values to a function (matlabComm) in which MATLAB communicates with microcontroller board through USB-to-TTL serial cable. This function enables the USB port that is connected to microcontroller board, which is programmed to set the output voltage of the DAC to the designated values by user. This will start the process as VCO will generate the desired frequency range determined by user. The generated RF signal is the input to DUT, the microstrip resonating at 1.98GHz. The output power of the resonator is captured by PD which converts them to a range of DC voltages. These voltages are captured by ADC on microcontroller board and then transmitted to MATLAB for post processing.

Using the captured information from the system, another function (Estimate_S21) is called within Control. This function estimates the amplitude of $S_{21}$of the resonator in the loop. In this system, the amplitude of $S_{21}$of the DUT is determined by its output and input power (P_{out}, P_{in}) as shown in (5-2). In this system $P_{out}$is determined by power of PD, and $P_{in}$is found by power of VCO. PD is assumed to have zero reflection in this estimation

$$S_{21}[dB] = P_{out} - P_{in} \tag{5-2}$$

To find these powers, first the voltages from ADC must be converted to power quantities; this is done by interpolating the output voltage and input power of PD indicated in its datasheet [88]. In addition, $P_{in}$is obtained by measuring the power of VCO using spectrum analyzer. Therefore (5-2) becomes

$$S_{21}[dB] = P_{PD} - P_{VCO} \tag{5-3}$$

Once the amplitude of $S_{21}$is calculated, the Control function plots the values from (5-3) versus the frequency vector that user determines before running the program, and calculates the peak frequency and amplitude to verify the resonance parameters of the DUT.

5.6 Experiments and Measurements

After implementing the hardware features and developing the software interfaces of the system, next step is to examine the designed readout circuitry and verify the results using VNA. As mentioned before, the operating range of frequency is determined by the dynamic range of DAC output voltage (0-10V) which leads to an operating range of 1.22 – 2 GHz. The frequency resolution of the system is determined by translating the ΔV_{outDAC} (5-1) into Δf_{outVCO}. Since DAC maps 1-bit to a certain output voltage, then using (5-1), the difference between two consecutive output voltages, ΔV_{outDAC} is calculated as

$$\Delta V_{outDAC} = \frac{(V_{REFP} - V_{REFN})}{2^{20} - 1} \quad (5\text{-}4)$$

where as mentioned before, $V_{REFP} = 10V$, and $V_{REFN} = -10V$, this leads to $\Delta V_{outDAC} = 19.1\mu V$. Using the performance data of VCO given in [85] and the fact that voltage and frequency present a linear relationship from 0 to 10V, the frequency resolution of VCO, and ultimately the proposed network analyzer, is calculated as

$$\Delta f_{system} = \frac{\Delta V_{outDAC} \times \Delta f_{VCO}}{\Delta V_{tuneVCO}} \cong 2kHz \quad (5\text{-}5)$$

where $\Delta V_{outDAC} = 19.1\mu V$, and for two points chosen from the table provided in [85], $\Delta f_{VCO} = 80MHz$, and $\Delta V_{tuneVCO} = 1V$.

In addition, the processing time of the measurement is defined as the time that takes the system to process, calculate, and plot the S21 response of the DUT in GUI. This time is determined by sampling frequency of the ADC, and frequency clock of SSC, the serial communication. According to section 5.4.2, the sampling frequency of ADC is set to its maximum value. However, the SSC clock is set to be 10 kHz. Using these parameters, the processing time is 1 minute and 28 second. This time can be reduced by increasing the clock frequency of SSC for a faster processing time but at the cost of more calculation load on MCU.

To verify the performance and functionality of the proposed system, a few sets of experiments have been considered. First, a group of planar microstrip resonators with different resonance frequencies are used as DUT to display their $S_{21}$and compare with VNA results. This experiment shows the accuracy of the proposed readout circuitry throughout its frequency span (1.2-1.98GHz). These resonators have peak frequencies at 1.72GHz, 1.95GHz, and 1.979GHz. It is worth mentioning that, these microwave resonators are same structures introduced in Chapter 3 and Chapter 4.

The second set of experiments are focused on glucose sensing. The purpose of this experiment is to investigate the capability of the system in capturing the frequency shift of the resonator due to the change in glucose concentration in sample solutions. Naturally, by changing the concentration of glucose, the permittivity of the resulting solution changes. Since microstrip resonators' performance change according to permittivity of the MUT, a shift in the peak frequency is observed. Now, to compare the performance of the system with VNA, the glucose sensing measurements are done using both the proposed readout circuitry and VNA. In these experiments, the modified SRR with extended gap introduced in this thesis (Ch. 3) is used for glucose sensing. This SRR has a resonance frequency at 1.96GHz.

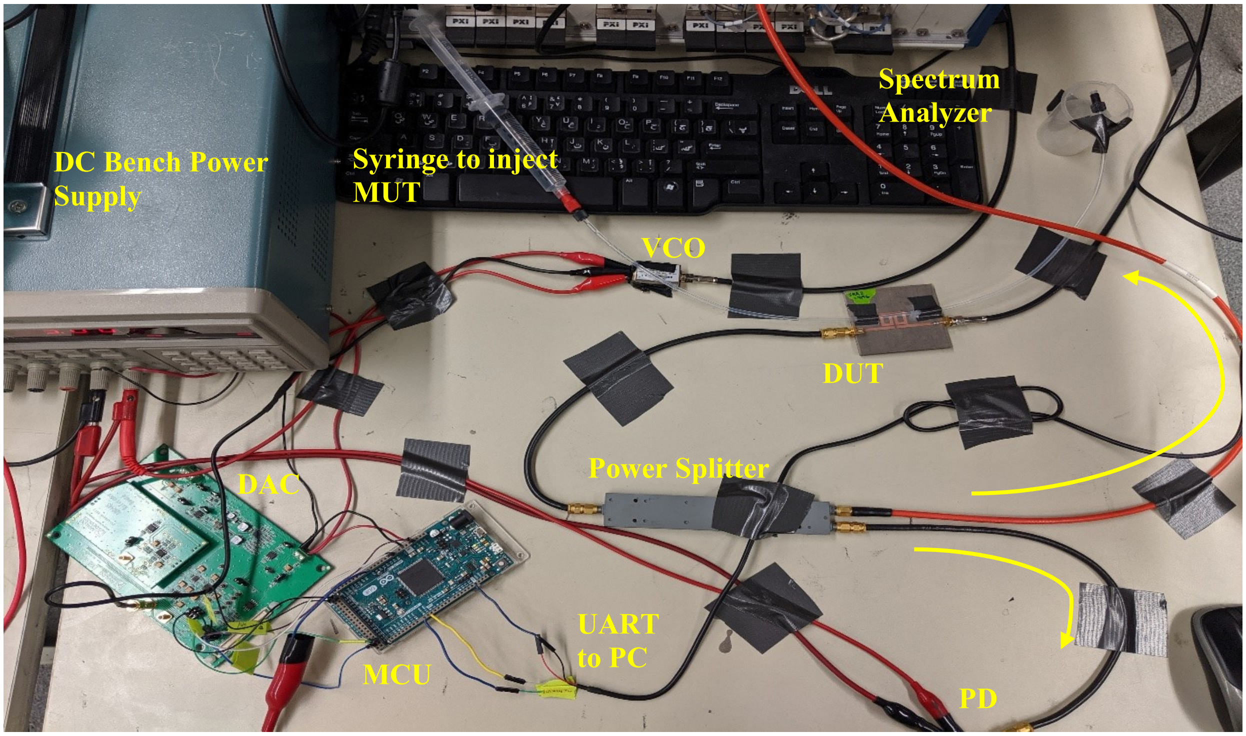

Fig. 5-6 Original experiment setup with power splitter, spectrum analyzer, and the syringe to inject glucose solutions for sensing measurements

These experiments are done using two set-ups, the original setup and the improved one that has the power board, attenuator, and the low pass filter. In the first setup shown in Fig. 5-6, the output power of DUT is going through a power splitter where one port goes to spectrum analyzer (NI PXIe-5601, 10MHz-6.6GHz) for monitoring purposes and the other port is connected to the power detector.

5.6.1 Initial Glucose Sensing Measurements

To verify the application of the proposed readout circuitry in sensing measurements using microwave resonators, it is necessary to perform similar tests on this system. Since glucose sensing measurements have been done in Ch. 3 using the extended gap SRR, this experiment is repeated using the same microwave resonator and glucose solutions with concentration range of 1 gr/dL to 42 gr/dL. The concentration range is chosen to be wide so that low, medium, and high concentrations of glucose in water can be determined using the sensor.

The lower concentration solutions are made by mixing glucose powder in 100mL of water to obtain gr/dL concentrations. For instance, to get a concentration of 5.5gr/dL, 5.5gr of glucose powder is mixed in 100mL of deionized (DI) water. However, for high concentrations of glucose, due to saturation of the mixture, the volume of solvent is increased to 200mL, and ounce is used as the measuring scale for glucose powder. For example, mixing 2oz of glucose in 200mL DI water leads to a 28.35gr/dL solution. In this calculation one ounce is assumed to be 28.35 gram.

After preparing the sample solutions at different concentrations, a PTFE tube is placed on the sensitive region of the sensor (as shown in Fig. 5-64 (b) in Ch. 4), and the sample materials are injected into the tube one at a time when the amplitude of S_{21} of the sensor is measured. This experiment is done using both the VNA and the designed system for comparison purposes. Before adding any enhancive components, such as the attenuator and the LPF, and calibration algorithm to improve the system, an initial set of measurements are done to acquire a primary knowledge of the system functionality. The experiment setup is shown in Fig. 5-6.

Fig. 5-7 presents the initial glucose sensing measurements done by the system (solid lines) versus the VNA (dashed lines). This experiment is done for 4 cases, where the tube is empty, and tube is filled with concentrations of 1.4, 5.5, and 15.1 gr/dL. From the data captured with VNA

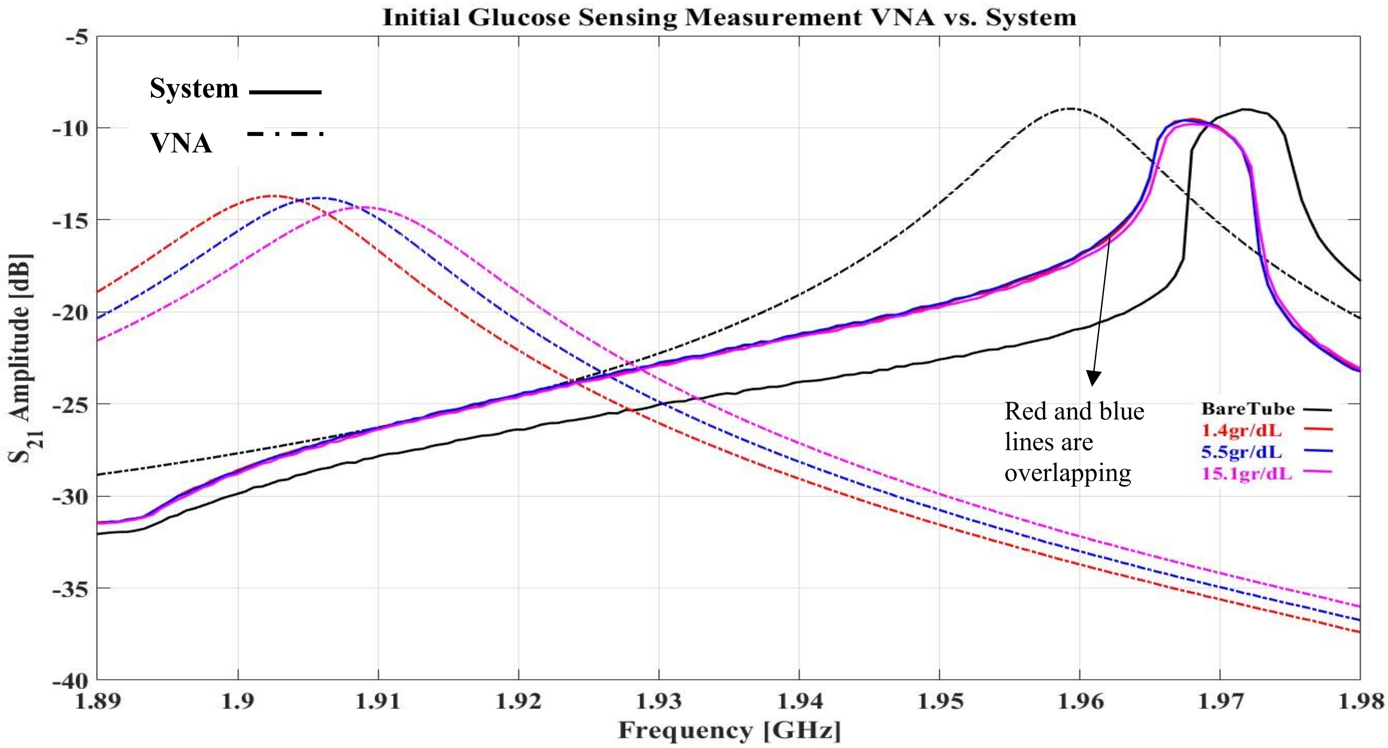

Fig. 5-7 Initial glucose sensing measurements with no enhancive components and calibration

(reference point), it is understood that with increasing the glucose concentration in MUT, an upshift of frequency is expected. On the other hand, even though the system is capable of measuring the transmission profile of the DUT poorly, it fails to determine the frequency shift of the resonator at different concentrations. This is due to instability and inaccuracy of the VCO in generating the frequency span, as well as the unwanted harmonics carried over to PD.

As it is observed from Fig. 5-7, these issues lead to error in both frequency and amplitude of the measured S_{21}. Even though the sensor can distinguish whether the tube is empty or filled with liquid, it cannot separate different concentrations of the sample solutions. This is called switching sensing, which means the sensor is only capable of sensing the existence of material, but fails to provide a spectrum of the MUT's property of interest. The results presented in this figure emphasize on the necessity of enhancing the stability of the VCO and eliminating the unwanted harmonics to generate an accurate frequency spectrum as well as amplitude values.

5.6.2 Effect of Low Pass Filter and Attenuator

As mentioned before, the VCO generates unwanted harmonics which are captured by PD and led to undesired response of the system. In addition, when VCO is directly connected to the DUT the loading effect causes instability in VCO performance and RF signal generation. This leads to inaccurate frequency generation which cause error in the results.

To resolve these issues, the 6dB attenuator is placed after VCO. This humble RF module is a great isolator for VCO to reduce the loading effect, increase the stability in output generation, and enhance the accuracy and performance of the whole system. In addition, the LPF with 3dB attenuation at cut-off frequency of 2.4GHz is added after the attenuator to attenuate the amplitude of the unwanted harmonics and reduce their impact on amplitude of S21 of the DUT. The filter provides 20dB and 40dB attenuation at 1.35× f_{cutoff} and 1.75× f_{cutoff}, respectively [87]. This

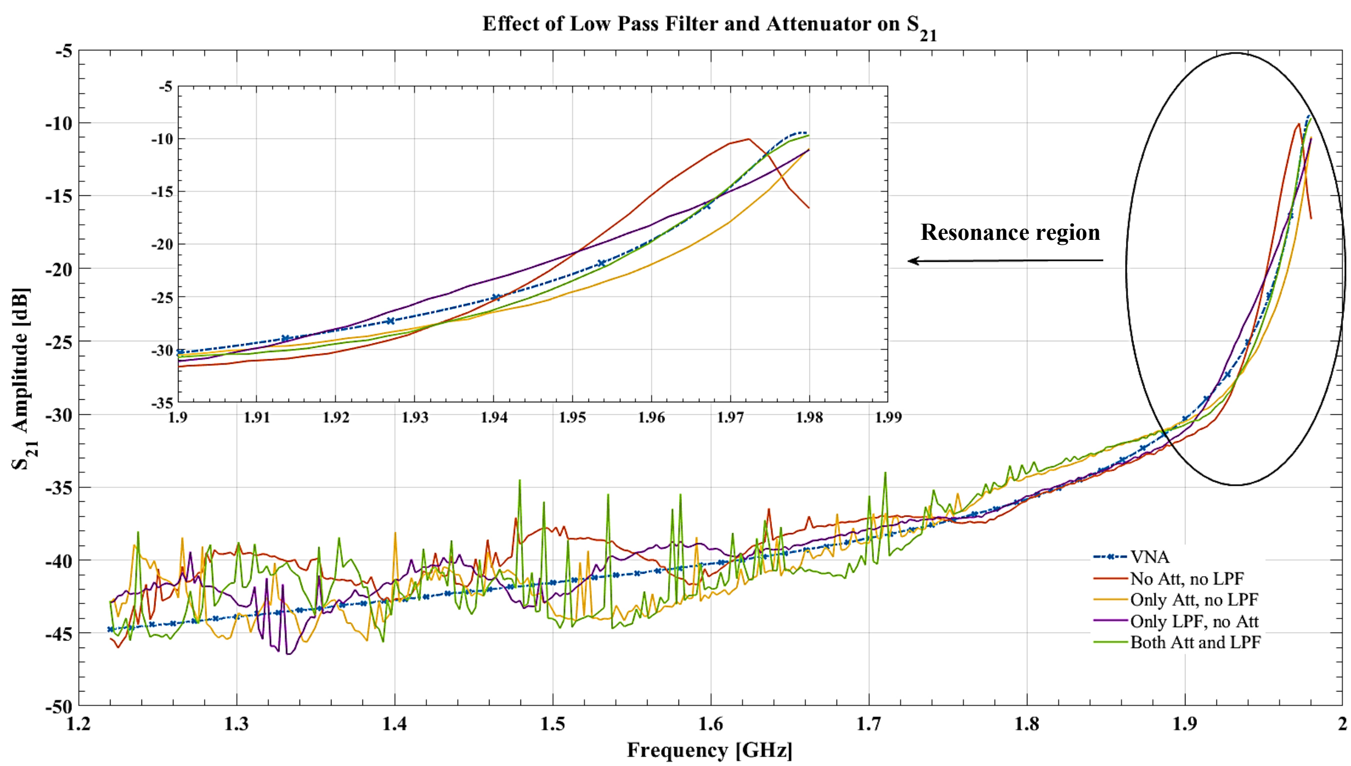

Fig. 5-8 Effect of LPF and Attenuator on the system in 4 possible scenarios

allows for sharp rejection of unwanted higher frequencies. To investigate the effect of Att. and LPF, all 4 possible cases are tested and compared in Fig. 5-8.

The blue curve with markers represents the S21 of the resonator captured by VNA, which is the reference and baseline of this investigation. The case where neither Att, nor the LPF is attached, both amplitude and frequency error is observed in the S21 response. This figure also shows that the result is inaccurate even if one of the components is placed. Therefore, the advantage of adding both attenuator and the LPF (green curve) is the high accuracy S21 measurement that agrees with the reference captured by VNA both in frequency and amplitude values.

However, Fig. 5-8 also shows the downside of the attenuator, and that is reducing the dynamic range of power. When Att brings down the output power of the DUT by 6dB, the measured S21 approaches the limits of power detector which has a power range of -44dB to 15dB. Looking at the VNA curve, the S21 goes below -40dB without any attenuation, therefore when the 6dB attenuator is added to the designed system the lower amplitudes reach even smaller power values, hence hitting the limits. This explains the spikes generated in the curves where Att exists.

Having said that, these values are below -30dB, and more importantly, the sensitive region is around the resonance peak of the DUT. This is the area of interest and where the frequency and amplitude parameters are used for sensing purposes. The enlarged plot shows this area, and once again, it is shown that placing both components (green curve) improve the results and accuracy of the system. Whereas, in the other scenarios, the curves are shifted from the reference (VNA). It is also worth mentioning that, the designed system provides 25-30dB dynamic range for amplitude within the area of interest.

5.6.3 Manual Calibration Procedure

Any system is only as effective as its accuracy in measurements, and this is done by calibrating the system. Calibration process compares the measured data provided by a DUT with those of a standard device with known accuracy. It is common to even calibrate the VNA for a given frequency range and number of points before each measurement.

A full 2-port calibration process in the VNA is done with so many built-in algorithms. The most common one is SOLT (short-open-load-thru) which uses well-defined standards that connect to the ports of interest to measure all the reflections and eliminate any possible errors in matching, directivity, and frequency response. The designed readout circuitry is considered to be a SNA (scalar network analyzer), because it only measures the amplitude of the transmission profile of the DUT (S_{21}). In this system, however, the calibration process is very simple and trivial.

To enhance the accuracy of the system a manual calibration algorithm is implemented to eliminate the errors in calculations which cause offset in the results. In this procedure, before

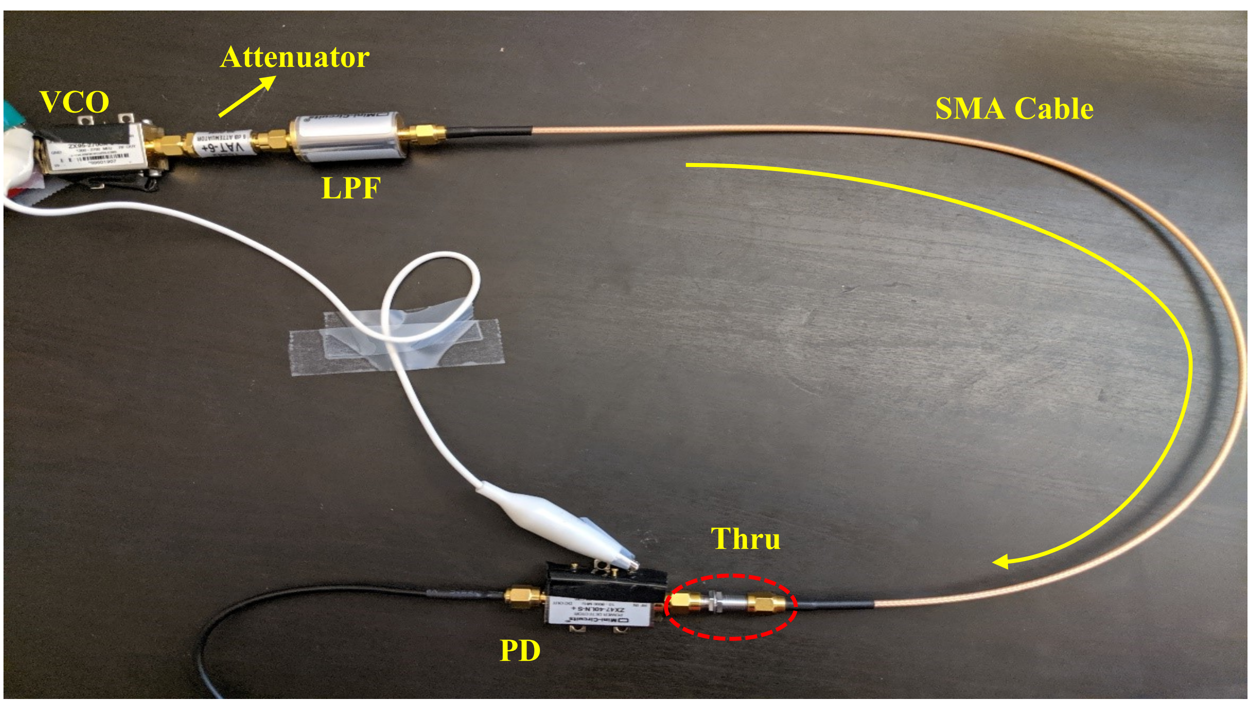

Fig. 5-9 Calibration setup using a female-to-female connector as thru

measuring the DUT, a female-to-female SMA connector is used as thru standard as the device under test. The thru connector is placed between the coaxial SMA cable coming from LPF and PD as shown in Fig. 5-9. Using this setup, first the $S_{21}$of the thru connector is measured within the frequency range of interest with desired number of points specified by the user, then the S_{21} data are saved in a file to be used for calibration. Then, when the DUT is placed, the saved data is subtracted from the output power of the DUT to compensate for the loss in the cable and other sources. The assumption is that female-to-female connector has an ideal $S_{21}$of 0dB, meaning all the power is transmitted and there is no attenuation. Then the following calculations are done based on (5-3):

$S_{21}[Thru] = P_{received,PD,thru} - P_{incident,cable}$, assuming $S_{21}[Thru] = 0dB$, then

$P_{incident,cable} = P_{received,PD,thru} = P_{received,PD}[\text{Calib}]$

Then when connecting the DUT, S_{21}calculation is changed to

$S_{21}[DUT] = P_{received,PD,DUT} - P_{received,PD}[Calib]$

Using the above calculation, the system is calibrated and provides higher accuracy in amplitude of the S_{21}. To present the efficiency and reliability of the system along with its calibration algorithm, three split ring resonators with different resonance behaviour are measured using the designed network analyzer, as well as the VNA.

5.6.4 Resonators Profiles with Improved Setup

After improving the system, a few split ring resonators are measured using the designed network analyzer, and their S21 profile is compared with VNA. The first two of these SRRs represents a peak at resonance frequency, and the third one illustrates a wider band notch. The latter is chosen to show the capability of this system to measure microwave resonators with various type of profiles while providing accurate result in all cases. Fig. 5-10 illustrates the measured transmission profile of these DUTs using proposed system as well as VNA. Also, summarizes the information from the resonance comparison using VNA versus the designed system. These results prove that adding the attenuator and LPF, as well as incorporating the calibration algorithm have improved the system's performance to a comparable level with a VNA.

Table 5-1 Comparison of resonance parameters of the three SRRs using VNA and the readout system

Resonance Parameters	$\boldsymbol{SRR_{(a)}}$	$\boldsymbol{SRR_{(b)}}$	$\boldsymbol{SRR_{(c)}}$
Frequency [GHz]	VNA: 1.979	1.953	1.727
	System: 1.980	1.952	1.726
S_{21} *Amplitude [dB]*	VNA: -9.452	-9.283	-31.99
	System: -9.625	-9.217	-33.45

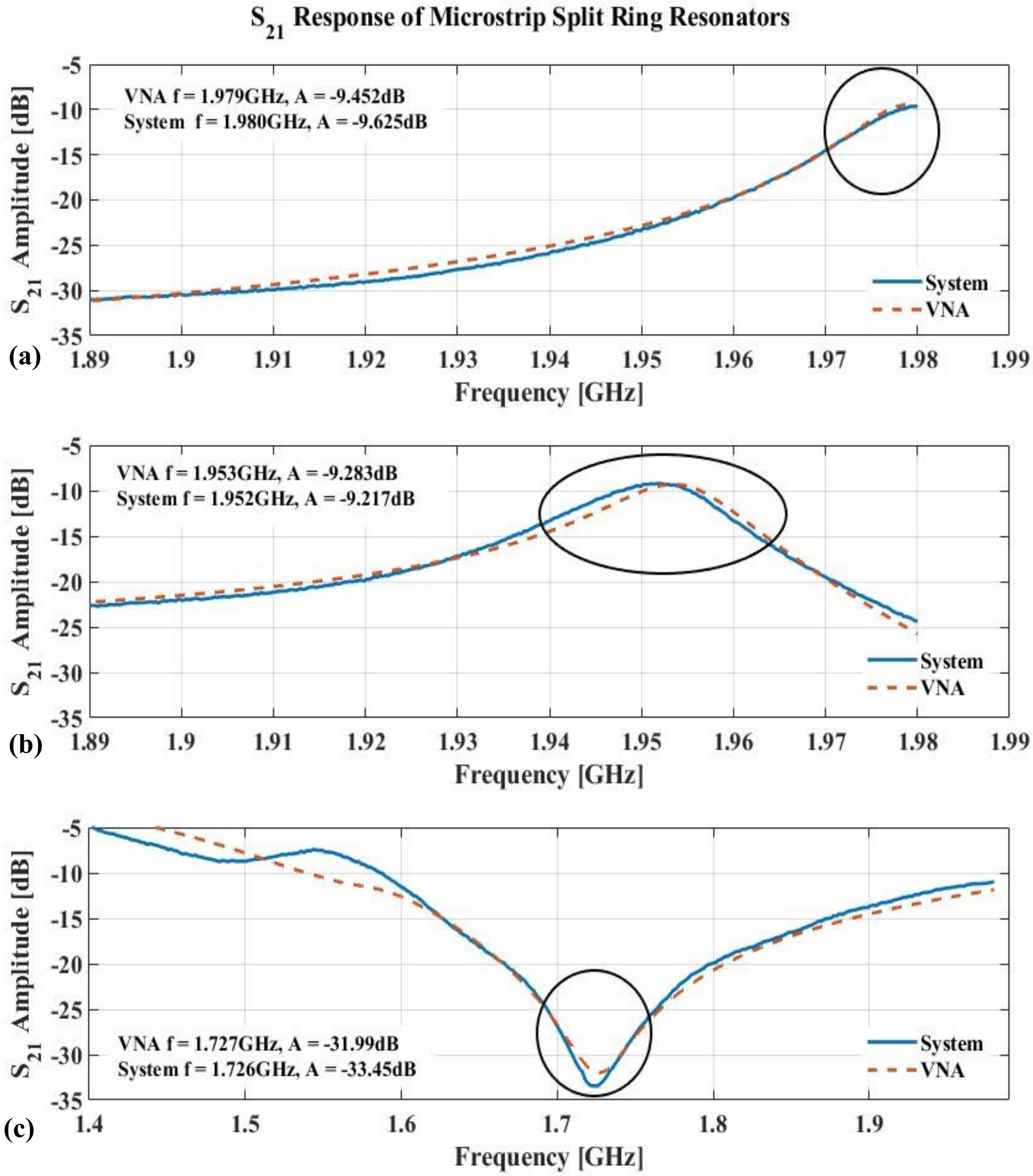

Fig. 5-10 Transmission profile of three resonators ($SRR_{(a)}, SRR_{(b)}, SRR_{(c)}$) measured with the system and VNA

5.6.5 Improved Glucose Sensing Measurements

As mentioned earlier, to increase the stability and accuracy of the network analyzer, the attenuator and LPF are added to the hardware (shown in Fig. 5-11), and the calibration algorithm is developed and applied on the calculation of S_{21}. The same glucose sensing measurement

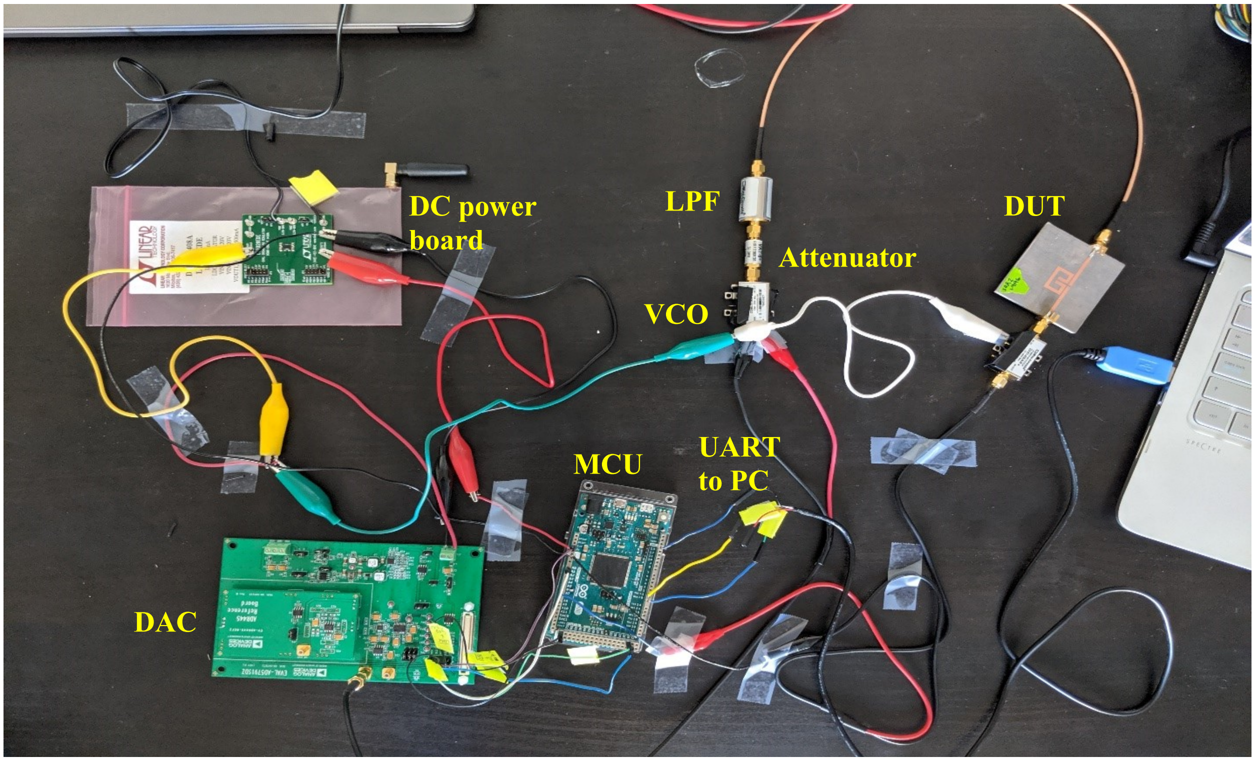

Fig. 5-11 Improved setup that includes the power board, attenuator and the low pass filter

explained in previous section is repeated with the enhanced system. In addition, higher concentration of glucose (28.35 gr/dL) is also tested in this experiment to show the dynamic range of sensitivity of this system. As it is illustrated in Fig. 5-12, the results have been substantially improved as opposed to the initial data. This figure shows a close agreement between the designed system and the VNA. This is due to eliminating the errors generating from the VCO, and also calibrating the system to compensate for any loss in the cables.

This figure shows that frequency and amplitude spectrum of the system is generated with minimum error. The offset in the peak can be explained due to poor holding of the PTFE tube on the sensor. It is very well possible that the tube is slightly moved after VNA tests are done and before the system measurements start. It is important to note that, this system is not only capable of sensing the presence of material, but also is accurate to distinguish between various

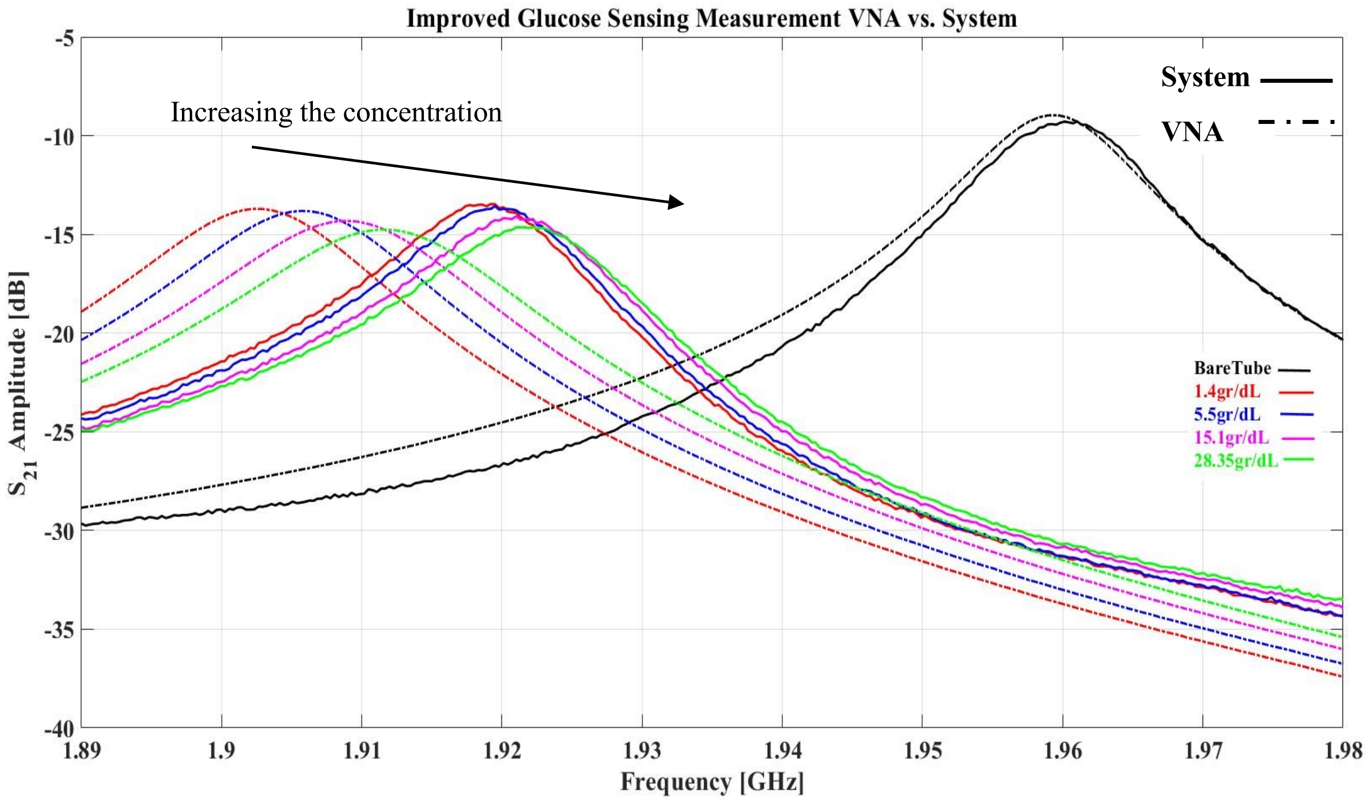

Fig. 5-12 Glucose sensing measurements using the enhanced system as compared to the VNA

concentrations. This leads to a full sensitivity spectrum where the system can provide information on low, medium, and high concentrations of glucose in MUT. The designed system shows the upshift in frequency when increasing the glucose concentration in sample solutions; this agrees with the behaviour of VNA. For more accurate glucose sensing measurements, it is recommended to use a more sensitive sensor which shows bigger shifts in frequency. This does not imply the system is incapable and low-precision, but rather shows the limitations of the DUT used in the experiment.

5.7 Summary

In this study, a simple, novel, compact, and high-precision readout circuitry is developed that can be used as a measuring and/or monitoring instrument for microwave resonance based sensors in the field. The motivation of this study is the fact that conventional VNAs are too large and expensive to be used for reading microwave resonators in the field. In addition, VNAs provide a wide range of applications and features that may not be used when only amplitude of transmission response is of an interest.

The proposed system is capable of measuring the amplitude of $S_{21}$of any microwave resonators in the range of its operation. This system operates from 1.2 – 1.98GHz, and has a frequency resolution of 2 kHz. In addition, its dynamic range of amplitude is from -44dB to +15dB. Developing this system requires a knowledge of handling RF components, configuring embedded systems such as microcontrollers, and implementing a user-friendly software that is available for users.

There are several factors that impact the accuracy of the system, such as supplying a clean and low-noise DC power to digital and analog components separately, stabilizing the VCO output for an accurate frequency span generation, and eliminating the unwanted harmonics of VCO using a LPF. It is also important to develop a calibration algorithm to compensate for any power loss in the cables and other components. This work shows that without considering these factors, the measured S_{21}contains error in both frequency and amplitude values, and provides inaccurate and unreliable performance.

Using the 6dB attenuator to eliminate the loading effects on VCO and the LPF at 2.4GHz to remove the unwanted harmonics, the performance of the system is considerably enhanced and the final results align with the data captured by the VNA. This proves that the designed system is a great candidate to be paired with any microwave resonance based sensor for sensing applications in the field. Compared to the VNA, the designed readout circuitry is extensively cheaper, smaller in size, and mobile which comes with a user-friendly interface. So far, the limitations of microwave sensors have been the lack of in-situ measuring instrument. Now, this successful work allows for a wide range of applications and commercialization of both the system and microwave sensors.

6 Conclusion and Future Work

This chapter summarizes the achievements and accomplishments of this thesis, and it also provides suggestions for future works.

6.1 Thesis Conclusions and Accomplishments

This thesis started with investigating the novel sensitivity enhancement techniques for passive planar microstrip ring resonators for material characterization, specifically liquid sensing applications in biomedical and food/beverage industries.

In Ch. 3, three different configurations with the conventional split ring resonator were analyzed in the resonant frequency of 2 GHz. The best configuration was chosen to be used in sensing for biomedical applications of glucose concentration sensing. Then, it was found that geometrically modifying the gap of the resonator with an inward extension results in sensitivity enhancement. After performing the glucose sensing measurements on the newly developed sensor, a 20% sensitivity improvement has been achieved.

In Ch. 4, three microwave resonant-based sensors were compared in terms of their sensitivity and performance for methanol-in-water sensing. These microwave resonators were conventional CSRR, SRR with extended gap from Ch. 3, and Circular-SRR with resonance frequencies of 1.7, 1.9, and 3.6 GHz, respectively. This work defined sensitivity from the volume of MUT's perspective. The electric field distribution and hot-spot of each resonator were simulated and analyzed, and sensitivity analysis were performed along with dielectric constant studies using Maxwell-Garnett's approximation. The most sensitive resonator was chosen to be examined further in terms of MUT placement either on top of the hot-spot or inside the substrate directly below the sensitive region.

It was concluded that, placing the MUT inside the substrate and between the resonator and ground leads to a significant enhancement in the sensitivity and performance of the conventional SRR. This results provided better sensitivity and accuracy for lossy mediums, such as liquids with verification on methanol-in-water concentration sensing within range of 0-50%. Another accomplishment of this study was integrating the MUT-in-substrate technique with microfluidic channel to prove the feasibility of using the embedding technique in small-scale sensing applications in biomedical and biological research.

In Ch. 5, the objective was to design and develop a RF sensor readout system to use as a measuring instrument for microwave resonance-based sensors in practice. This work successfully delivered an accurate, cheap, and mobile product that measures the amplitude of the transmission profile of any DUT in the range of 1.2 - 1.98GHz. This system had the frequency resolution of 2kHz and dynamic range of amplitude from -44dB to +15dB, which is ideal for resonance-based sensing applications. A simple and trivial GUI was made for the user to easily operate the system with their desired DUT and application. A calibration procedure was also implemented within the GUI software to increase the accuracy and enhance the performance of the system.

6.2 Suggestions for Future Work

The suggestions for improving this research are as follow:

- In Ch. 3, the sensitivity of the passive resonator can be increased by introducing an active feed-back loop. This method considerably increases the quality factor of the resonator, and hence the resolution of the passive sensor. Higher resolution in sensing is under exploration for next generations of the proposed sensor in future work.

- In Ch. 4, embedding the MUT inside the substrate and manufacturing such sensor that has this capability is a big challenge. However, sophisticated micro/nano fabrication procedures can make it possible. In addition, with the rising popularity of 3D printers in research, design and building this type of sensor with the ability to engulf the MUT within its substrate can be simply done by prevailing innovative 3D-printing technologies.
- In Ch. 5, separate modules and components are used to build the hardware of the system. This work can improve by employing all the analog and digital components in one compact PCB using high-end IC chips and integrative components. In terms of software development, more features can be added to the GUI depending on the application, such as measuring the quality factor of the device under test. The frequency span of the system can also be improved by increasing the reference voltage of DAC which is directly dependent of the voltage supplied to DAC.
- In Ch. 5, the scanning time of the system can also be improved by modifying the firmware of the microcontroller to provide higher clock frequency to SSC module for faster communication with the hardware.

References

[1] R. Di Sante, “Fibre Optic Sensors for Structural Health Monitoring of Aircraft Composite Structures: Recent Advances and Applications,” *Sensors*, vol. 15, no. 8, pp. 18666–18713, 2015.

[2] J. Villatoro, A. Van Newkirk, E. Antonio-Lopez, J. Zubia, A. Schülzgen, and R. Amezcua-Correa, “Ultrasensitive vector bending sensor based on multicore optical fiber,” *Opt. Lett.*, vol. 41, no. 4, pp. 832–835, 2016.

[3] V. A. Trofimov and S. A. Varentsova, “Essential Limitations of the Standard THz TDS Method for Substance Detection and Identification and a Way of Overcoming Them,” *Sensors*, vol. 16, no. 4, 2016.

[4] M. Abdolrazzaghi and M. Daneshmand, “Enhanced Q double resonant active sensor for humidity and moisture effect elimination,” in *Microwave Symposium (IMS), 2016 IEEE MTT-S International*, 2016, pp. 1–3.

[5] M. Abdolrazzaghi, M. Daneshmand, and A. K. Iyer, “Strongly Enhanced Sensitivity in Planar Microwave Sensors Based on Metamaterial Coupling,” *IEEE Trans. Microw. Theory Tech.*, vol. 66, no. 4, pp. 1843–1855, Apr. 2018.

[6] M. Abdolrazzaghi, M. H. Zarifi, W. Pedrycz, and M. Daneshmand, “Robust {Ultra-High} Resolution Microwave Planar Sensor Using Fuzzy Neural Network Approach,” *IEEE Sens. J.*, vol. 17, no. 2, pp. 323–332, Jan. 2017.

[7] M. Fayaz, M. H. Zarifi, M. Abdolrazzaghi, P. Shariaty, Z. Hashisho, and M. Daneshmand, “A Novel Technique for Determining the Adsorption Capacity and Breakthrough Time of

Adsorbents Using a Noncontact {High-Resolution} Microwave Resonator Sensor," *Environ. Sci. Technol.*, vol. 51, no. 1, pp. 427–435, Jan. 2017.

[8] M. H. Zarifi, S. Farsinezhad, M. Abdolrazzaghi, M. Daneshmand, and K. Shankar, "Selective microwave sensors exploiting the interaction of analytes with trap states in {TiO2} nanotube arrays," *Nanoscale*, vol. 8, no. 14, pp. 7466–7473, Jan. 2016.

[9] H. J. Lee, K. A. Hyun, and H. Il Jung, "A high-Q resonator using biocompatible materials at microwave frequencies," *Appl. Phys. Lett.*, vol. 104, no. 2, p. 023509, Jan. 2014.

[10] M. H. Zarifi, M. Fayaz, J. Goldthorp, M. Abdolrazzaghi, Z. Hashisho, and M. Daneshmand, "Microbead-assisted high resolution microwave planar ring resonator for organic-vapor sensing," *Appl. Phys. Lett.*, vol. 106, no. 6, p. 62903, Feb. 2015.

[11] N. Sharafadinzadeh, M. Abdolrazzaghi, and M. Daneshmand, "Investigation on planar microwave sensors with enhanced sensitivity from microfluidic integration," *Sensors Actuators A Phys.*, p. 111752, Nov. 2019.

[12] M. Hofmann, "Six-port-based microwave spectroscopy of dielectric materials for non-invasive ISM applications," d-nb.info, 2015.

[13] S. Pinon *et al.*, "Fabrication and characterization of a fully integrated biosensor associating microfluidic device and {RF} circuit," in *2012 {IEEE/MTT-S} International Microwave Symposium Digest*, 2012, pp. 1–3.

[14] M. Abdolrazzaghi, M. H. Zarifi, M. Daneshmand, and C. F. A. Floquet, "Contactless asphaltene solid particle deposition monitoring using active microwave resonators," in *2016 {IEEE} {SENSORS}*, 2016, pp. 1–3.

[15] M. H. Zarifi, T. Thundat, and M. Daneshmand, "High resolution microwave microstrip resonator for sensing applications," *Sens. Actuators A Phys.*, vol. 233, pp. 224–230, Sep. 2015.

[16] M. A. Karimi, M. Arsalan, and A. Shamim, "Low Cost and Pipe Conformable {Microwave-Based} {Water-Cut} Sensor," *IEEE Sens. J.*, vol. 16, no. 21, pp. 7636–7645, Nov. 2016.

[17] S. W. Kim, S. B. Choi, Y.-J. An, B.-H. Kim, D. W. Kim, and J.-G. Yook, "Heart Rate Detection During Sleep Using a Flexible {RF} Resonator and {Injection-Locked} {PLL} Sensor," *IEEE Trans. Biomed. Eng.*, vol. 62, no. 11, pp. 2568–2575, Nov. 2015.

[18] H. Li *et al.*, "{Multi-Frequency} Measurement of Volatile Organic Compounds With a {Radio-Frequency} Interferometer," *IEEE Sens. J.*, vol. 17, no. 11, pp. 3323–3331, Jun. 2017.

[19] C. S. Lee, C. Y. Wu, and Y. L. Kuo, "Wearable Bracelet Belt Resonators for Noncontact Wrist Location and Pulse Detection," *IEEE Trans. Microw. Theory Tech.*, vol. PP, no. 99, pp. 1–8, 2017.

[20] Y.-J. An, B.-H. Kim, G.-H. Yun, S.-W. Kim, S.-B. Hong, and J.-G. Yook, "Flexible {Non-Constrained} {RF} Wrist Pulse Detection Sensor Based on Array Resonators," *IEEE Trans. Biomed. Circuits Syst.*, vol. 10, no. 2, pp. 300–308, Apr. 2016.

[21] R. Dhakal *et al.*, "An exploration of ocular glucose levels with flexible RF biosensor using polyethylene terephthalate," in *2014 IEEE MTT-S International Microwave Workshop Series on RF and Wireless Technologies for Biomedical and Healthcare Applications (IMWS-Bio2014)*, 2014, pp. 1–3.

[22] V. Rawat, S. Dhobale, and S. N. Kale, “Ultra-fast selective sensing of ethanol and petrol using microwave-range metamaterial complementary split-ring resonators,” *J. Appl. Phys.*, vol. 116, no. 16, p. 164106, Oct. 2014.

[23] M. Abdolrazzaghi, M. H. Zarifi, and M. Daneshmand, “Wireless Communication in {Feedback-Assisted} Active Sensors,” *IEEE Sens. J.*, vol. 16, no. 22, pp. 8151–8157, Nov. 2016.

[24] M. Abdolrazzaghi, M. H. Zarifi, and M. Daneshmand, “Sensitivity enhancement of split ring resonator based liquid sensors,” in *2016 {IEEE} {SENSORS}*, 2016, pp. 1–3.

[25] H.-J. Lee and J.-G. Yook, “Recent research trends of radio-frequency biosensors for biomolecular detection,” *Biosens. Bioelectron.*, vol. 61, pp. 448–459, Nov. 2014.

[26] M. U. Memon, H. Jeong, and S. Lim, “Metamaterial-Inspired Radio Frequency Based Touchpad Sensor System,” *IEEE Trans. Instrum. Meas.*, p. 1, 2019.

[27] A. Mason, O. Korostynska, M. Ortoneda-Pedrola, A. Shaw, and A. Al-Shamma’a, “A resonant co-planar sensor at microwave frequencies for biomedical applications,” *Sens. Actuators A Phys.*, vol. 202, pp. 170–175, Nov. 2013.

[28] R. Khalifeh, B. Lescop, F. Gallée, and S. Rioual, “Development of a radio frequency resonator for monitoring water diffusion in organic coatings,” *Sens. Actuators A Phys.*, vol. 247, pp. 30–36, Aug. 2016.

[29] A. A. Abduljabar, A. Porch, and D. A. Barrow, “Real-time measurements of size, speed, and dielectric property of liquid segments using a microwave microfluidic sensor,” in *2014 {IEEE} {MTT-S} International Microwave Symposium ({IMS2014})*, 2014, pp. 1–4.

[30] M. H. Zarifi, A. Sohrabi, P. M. Shaibani, M. Daneshmand, and T. Thundat, "Detection of Volatile Organic Compounds Using Microwave Sensors," *IEEE Sens. J.*, vol. 15, no. 1, pp. 248–254, Jan. 2015.

[31] H. Moghadas, M. Daneshmand, and P. Mousavi, "A passive non-contact microwave loop resonance sensor for liquid interface," *Sens. Actuators B Chem.*, vol. 241, pp. 96–98, Mar. 2017.

[32] L. Yang, R. Zhang, D. Staiculescu, C. P. Wong, and M. M. Tentzeris, "A Novel Conformal {RFID-Enabled} Module Utilizing {Inkjet-Printed} Antennas and Carbon Nanotubes for {Gas-Detection} Applications," *IEEE Antennas Wirel. Propag. Lett.*, vol. 8, pp. 653–656, 2009.

[33] A. Chahadih, P. Y. Cresson, Z. Hamouda, S. Gu, C. Mismer, and T. Lasri, "Microwave/microfluidic sensor fabricated on a flexible kapton substrate for complex permittivity characterization of liquids," *Sens. Actuators. A. Phys.*, vol. 229, pp. 128–135, 2015.

[34] M. H. Zarifi *et al.*, "A Microwave Ring Resonator Sensor for Early Detection of Breaches in Pipeline Coatings," *IEEE Trans. Ind. Electron.*, vol. 65, no. 2, pp. 1626–1635, Feb. 2018.

[35] O. Korostynska, A. Mason, M. Ortoneda-Pedrola, and A. Al-Shamma'a, "Electromagnetic wave sensing of NO3 and COD concentrations for real-time environmental and industrial monitoring," *Sens. Actuators. B. Chem.*, vol. 198, pp. 49–54, 2014.

[36] M. H. Zarifi, M. Rahimi, M. Daneshmand, and T. Thundat, "Microwave ring resonator-based non-contact interface sensor for oil sands applications," *Sens. Actuators B Chem.*,

vol. 224, pp. 632–639, 2016.

[37] A. Salim and S. Lim, “Complementary {Split-Ring} {Resonator-Loaded} Microfluidic Ethanol Chemical Sensor,” *Sensors*, vol. 16, no. 11, Oct. 2016.

[38] A. Sieg, R. H. Guy, and M. B. Delgado-Charro, “Noninvasive and minimally invasive methods for transdermal glucose monitoring,” *Diabetes Technol. Ther.*, vol. 7, no. 1, pp. 174–197, Feb. 2005.

[39] N.-Y. Kim, K. K. Adhikari, R. Dhakal, Z. Chuluunbaatar, C. Wang, and E.-S. Kim, “Rapid, sensitive, and reusable detection of glucose by a robust radiofrequency integrated passive device biosensor chip,” *Sci. Rep.*, vol. 5, p. 7807, Jan. 2015.

[40] V. Turgul and I. Kale, “Characterization of the complex permittivity of glucose/water solutions for noninvasive {RF/Microwave} blood glucose sensing,” in *2016 {IEEE} International Instrumentation and Measurement Technology Conference Proceedings*, 2016, pp. 1–5.

[41] A. Ebrahimi, W. Withayachumnankul, S. F. Al-Sarawi, and D. Abbott, “Microwave microfluidic sensor for determination of glucose concentration in water,” in *2015 {IEEE} 15th Mediterranean Microwave Symposium ({MMS})*, 2015, pp. 1–3.

[42] T. Yilmaz and Y. Hao, “Electrical property characterization of blood glucose for on-body sensors,” in *Proceedings of the 5th European Conference on Antennas and Propagation ({EUCAP})*, 2011, pp. 3659–3662.

[43] M. Hofmann, G. Fischer, R. Weigel, and D. Kissinger, “{Microwave-Based} Noninvasive Concentration Measurements for Biomedical Applications,” *IEEE Trans. Microw. Theory*

Tech., vol. 61, no. 5, pp. 2195–2204, May 2013.

[44] J. Kim, A. Babajanyan, A. Hovsepyan, K. Lee, and B. Friedman, "Microwave dielectric resonator biosensor for aqueous glucose solution," *Rev. Sci. Instrum.*, vol. 79, no. 8, p. 86107, Aug. 2008.

[45] K. Saeed, A. C. Guyette, I. C. Hunter, and R. D. Pollard, "Microstrip Resonator Technique for Measuring Dielectric Permittivity of Liquid Solvents and for Solution Sensing," in *2007 {IEEE/MTT-S} International Microwave Symposium*, 2007, pp. 1185–1188.

[46] "What is a Vector Network Analyzer, VNA » Electronics Notes." [Online]. Available: https://www.electronics-notes.com/articles/test-methods/rf-vector-network-analyzer-vna/what-is-a-vna.php. [Accessed: 20-Oct-2019].

[47] "What is a Vector Network Analyzer and how does it work? | Tektronix." [Online]. Available: https://www.tek.com/dokument/primer/what-vector-network-analyzer-and-how-does-it-work. [Accessed: 20-Oct-2019].

[48] D. M. Pozar, *Microwave Engineering*, Fourth. Wiley Subscription Services, Inc., A Wiley Company.

[49] M. A. Abou-Khousa, M. A. Baumgartner, S. Kharkovsky, and R. Zoughi, "Novel and simple high-frequency single-port vector network analyzer," *IEEE Trans. Instrum. Meas.*, vol. 59, no. 3, pp. 534–542, Mar. 2010.

[50] M. Puentes, C. Weiß, M. Schüßler, and R. Jakoby, "Sensor array based on split ring resonators for analysis of organic tissues," in *IEEE MTT-S International Microwave*

Symposium Digest, 2011.

[51] M. Schüßeler, C. Mandel, M. Puentes, and R. Jakoby, “Metamaterial inspired microwave sensors,” in *IEEE Microwave Magazine*, 2012, vol. 13, no. 2, pp. 57–68.

[52] A. Bababjanyan, H. Melikyan, S. Kim, J. Kim, K. Lee, and B. Friedman, “Real-Time Noninvasive Measurement of Glucose Concentration Using a Microwave Biosensor,” *J. Sensors*, vol. 2010, 2010.

[53] J. H. Goh, A. Mason, A. I. Al-Shamma’a, M. Field, and P. Browning, “LACTATE DETECTION USING MICROWAVE SPECTROSCOPY FOR IN-SITU MEDICAL APPLICATIONS,” *Int. J. Smart Sens. Intell. Syst.*, vol. 4, no. 3, 2011.

[54] C. Bernou, D. Rebière, and J. Pistré, “Microwave sensors: a new sensing principle. Application to humidity detection,” *Sens. Actuators. B. Chem.*, vol. 68, no. 1, pp. 88–93, 2000.

[55] O. Korostynska, A. Mason, and A. Al-Shamma’a, “Microwave sensors for the non-invasive monitoring of industrial and medical applications,” *Sens. Rev.*, vol. 34, no. 2, pp. 182–191, 2014.

[56] H.-J. Lee, H.-S. Lee, K.-H. Yoo, and J.-G. Yook, “DNA sensing using split-ring resonator alone at microwave regime,” *J. Appl. Phys.*, vol. 108, no. 1, p. 14908, 2010.

[57] H.-J. Lee, J.-H. Lee, S. Choi, I.-S. Jang, J.-S. Choi, and H.-I. Jung, “Asymmetric split-ring resonator-based biosensor for detection of label-free stress biomarkers,” *Appl. Phys. Lett.*, vol. 103, no. 5, p. 53702, 2013.

[58] A. K. Horestani, C. Fumeaux, S. F. Al-Sarawi, and D. Abbott, “Displacement Sensor

Based on Diamond-Shaped Tapered Split Ring Resonator," *IEEE Sens. J.*, vol. 13, no. 4, pp. 1153–1160, Apr. 2013.

[59] J. Naqui, M. Durán-Sindreu, and F. Martín, "Novel sensors based on the symmetry properties of split ring resonators (SRRs)," *Sensors*, vol. 11, no. 8, pp. 7545–7553, 2011.

[60] A. A. Abduljabar, D. J. Rowe, A. Porch, and D. A. Barrow, "Novel microwave microfluidic sensor using a microstrip split-ring resonator," *IEEE Trans. Microw. Theory Tech.*, vol. 62, no. 3, pp. 679–688, 2014.

[61] A. Ebrahimi, W. Withayachumnankul, S. Al-Sarawi, and D. Abbott, "{High-Sensitivity} {Metamaterial-Inspired} Sensor for Microfluidic Dielectric Characterization," *IEEE Sens. J.*, vol. 14, no. 5, pp. 1345–1351, May 2014.

[62] M. S. Boybay and O. M. Ramahi, "Material Characterization Using Complementary Split-Ring Resonators," *IEEE Trans. Instrum. Meas.*, vol. 61, no. 11, pp. 3039–3046, Nov. 2012.

[63] O. Korostynska, A. Mason, and A. I. Al-Shammaa, "Flexible microwave sensors for real-time analysis of water contaminants," *J. Electromagn. Waves Appl.*, vol. 27, no. 16, pp. 2075–2089, Nov. 2013.

[64] A. K. Horestani, D. Abbott, and C. Fumeaux, "Rotation sensor based on horn-shaped split ring resonator," *IEEE Sensors Journal*, vol. 13, no. 8. pp. 3014–3015, 2013.

[65] J. Naqui and F. Martin, "Transmission lines loaded with bisymmetric resonators and their application to angular displacement and velocity sensors," *IEEE Trans. Microw. Theory Tech.*, vol. 61, no. 12, pp. 4700–4713, Dec. 2013.

[66] L. Su, J. Mata-Contreras, P. Velez, and F. Martin, “Splitter/combiner microstrip sections loaded with pairs of Complementary Split Ring Resonators (CSRRs): Modeling and optimization for differential sensing applications,” *IEEE Trans. Microw. Theory Tech.*, vol. 64, no. 12, pp. 4362–4370, Dec. 2016.

[67] A. K. Horestani, J. Naqui, D. Abbott, C. Fumeaux, and F. Martín, “Two-dimensional displacement and alignment sensor based on reflection coefficients of open microstrip lines loaded with split ring resonators,” *Electron. Lett.*, vol. 50, no. 8, pp. 620–622, Apr. 2014.

[68] C. Sen Lee and C. L. Yang, “Complementary split-ring resonators for measuring dielectric constants and loss tangents,” *IEEE Microw. Wirel. Components Lett.*, vol. 24, no. 8, pp. 563–565, 2014.

[69] L. Su, J. Mata-Contreras, P. Vélez, A. Fernández-Prieto, and F. Martín, “Analytical method to estimate the complex permittivity of oil samples,” *Sensors (Switzerland)*, vol. 18, no. 4, Apr. 2018.

[70] P. Velez, L. Su, K. Grenier, J. Mata-Contreras, D. Dubuc, and F. Martin, “Microwave Microfluidic Sensor Based on a Microstrip Splitter/Combiner Configuration and Split Ring Resonators (SRRs) for Dielectric Characterization of Liquids,” *IEEE Sens. J.*, vol. 17, no. 20, pp. 6589–6598, Oct. 2017.

[71] P. Velez, K. Grenier, J. Mata-Contreras, D. Dubuc, and F. Martin, “Highly-sensitive microwave sensors based on Open Complementary Split Ring Resonators (OCSRRs) for dielectric characterization and solute concentration measurement in liquids,” *IEEE Access*, vol. 6, pp. 48324–48338, Aug. 2018.

[72] P. Velez, J. Munoz-Enano, K. Grenier, J. Mata-Contreras, D. Dubuc, and F. Martin, "Split Ring Resonator-Based Microwave Fluidic Sensors for Electrolyte Concentration Measurements," *IEEE Sens. J.*, vol. 19, no. 7, pp. 2562–2569, Apr. 2019.

[73] C. L. Yang, C. Sen Lee, K. W. Chen, and K. Z. Chen, "Noncontact measurement of complex permittivity and thickness by using planar resonators," *IEEE Trans. Microw. Theory Tech.*, vol. 64, no. 1, pp. 247–257, Jan. 2016.

[74] M. H. Zarifi and M. Daneshmand, "Non-contact liquid sensing using high resolution microwave microstrip resonator," in *Microwave Symposium (IMS), 2015 IEEE MTT-S International*, 2015, pp. 1–4.

[75] S. R. Narayanan, T. I. Valdez, and W. Chun, "Design and Operation of an Electrochemical Methanol Concentration Sensor for Direct Methanol Fuel Cell Systems," *Electrochem. Solid-State Lett.*, vol. 3, no. 3, pp. 117–120, 2000.

[76] R. J. Stanis *et al.*, "Evaluation of hydrogen and methanol fuel cell performance of sulfonated diels alder poly(phenylene) membranes," *J. Power Sources*, vol. 195, no. 1, pp. 104–110, 2010.

[77] S. Celik and M. D. Mat, "Measurement and estimation of species distribution in a direct methanol fuel cell," *Int. J. Hydrogen Energy*, vol. 35, no. 5, pp. 2151–2159, 2010.

[78] Y.-N. Wang, C.-C. Liu, R.-J. Yang, W.-J. Ju, and L.-M. Fu, "Microfluidic distillation chip for methanol concentration detection," *Anal. Chim. Acta*, vol. 912, pp. 97–104, 2016.

[79] C. Wongchoosuk, A. Wisitsoraat, A. Tuantranont, and T. Kerdcharoen, "Portable electronic nose based on carbon nanotube-SnO2 gas sensors and its application for

detection of methanol contamination in whiskeys," *Sens. Actuators. B. Chem.*, vol. 147, no. 2, pp. 392–399, 2010.

[80] J. Yeo and J.-I. Lee, "High-Sensitivity Microwave Sensor Based on An Interdigital-Capacitor-Shaped Defected Ground Structure for Permittivity Characterization," *Sensors*, vol. 19, no. 3, 2019.

[81] A. M. Albishi and O. M. Ramahi, "Highly Sensitive Microwaves Sensors for Fluid Concentration Measurements," *IEEE Microw. Wirel. Components Lett.*, vol. 28, no. 4, pp. 287–289, Apr. 2018.

[82] Y. Wei and S. Sridhar, "Technique for measuring the frequency-dependent complex dielectric constants of liquids up to 20 GHz," *Rev. Sci. Instrum.*, vol. 60, no. 9, pp. 3041–3046, 1989.

[83] V. A. Markel, "Introduction to the Maxwell Garnett approximation: tutorial," *J. Opt. Soc. Am. A. Opt. Image Sci. Vis.*, vol. 33, no. 7, pp. 1244–1256, 2016.

[84] L. Noise and M. L. Regulator, "DEMONSTRATION CIRCUIT 1408," pp. 1–3.

[85] V. S.- Port, R. Tivity, C. A. P. Modulation, M. Max, and M. Max, "Voltage Controlled Oscillator," pp. 2–3.

[86] "SMA Fixed Attenuator," p. 151107.

[87] "Low Pass Filter 50," vol. 0003, no. 718, p. 350166.

[88] M. Ratings, "Power Detector," pp. 2–5.

[89] O. Technology, W. P. O. Box, and U. S. A. T. Fax, "EVAL-AD5791SDZ User Guide UG-1152 with Single and Dual Supply EVAL-AD5791SDZ User Guide."

[90] A. S. A. Mcu, “SAM3X / SAM3A Series.”

[91] D. Sheet, “Voltage Output DAC Data Sheet,” 2018.

Appendix A

Manual Instructions to Use RF Sensor Readout System

A. 1 Calibration Procedure

After turning on the system and before connecting and measuring the resonator, the user needs to calibrate the system according to their desired range of frequency and number of points. The calibration procedure is as follows:

Step 1) Connect the SMA Female-Female connector as a thru connector.

Step 2) Open the GUI of the system and enter the desired narrow band start and stop frequencies (any range within **1.22 – 1.98GHz** is acceptable), number of points for sampling, as well as, points for averaging and move mean for signal processing purposes. To better calculate the resonance parameters, check the box for either **notch** or **peak** resonance. Please note, for better resolution in the results, the optimized values for number of points, averaging and move mean are found to be **300**, **100**, and **5** (Fig. A- 1). However, these values are optional and one can increase or decrease the values for their specific optimum results. Increasing these values will lead to a longer scanning time.

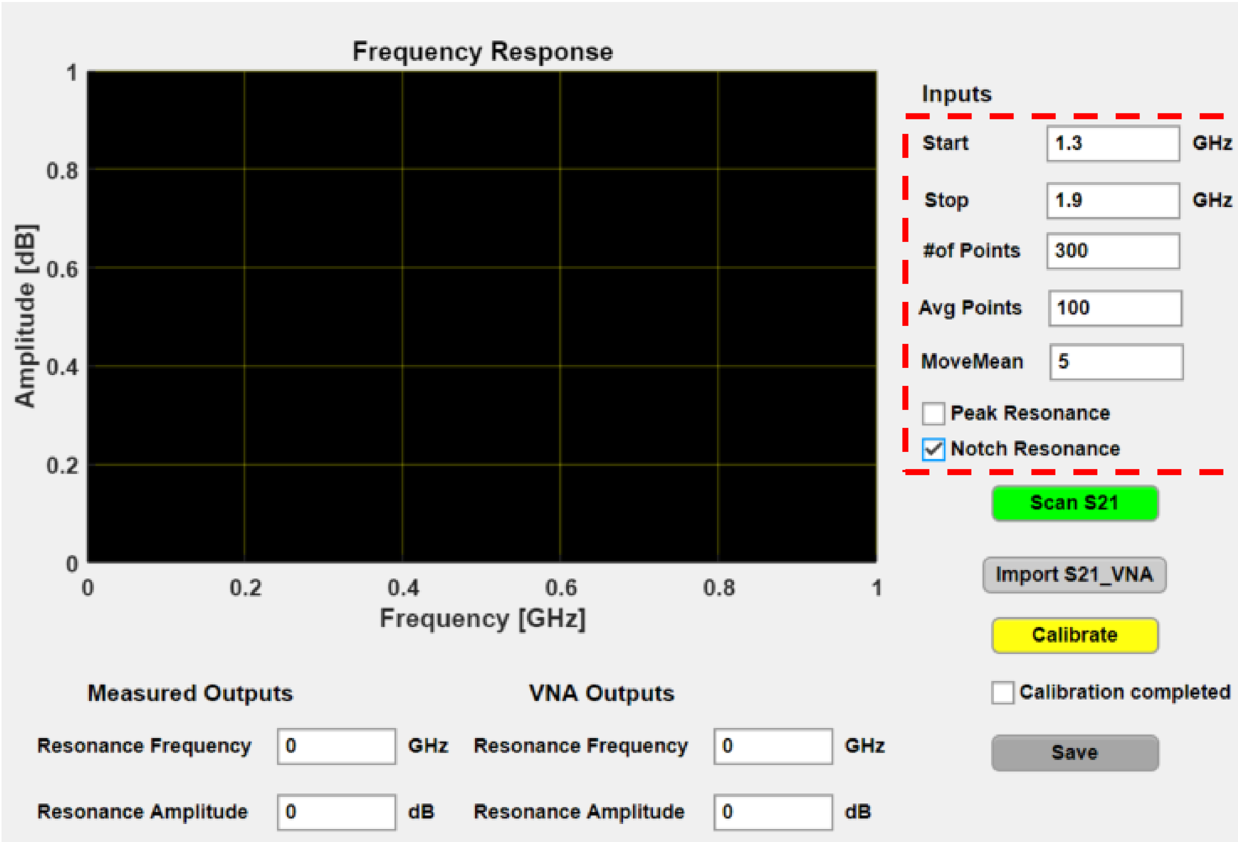

Fig. A- 1 Screenshot of the user interface with sample frequency range and optimum processing number of points are entered

Step 3) Once the desired range of frequency and processing parameters are entered, click on 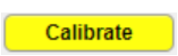

which then prompts a message to ensure thru is connected and instructs the user to check the calibration box 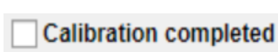

after the process is done. This ensures that the program will use this calibration data to measure S_{21} of the resonator.

A. 2 Narrow Band S_{21} Amplitude Measurement

Step 1) Remove the thru connector and connect the resonator of the interest. Ensure the calibration box is checked before scanning.

Step 2) Without changing any of the input parameters, click on 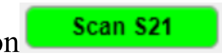

. A progress dialog box pops up to show how much of the process is done. With the current design, scanning time for 300 sampling points and 100 averaging points take about 1minute and 28 seconds. Reducing the number of points will also reduce the measuring time, as well as the resolution. Once the scanning is done, the plot of the S_{21}amplitude [dB] is displayed on the axes. This plot shows the resonance peak or notch of the device under test. In addition the resonance frequency and amplitude are shown under **Measured Outputs**.

Step 3) After scanning is done, user can save the data in the format of .mat (MATLAB data file) by clicking on 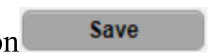

.

Step 4) **Optional**: This GUI provides an option to import the resonator's S_{21}data (.s2p file) captured by a VNA for comparison purposes. User can plot the $S_{21}$from VNA on top of the measured profile plotted by the system. The resonance frequency and amplitude of the VNA can

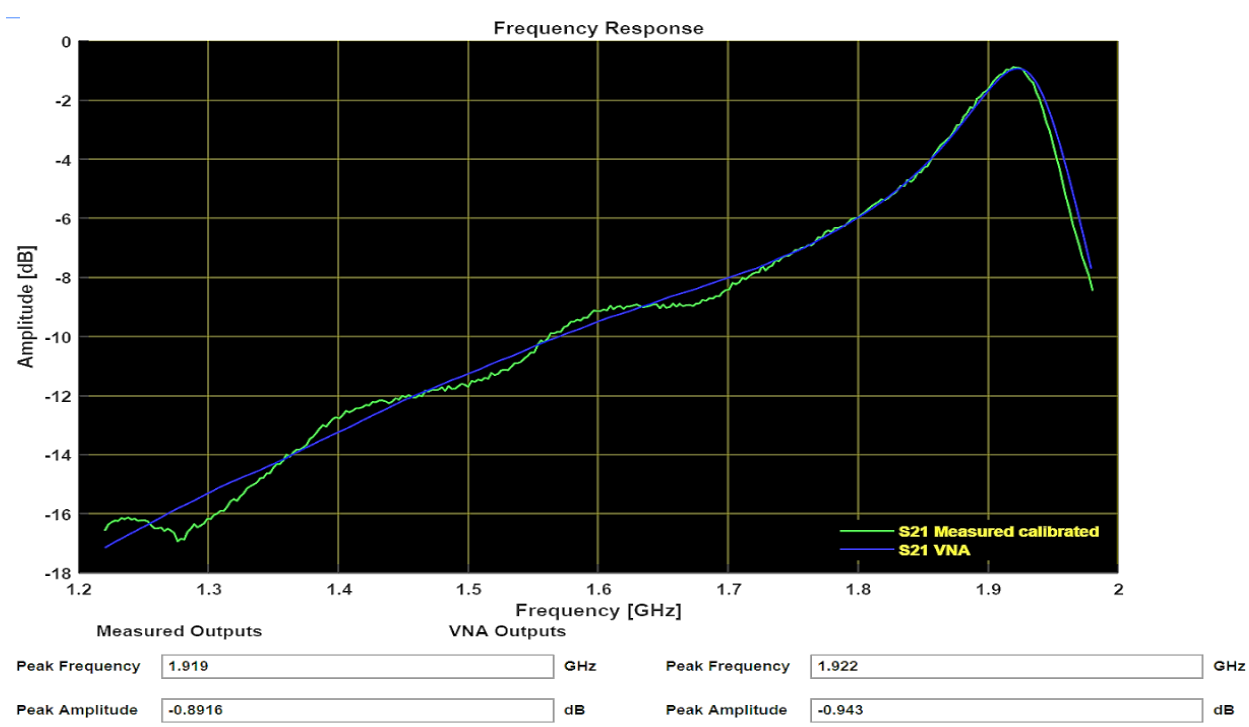

Fig. A- 2 Screenshot of S_{21}measurements of a resonator with the system and imported from VNA also be seen under **VNA Outputs**. This allow the user to compare the transmission profile of the DUT measured by the system with VNA. Fig. A- 2 shows an example of a resonator measurement with VNA data imported and plotted in the GUI.